Universidade Federal de Pernambuco
Centro de Ciências Exatas e da Natureza
Departamento de Física

Pós-graduação em Física

VORTEX MOTION AROUND A CIRCULAR CYLINDER BOTH IN AN UNBOUNDED DOMAIN AND NEAR A PLANE BOUNDARY

Marcel Nascimento de Moura

DISSERTAÇÃO DE MESTRADO

Recife
17 de maio de 2012

Universidade Federal de Pernambuco
Centro de Ciências Exatas e da Natureza
Departamento de Física

Marcel Nascimento de Moura

VORTEX MOTION AROUND A CIRCULAR CYLINDER BOTH IN AN UNBOUNDED DOMAIN AND NEAR A PLANE BOUNDARY

Trabalho apresentado ao Programa de Pós-graduação em Física do Departamento de Física da Universidade Federal de Pernambuco como requisito parcial para obtenção do grau de Mestre em Física.

Orientador: *Giovani Lopes Vasconcelos*

Banca examinadora:
Prof. Giovani Lopes Vasconcelos (Departamento de Física - UFPE)
Prof. Darren Gregory Crowdy (Department of Mathematics - Imperial College London)
Prof. Clécio Clemente de Souza Silva (Departamento de Física - UFPE)

Recife
17 de maio de 2012

Catalogação na fonte
Bibliotecária Joana D'Arc L. Salvador, CRB 4-572

Moura, Marcel Nascimento de.
Vortex motion around a circular cylinder both in an unbounded domain and near a plane boundary / Marcel Nascimento de Moura. – Recife: O Autor, 2012.
xiv, 93 f.: fig.

Orientador: Giovani Lopes Vasconcelos.
Dissertação (Mestrado) - Universidade Federal de Pernambuco. CCEN. Física, 2012.
Inclui bibliografia e apêndice.

1. Dinâmica dos fluidos. 2. Dinâmica de vórtices. 3. Sistemas hamiltonianos. I. Vasconcelos, Giovani (orientador). II. Título.

.

532.05 (22. ed.) FQ 2012-020

Universidade Federal de Pernambuco
Departamento de Física – CCEN
Programa de Pós-Graduação em Física
Cidade Universitária - 50670-901 Recife PE Brasil
Fone (++ 55 81) 2126-8449/2126-8450 - Fax (++ 55 81) 3271-0359
http://www.df.ufpe.br/pg e-mail: posgrad@df.ufpe.br

Parecer da Banca Examinadora de Defesa de Dissertação de Mestrado

Marcel Nascimento de Moura

"VORTEX MOTION AROUND A CIRCULAR CYLINDER BOTH IN AN UNBOUNDED DOMAIN AND NEAR A PLANE BOUNDARY"

A Banca Examinadora composta pelos Professores Giovani Lopes Vasconcelos (Presidente e Orientador), Clécio Clemente de Souza Silva, ambos do Departamento de Física da Universidade Federal de Pernambuco e Darren Greg Crowdy, do Imperial College, Londres, consideram o candidato:

( ) Aprovado ( ) Reprovado ( ) Em exigência

Secretaria do Programa de Pós-Graduação em Física do Departamento de Física do Centro de Ciências Exatas e da Natureza da Universidade Federal de Pernambuco em dezessete de maio de dois mil e doze.

_____ _____

Prof. Giovani Lopes Vasconcelos
Presidente e Orientador

Prof. Clécio Clemente de Souza e Silva

_____

Prof. Darren Greg Crowdy

Ao meu avô, Mauricio do Nascimento.
Por ter me mostrado as estrelas, os planetas, os peixes, os matos e os seixos.
Por ter me nutrido com curiosidade para uma vida inteira.
Por ter me ensinado, no meio de andanças, conversas e muitas piadas, todas as coisas importantes.

AGRADECIMENTOS

Agradeço.

Aos meus pais, Marco e Thelma, por me amarem incondicionalmente, e às minhas avós, Maria Izabel e Maria do Socorro, pela torcida e estímulo constantes. A Deus por estar sempre comigo.

Ao meu orientador, Prof. Giovani Vasconcelos, pela confiança que sempre depositou em mim, pela disponibilidade constante em me ajudar, pela liberdade que me concedeu e que fez com que esse trabalho fosse o produto final de um cotidiano amistoso e agradável.

Aos meus amigos da faculdade e da vida, em especial a Erton, Walter, Saulo, Rafael e Ceará (vulgo Tiago), por tudo de excelente que vivemos juntos nesses últimos seis(!) anos.

A Moacyr, pela amizade sincera, pelo café, pelas discussões, pela literatura e pelo sonho (ainda não realizado) de construir um laboratório de dinâmica de fluidos no terceiro andar! Pela utopia, sobretudo.

Ao CNPq pelo apoio financeiro.

Dear sir or madam, will you read my book?
It took me years to write, will you take a look?

—THE BEATLES (Paperback Writer)

RESUMO

Nessa dissertação estudamos a dinâmica de vórtices próximos a fronteiras sólidas em um fluido ideal, através do modelo de vórtices puntiformes. Obtivemos as configurações estacionárias de vórtices na presença de um cilindro circular colocado em um escoamento uniforme e investigamos suas propriedades de estabilidade sob pequenas perturbações. Dois sistemas distintos foram estudados. Consideramos inicialmente o caso clássico de um cilindro circular colocado em um escoamento uniforme ilimitado. Nesse caso, como se sabe, um par de vórtices com sentidos opostos é observado na esteira do cilindro, para números de Reynolds até cerca de 50, ao passo que para números de Reynolds maiores, essa configuração torna-se instável dando lugar à emissão alternada de vórtices. Este sistema foi tratado analiticamente pela primeira vez, através de um modelo de vórtices puntiformes, por Föppl em 1913. Na primeira parte dessa dissertação, o modelo de Föppl é revisto e várias características novas desse sistema são apresentadas, incluindo a existência de um ponto de sela nilpotente no infinito, até então não percebido, cujas órbitas homoclínicas definem a região de estabilidade não-linear do chamado equilíbrio de Föppl. Além disso, estudamos também a dinâmica não-linear resultante de perturbações anti-simétricas do equilíbrio de Föppl e discutimos sua relevância para a emissão alternada de vórtices. Na segunda parte, consideramos o movimento de um vórtice em torno de um cilindro circular colocado acima de uma parede plana infinita. Em experimentos com esse arranjo, um vórtice estacionário é observado na frente do cilindro, uma situação que não é encontrada no caso clássico (i.e., sem o plano). Para estudar a dinâmica de vórtices nessa situação, a região do fluido é inicialmente mapeada em um anel em um plano complexo auxiliar, e o potencial complexo correspondente é então obtido em termos da chamada função prima de Schottky-Klein, que neste caso pode ser escrita em termos de funções elípticas. As configurações estacionárias são então calculadas e suas propriedades de estabilidade são determinadas. Discutimos também, como as soluções do modelo de vórtice puntiforme podem ajudar a explicar as observações experimentais envolvendo a formação de vórtices na frente de um cilindro colocado próximo a um plano.

Palavras-chave: dinâmica de vórtices, vórtice puntiforme, dinâmica hamiltoniana, par de Föppl, domínio multiplamente conexo, Schottky-Klein.

ABSTRACT

In this thesis the dynamics of vortices near solid boundaries in an ideal fluid is studied using the point vortex model. Stationary configurations of vortices in the presence of a circular cylinder placed in a uniform stream are obtained and their stability properties under small disturbances are investigated. Two different systems are studied. First, the classical case of a circular cylinder placed in a uniform stream in an otherwise unbounded domain is considered. As is well known, in this case a pair of counter-rotating eddies is observed downstream of the cylinder for Reynolds numbers up to about 50, whereas for larger Reynolds number this configuration becomes unstable, leading to vortex shedding. This system was first treated analytically using point vortices by Föppl in 1913. In the first part of the thesis, the Föppl model is revisited and several novel features of this system are presented, including the existence of a hitherto unnoticed nilpotent saddle point at infinity whose homoclinic orbits define the region of nonlinear stability of the so-called Föppl equilibrium. In addition, the nonlinear dynamics resulting from antisymmetric perturbations of the Föppl equilibrium is studied and its relevance to vortex shedding is discussed. In the second part, the motion of a vortex around a cylinder placed above an infinite plane wall is considered. In experiments using this arrangement, a stationary eddy is observed in front of the cylinder, a situation that is not found in the classical case (i.e., without the plane). To study the vortex dynamics in this case, the flow domain is first mapped to an annulus in an auxiliary complex plane and the corresponding complex potential is obtained in terms of the so-called Schottky-Klein prime function, which in this case can be written in terms of elliptic functions. The stationary configurations are then calculated and their stability properties are determined. It is also discussed how the solutions of the point vortex model can help to explain the experimental findings for the vortex formation in front of a cylinder placed near a plane.

Keywords: vortex dynamics, point vortex, hamiltonian dynamics, Föppl pair, multiply connected domain, Schottky-Klein.

CONTENTS

LIST OF FIGURES

CHAPTER 1

INTRODUCTION

Vortex phenomena are very common in Nature. They occur in a wide variety of length and velocity scales. In the next few pages we will present a collection of pictures (Figures 1.1 to 1.5) showing some of these phenomena, with lengths varying from about $10^7\,m$ to $10^{-1}\,m$.

Fig. 1.1 shows two vortex formations on the planetary and astronomical scales: on the left side we see a satellite picture showing a von Karman vortex street near the coast of California. On the right side is Jupiter's Great Red Spot, a giant anticyclonic storm lasting for more than 200 years.

Tornadoes and waterspouts like the ones shown in Fig. 1.2 are two common examples of vortices, but these are not the only existing vortex-related atmospherical phenomena. Fig. 1.3 shows a strange cloud formation that is created due to a vortex sheet hydrodynamic instability, known as the Kelvin-Helmholtz instability.

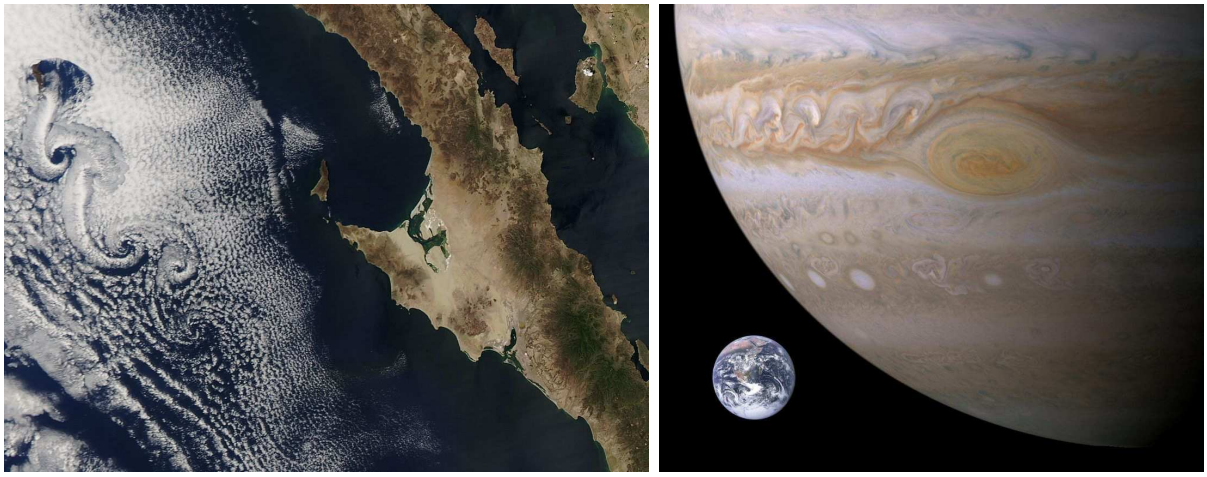

Figure 1.1 (left) von Karman vortex street caused by the interaction of wind currents with an island west of California (the wind comes from northwest). (right) Jupiter's Great Red Spot, an anticyclonic storm larger than the Earth, is an example of vortex lasting for more than 200 years.

Figure 1.2 (left) Tornadoes and waterspouts are not commonly seen in the Northeast Region of Brazil but in May of 2011 this unusual waterspout (right) was observed in Tamandaré, a city about 100 km away from Recife.

Vortex phenomena are also fundamental to many important practical applications such as the generation of lift in an airplane wing and the mixing of chemical substances. Civil and mechanical engineers must also take into account the effect of vortex induced vibrations in their projects. Fig. 1.4 shows the formation of a vortex structure behind a big airplane (actually, there are two vortices, one for each wing). These wingtip vortices may be dangerous for small aircrafts because if these aircraft happen to enter the vortex core, a rotation is induced which may cause a reduction of lift. An active area of research in Aeronautical Engineering concerns the creation of devices not only to reduce the formation of these vortices but also to detect in advance their presence in the air surrounding an aircraft (Ref. [1]).

Another interesting vortex-related phenomena is the vortex ring, the most common example being the smoke ring that some skilled smokers can produce. These rings can also be produced by making use of a box filled with smoke having a small hole in one side

Figure 1.3 (left) This frightening cloud formation is due to a vortex sheet hydrodynamic instability called the Kelvin-Helmholtz instability. These clouds may have served as an inspiration to Van Gogh's masterpiece *Starry Night* (right).

Figure 1.4 Wingtip vortex generated by a Boeing 747 on landing approach, made visible by industrial smoke. These vortices can be dangerous, specially for small aircrafts which can lose lift if entering the vortex core. Wingtip devices named *winglets* are used to reduce the vortex formation. Figure from Ref. [1].

and a rubber sheet attached to the other side. By giving a fast punch to the rubber sheet it is possible to make a very stable vortex ring, as shown in Fig. 1.5. As a historical side note, it is worth noticing that the stability of these rings and their vibrational properties impressed so much the Irish physicist William Thomson (later known as Lord Kelvin) that he considered the possibility that vortex rings in an etherial fluid could be the very constituents of all matter, giving rise, therefore, to the idea of a *vortex theory of matter*. Actually, this strong belief (and not the description of fluid mechanical phenomena) was the main reason that led this famous physicist to study vortex dynamics so deeply. The following excerpt, taken from an 1867 correspondence from Lord Kelvin to his friend, the German physicist Hermann von Helmholtz (founder of the field of Vortex Dynamics), describes his idea:

> My dear Helmholtz - I have allowed too long a time to pass without thanking you for your kind letter [...] Tait showed me in Edinburgh a magnificent way of producing them (the vortex rings). Take one side (or the lid) off a box (any old packing-box will serve) and cut a large hole in the opposite side. Stop the open side loosely with a piece of cloth, and strike the middle of the cloth with your hand. If you leave anything smoking in the box, you will see a magnificent ring shot out by every blow. A piece of burning phosphorus gives very good smoke for the purpose. [...] If you try it, you will easily make rings of a foot in diameter and an inch or so in section, and be able to follow them and see the constituent rotatory motion. The vibrations make good subject for mathematical work. [...] The absolute permanence of the rotation, and the unchangeable relation between it and the portion of the fluid once acquiring such motion in a perfect fluid, shows that if there is a perfect fluid all through space, constituting the substance of all matter, a vortex-ring would be as permanent as the solid hard atoms assumed by Lucretius and his followers (and predecessors) to account for the permanent properties of bodies (as gold, lead, etc.) and the differences of their characters.

Although Kelvin's ideas impressed many of the major scientific personalities of the

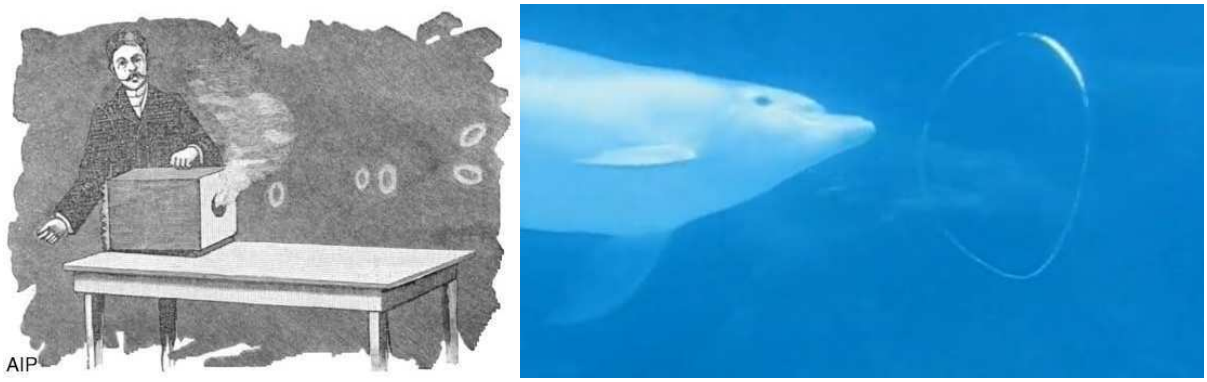

Figure 1.5 Smoke rings, as those shown on the 1897 sketch above (left), are examples of vortex rings. Dolphins like to play with bubble rings (right), which are vortex rings they produce by quickly pushing air from their blowholes.

19th century (the Scottish physicist James Clerk Maxwell said "it satisfies more of the conditions than any atom hitherto considers"), the vortex-atom theory was shown to be incorrect and Kelvin himself concluded later, motivated by instability arguments, that it could not serve as a theory of matter.

After this general motivation of the importance of vortex-related phenomena, we state the kind of problem that we are going to address in this thesis: we are interested here in the dynamics of vortices in the vicinity of solid obstacles. Fig. 1.6 shows an example of a flow past a circular cylinder placed in a uniform stream. In this case a pair of counter-rotating vortices is formed downstream of the cylinder, in the regime of low Reynolds number (when the velocity of the incoming stream is not too high). As the Reynolds number is increased, the vortex pair configuration becomes unstable, giving rise to transversal oscillations that ultimately lead to the formation of the so-called von Karman vortex street, a regime in which vortices are continuously shed from both sides of the cylinder; see Fig. 1.7 and compare it with the left side of Fig. 1.1. The dynamics of a vortex pair behind a cylinder will be studied in detail in Chapter 3. The instability properties of this system are believed to constitute the basic mechanism that leads to vortex shedding and the formation of the vortex street.

In this thesis, we will use the model of point vortices in an ideal fluid to describe

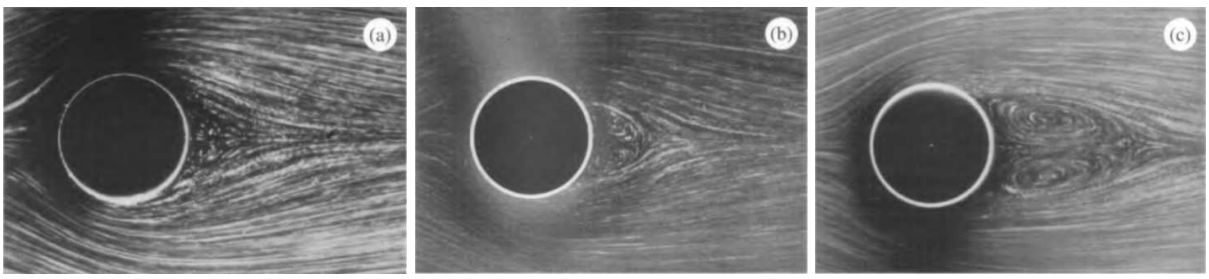

Figure 1.6 Formation of a vortex pair downstream of a cylinder. From left to right, the velocity of the incident stream is increased by a total factor of 2.7 (figure from Ref. [2]).

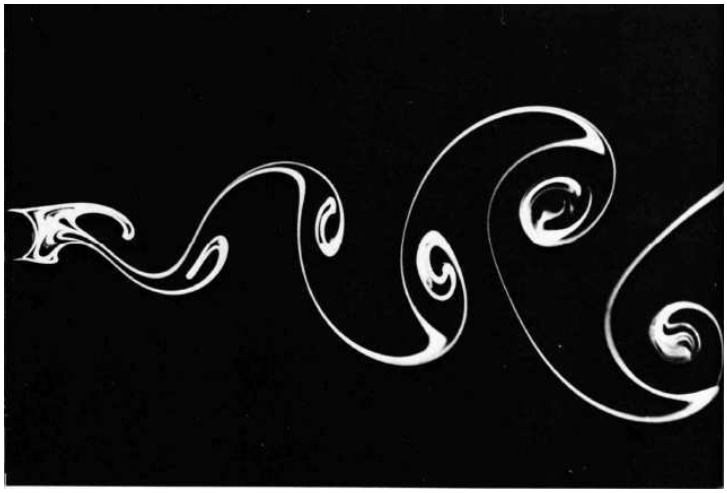

Figure 1.7 The von Karman vortex street. The cylinder is the small black circle on the extreme left (figure from Ref. [2]).

the vortices observed in flows past a cylinder. This model will be briefly explained in this chapter—a more detailed discussion will be deferred to Chapter 2—but first let us introduce the important concept of vorticity, $\vec{\omega}$, which is defined as the curl of the velocity field $\vec{v}$:

$$\vec{\omega} = \vec{\nabla} \times \vec{v} \,. \tag{1.1}$$

As can be easily found in the fluid mechanics literature (see, for example, Ref. [3]), the vorticity gives twice the average angular velocity of an infinitesimal fluid element around its center. If the vorticity in a region of the flow is zero, the fluid elements in that region are not rotating around their centers.

In the particular case of two-dimensional (2D) flows,

$$\vec{v} = (u(x,y), v(x,y), 0) \,, \tag{1.2}$$

we have

$$\vec{\omega} = (0, 0, \omega) \,, \tag{1.3}$$

i.e., the vorticity vector is in the z direction. If the vorticity is concentrated in a single point, we call it a *point vortex*. The vorticity field for a point vortex of intensity Γ located at $\vec{r_0} = (x_0, y_0)$ is thus given by

$$\omega(x,y) = \Gamma \delta(\vec{r} - \vec{r_0}) \,. \tag{1.4}$$

The velocity field of such a point vortex can be calculated by the fluid mechanical analog of Biot-Savart law and is given by

$$\vec{v} = \frac{\Gamma}{2\pi r} \, \hat{\theta} \,. \tag{1.5}$$

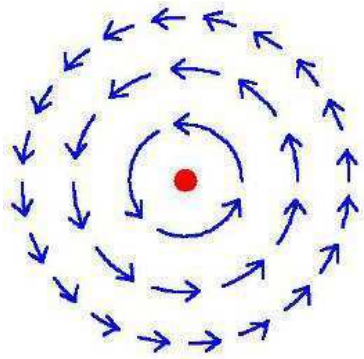

Figure 1.8 Sketch of the velocity field due to a point vortex of positive intensity (for negative intensity, the arrows would be clockwise).

where $r = |\vec{r} - \vec{r_0}| = \sqrt{(x - x_0)^2 + (y - y_0)^2}$ and $\hat{\theta}$ is the unit vector in the azimuthal direction. As can be easily verified, the constant Γ gives the value of the circulation around a contour enclosing the vortex:

$$\oint_C \vec{v} \cdot d\vec{x} = \oint_C \frac{\Gamma}{2\pi r} \hat{\theta} \cdot d\vec{x} = \Gamma \tag{1.6}$$

The velocity field due to a point vortex is thus strong near the vortex core and decreases as $1/r$ with the distance. The streamlines (lines tangent at each point to the local velocity vector) are circles centered at the vortex core. Fig. 1.8 shows a sketch of this velocity field.

In this thesis we will consider only the the case of ideal fluids, for which the viscosity is zero. In addition, we will impose two other conditions: the first one is that the fluid is incompressible ($\vec{\nabla} \cdot \vec{v} = 0$), meaning that the fluid density is constant everywhere, and the second one is that the flow is irrotational ($\vec{\omega} = 0$) everywhere, except at the singular isolated points where the vortices are located. In summary, the flows to be treated in this work will always be inviscid, incompressible and irrotational.

Considering irrotational flows when studying systems containing vortices may seem illogical at first, but the fact that the flow is irrotational does not necessarily mean that the fluid is not rotating. It means only that an element of fluid does not rotate around itself. Fig. 1.9 shows an example in which two small leaves are dropped in a point vortex flow: they rotate around the center of the vortex but they do that *without* rotating around their own centers. It is in this sense that the flow is said to be irrotational.

Although an inviscid fluid is capable of maintaining vorticity, its creation is usually due to viscous effects. Here, however, we will not analyze the mechanisms that lead to the formation of vortices. All analyses will be carried out considering that the vortices are already present in the flow.

The flows that we will consider here are two-dimensional, being constrained to the x-y plane, so that gravity will not be relevant and the only force responsible for the motion is the pressure field. The experiments we are going to refer to are also essentially two-dimensional, in the sense that the velocity fields are always of the form $\vec{v}(x, y, z) =$

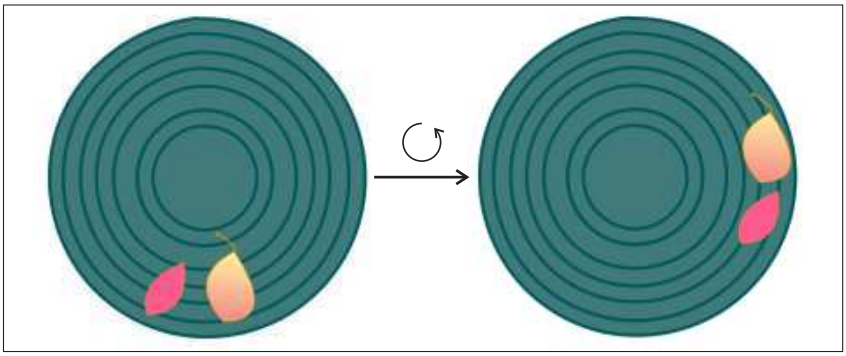

Figure 1.9 Two small leaves dropped at a point vortex flow. As time passes, they rotate around the vortex center, but they do not rotate around themselves.

$(v_x(x, y), v_y(x, y), 0)$.

Thus, in this thesis we study the dynamics of *point vortices in two-dimensional classical ideal fluids*, which form a simplified model of real vortical systems. We analyze possible stationary vortex configurations and study their stability under small displacements. Extensive use was made of the software *Wolfram Mathematica 6.0*, to generate plots, integrate nonlinear differential equations, and aid in some complicated numerical calculations that would otherwise take too long to be treated by hand.

The structure of this thesis is as follows. In chapter 2 we will give a brief account of the main theoretical results of vortex dynamics in 2D classical ideal fluids. The important theorems and mathematical techniques are presented and some simple examples will be given. In Chapter 3 we study the well-known problem of a pair of counter-rotating vortices in the presence of a circular cylinder placed in a uniform stream—the so-called Föppl pair. The dynamical aspects of this system are analyzed both analytically and numerically. Although this is a century-old problem (Föppl's original analysis dates back to 1913), we uncovered several new dynamical features of this system. Next, we study vortex configurations in domains involving more than one obstacle. The analysis of the dynamics of vortices in such a multiply connected domain is much more complicated than the one performed in Chapter 3. A new mathematical apparatus is needed, which is not yet found in modern textbooks on fluid mechanics. In Chapter 4, we briefly explain the basic mathematical formalism necessary to treat the dynamics of vortices in multiply connected domains. These results are used in Chapter 5 to study the dynamics of a single vortex near a cylinder placed above an infinite plane boundary in a uniform stream. Chapter 6 summarizes our main conclusions and discusses some possible extensions of this work.

CHAPTER 2

POTENTIAL FLOWS AND VORTEX DYNAMICS

This chapter is devoted to the description of the basic formalism that will be employed in rest of this thesis to analyze the vortex dynamics of some systems of interest. The content of this chapter can be found in practically any textbook on Fluid Mechanics having a chapter devoted to vortex dynamics. Nonetheless, it was thought desirable to collect here some basic results on two-dimensional vortex dynamics to render this thesis as self-contained as possible. In the beginning of the chapter, we will derive Bernoulli equation and introduce the important concepts of *potential flow* and *complex potential* that will be frequently used hereafter. The important theorems due to Kelvin and Helmholtz on the dynamics of vortices will be presented. Next we will introduce the point-vortex model, and the Hamiltonian nature of point-vortex dynamics will be explained. At the end of the chapter, some simple examples will be given to illustrate the techniques presented.

2.1 BERNOULLI EQUATION

Ideal fluid flows are governed by Euler equation

$$\rho \frac{D\vec{v}}{Dt} = -\vec{\nabla} P + \rho \vec{g} \,, \tag{2.1}$$

where ρ is the fluid density, $\vec{v}$ is the velocity field, P is the pressure field, $\vec{g}$ is the gravity, and the differential operator on the left side of the equation is the material derivative, meaning

$$\frac{D}{Dt} = \frac{\partial}{\partial t} + \vec{v} \cdot \vec{\nabla} \,, \tag{2.2}$$

which is responsible for taking the derivative "following" the fluid particles.

Since the gravitational force is conservative, it can be written as the gradient of a potential χ:

$$\vec{g} = -\vec{\nabla}\chi \,, \qquad \chi = gz \,. \tag{2.3}$$

Now, plugging this into Euler equation and considering that the flow is steady, which means $\frac{\partial \vec{u}}{\partial t} = 0$, we have

$$(\vec{v} \cdot \vec{\nabla})\vec{v} = -\vec{\nabla}\left(\frac{P}{\rho} + \chi\right) \,. \tag{2.4}$$

Using the vector identity

$$(\vec{v} \cdot \vec{\nabla})\vec{v} = (\vec{\nabla} \times \vec{v}) \times \vec{v} + \vec{\nabla}\left(\frac{1}{2}\left|\vec{v}\right|^2\right) \,, \tag{2.5}$$

into Eq. (2.4), we then have

$$\vec{\omega} \times \vec{v} = -\vec{\nabla} H \,, \tag{2.6}$$

where, as already discussed, $\vec{\omega} = \vec{\nabla} \times \vec{v}$ is the vorticity and $H = \frac{P}{\rho} + \frac{1}{2}\left|\vec{u}\right|^2 + \chi$. If we take a scalar product of Eq. (2.6) with the velocity vector, the left side vanishes, yielding

$$(\vec{v} \cdot \vec{\nabla}) H = 0 \,. \tag{2.7}$$

On the other hand, one can easily verify that the operator $\vec{v} \cdot \vec{\nabla}$ corresponds to taking the derivative along a streamline

$$(\vec{v} \cdot \vec{\nabla}) H = |\vec{v}| (\hat{n} \cdot \vec{\nabla}) H = |\vec{v}| \frac{dH}{ds} \tag{2.8}$$

where, $\hat{n}$ is a unit vector in the direction of the velocity field and ds is an infinitesimal element along a streamline (a line that is tangent at each point to the local velocity vector). This leads to the following important conclusion: *for an ideal fluid in a steady flow, H is constant along a streamline.*

Moreover, if the flow is irrotational, i.e. $\vec{\omega} = 0$, Eq. (2.6) reduces to

$$\vec{\nabla} H = 0 \tag{2.9}$$

which means

$$H = \frac{P}{\rho} + \frac{1}{2}\left|\vec{v}\right|^2 + \chi = const. \tag{2.10}$$

We then conclude that *for an ideal fluid in an irrotational steady flow, H is constant in the whole fluid domain.* Eq. (2.10) is known as *Bernoulli equation*, a very useful relation between the pressure, velocity and gravity. It is possibly the most used fluid dynamical equation in engineering problems.

Since the systems to be treated here are all two-dimensional, constrained to the x-y plane, the gravity will not be important and only the pressure and velocity terms will be present in the Bernoulli equation. A general statement about fluid flows then follows: high pressure $\Leftrightarrow$ low velocity / low pressure $\Leftrightarrow$ high velocity.

If we happen to find a velocity field that matches the boundary conditions to a given problem, then Eq. (2.10) can be used to find the respective pressure field satisfying Euler equation for an ideal irrotational steady flow. This means that, in the context of ideal fluids, one need not to worry about the pressure. The problem then reduces to finding the appropriate velocity field (from which the pressure can be later computed). In the next sections, we will show how to construct the velocity fields for some useful flow systems that satisfy the irrotationality condition.

2.2 POTENTIAL FLOW

Let us recall here the three conditions that will apply to all the flows treated in this work: the flows are *inviscid*, *incompressible* and *irrotational* (except for the singular points at

the vortex centers). Let $\vec{v} = (u, v)$ be the velocity field. The irrotationality condition (in two dimensions),

$$\vec{\nabla} \times \vec{v} = \left(\frac{\partial v}{\partial x} - \frac{\partial u}{\partial y} \right) \hat{k} = 0 \,, \tag{2.11}$$

where $\hat{k}$ is the unit vector in the z direction, implies that the velocity field can be represented as the gradient of a certain function ϕ,

$$\vec{v} = \vec{\nabla} \phi \,. \tag{2.12}$$

Flows obeying this condition are called *potential flows*. The function ϕ is the *velocity potential*. In two dimensions, Eq. (2.12) is written

$$u = \frac{\partial \phi}{\partial x} \quad , \quad v = \frac{\partial \phi}{\partial y} \,. \tag{2.13}$$

In a similar manner, the condition of incompressibility (in two dimensions),

$$\vec{\nabla} \cdot \vec{v} = \frac{\partial u}{\partial x} + \frac{\partial v}{\partial y} = 0 \,, \tag{2.14}$$

implies that the velocity can also be expressed in terms of another function ψ in the following manner:

$$u = \frac{\partial \psi}{\partial y} \quad , \quad v = -\frac{\partial \psi}{\partial x} \,. \tag{2.15}$$

The derivative of ψ with respect to a given direction gives the velocity component in a direction rotated by 90° clockwisely in relation to the direction of differentiation. Eq. (2.15) can be written in vectorial notation as

$$\vec{v} = \vec{\nabla} \times (\psi \, \hat{k}) \,. \tag{2.16}$$

Notice that with this definition, the condition of incompressibility is automatically satisfied. The function ψ is called the *streamfunction* because its contour lines, defined by

$$\psi(x, y) = const. \,, \tag{2.17}$$

are streamlines of the flow. To see why this is so, we consider the change in ψ as we move from a point (x, y) to a point $(x + dx, y + dy)$, at a fixed time, following the direction of the flow:

$$\begin{aligned} d\psi &= \psi(x + dx, y + dy) - \psi(x, y) \\ &= \frac{\partial \psi}{\partial x} dx + \frac{\partial \psi}{\partial y} dy \\ &= \frac{\partial \psi}{\partial x} dx + \frac{\partial \psi}{\partial y} \frac{v}{u} \, dx \,, \end{aligned} \tag{2.18}$$

where we used $dy = (v/u)\,dx$, because we are considering a displacement in the direction of the flow at the point (x, y). Using Eq. (2.15), we have

$$d\psi = \left(\frac{\partial\psi}{\partial x} - \frac{\partial\psi}{\partial x}\right) dx = 0\,. \tag{2.19}$$

So the streamfunction ψ is constant on each streamline. To visualize a streamline pattern of the flow, all that is necessary is to take the level set $\psi(x, y) = k$, for many different values of the constant k.

2.3 COMPLEX POTENTIAL

Combining Eqs. (2.13) and (2.15) we have

$$\frac{\partial\phi}{\partial x} = \frac{\partial\psi}{\partial y}\,, \tag{2.20}$$

$$\frac{\partial\phi}{\partial y} = -\frac{\partial\psi}{\partial x}\,. \tag{2.21}$$

These are the well-known Cauchy-Riemann equations of complex analysis. It follows then that if the partial derivatives of Eqs. (2.20) and (2.21) are continuous, the function w defined as

$$w(z) = \phi(x, y) + i\psi(x, y) \tag{2.22}$$

is an analytic function of the complex variable $z = x + iy$. The function $w(z)$ thus defined is called the *complex potential* associated with the flow. The derivative of w with respect to the complex variable z is

$$\begin{aligned} \frac{dw}{dz} &= \frac{\partial\phi}{\partial x} + i\frac{\partial\psi}{\partial x} \\ \frac{dw}{dz} &= u - iv\,, \end{aligned} \tag{2.23}$$

which is called the *complex velocity* and is simply the complex conjugate of the velocity vector treated as a complex number. The complex potential for a particular flow can be defined up to an additive irrelevant (complex) constant.

Notice that both the velocity potential ϕ and the streamfunction ψ obey the Laplace equation, as can be readily verified by taking the derivatives of the Cauchy-Riemann Eqs. (2.20) and (2.21):

$$\nabla^2\phi(x, y) = \frac{\partial^2\phi}{\partial x^2} + \frac{\partial^2\phi}{\partial y^2} = 0\,, \tag{2.24}$$

$$\nabla^2\psi(x, y) = \frac{\partial^2\psi}{\partial x^2} + \frac{\partial^2\psi}{\partial y^2} = 0\,. \tag{2.25}$$

In fact any analytic function satisfies Eqs. (2.24) and (2.25) for its real and imaginary part, as is well known. So, *any* analytic function can represent a complex potential for some two-dimensional potential flow. Since Laplace equation is linear, we can apply the superposition principle and add different contributions to form another complex potential.

The boundary condition usually encountered in irrotational flows are of two types:

1. Condition on solid surfaces: on any obstacle present in the flow, the velocity component normal to the surface must vanish. Therefore, the surface must be a streamline of the flow.

$$\frac{\partial \phi}{\partial n} = 0 \quad \text{or} \quad \frac{\partial \psi}{\partial s} = 0 \quad \Longrightarrow \quad \psi(x, y) = const. \,, \tag{2.26}$$

   where dn is an infinitesimal element along a direction normal to the surface and ds is an infinitesimal element along the direction of the surface.

2. Condition at infinity: typically (for our problems) the flow at infinity will be a uniform stream, in the, say, x direction, so the boundary condition reads

$$\frac{\partial \phi}{\partial x} = U \;, \; \frac{\partial \phi}{\partial y} = 0 \quad \text{or} \quad \frac{\partial \psi}{\partial y} = U \;, \; \frac{\partial \psi}{\partial x} = 0 \,, \tag{2.27}$$

   where U is the velocity of the uniform flow.

Solving the Laplace equation for the velocity potential (or alternatively for the streamfunction) subject to these boundary conditions can be difficult. Typically what is done is to consider the problem in the opposite way: take an analytical function $w(z)$, obtain its real and imaginary parts, which are respectively the velocity potential and the streamfunction for some particular flow, and then see what boundary conditions are satisfied by this complex potential. After that, one can use the superposition principle to add many contributions to form a different complex potential, satisfying the desired boundary conditions.

Once the complex potential is obtained, the velocity field can be immediately calculated, since it is given by the gradient of the velocity potential; see Eq. (2.12). The pressure field associated with this velocity field is easily calculated by means of Bernoulli equation (2.10). So if one finds a way to calculate the complex potential related to a particular irrotational flow, satisfying the appropriate boundary conditions, then a solution to Euler nonlinear equation (2.1) is immediately obtained by computing the pressure field using the Bernoulli equation (2.10).

Let $\vec{v_1}$ and P_1 be the velocity and pressure fields, respectively, for a given flow. Let $\vec{v_2}$ and P_2 be the same quantities for another flow. The superposition of the two flows produce a third flow with $\vec{v_3}$ and P_3 given by

$$\vec{v_3} = \vec{v_1} + \vec{v_2} \,, \tag{2.28}$$

$$P_3 = P_1 + P_2 - \rho \vec{v_1} \cdot \vec{v_2} \,, \tag{2.29}$$

where ρ is the fluid density. To see why the correction term to the pressure fields emerges, let us consider again Euler equation (without the gravity term),

$$\frac{\partial \vec{v}}{\partial t} + (\vec{v}\cdot\vec{\nabla})\vec{v} = -\vec{\nabla}\left(\frac{P}{\rho}\right) . \tag{2.30}$$

Now, using the vector identity (2.5) and considering the case of irrotational flows ($\vec{\nabla}\times\vec{v} = 0$), this equation can be rewritten as

$$\frac{\partial \vec{v}}{\partial t} = -\vec{\nabla}\left(\frac{P}{\rho} + \frac{1}{2}|\vec{v}|^2\right) , \tag{2.31}$$

which is valid for both set of variables $\vec{v_1}, P_1$, and $\vec{v_2}, P_2$. Adding the contributions of these two flows, we have

$$\begin{aligned}
\frac{\partial(\vec{v_1}+\vec{v_2})}{\partial t} &= -\vec{\nabla}\left(\frac{P_1+P_2}{\rho} + \frac{1}{2}\left(|\vec{v_1}|^2 + |\vec{v_2}|^2\right)\right) \\
&= -\vec{\nabla}\left(\frac{P_1+P_2}{\rho} + \frac{1}{2}\left(|\vec{v_1}+\vec{v_2}|^2 - 2\vec{v_1}\cdot\vec{v_2}\right)\right) \\
&= -\vec{\nabla}\left(\frac{P_1+P_2-\rho\vec{v_1}\cdot\vec{v_2}}{\rho} + \frac{1}{2}\left(|\vec{v_1}+\vec{v_2}|^2\right)\right) ,
\end{aligned} \tag{2.32}$$

thus showing that the Euler equation is satisfied for the velocity and pressure fields given in Eqs. (2.28) and (2.29). In the next subsection we show examples of complex potentials for several simple flows.

2.3.1 Uniform Flow

The velocity field due to a uniform flow of intensity U, making an angle α with the horizontal is

$$\vec{v} = U\cos(\alpha)\hat{x} + U\sin(\alpha)\hat{y} , \tag{2.33}$$

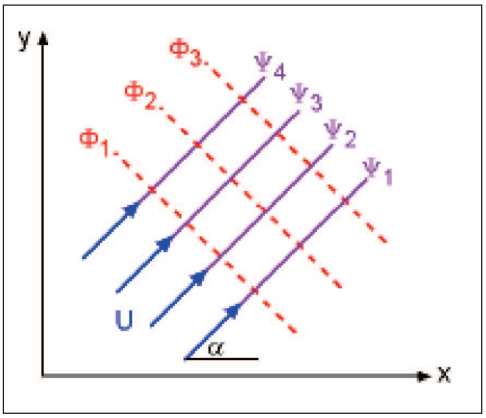

Figure 2.1 Streamlines (purple) and equipotential lines (red) for a uniform flow.

which can be obtained as the gradient of the potential

$$\phi(x, y) = U\cos(\alpha)x + U\sin(\alpha)y\,. \tag{2.34}$$

This function is the real part of the following analytical complex function:

$$w = Ue^{-i\alpha}z\,, \tag{2.35}$$

as can be readily verified:

$$\begin{aligned} w &= Ue^{-i\alpha}z \\ &= U(\cos(\alpha) - i\sin(\alpha))(x + iy) \\ &= \underbrace{U(\cos(\alpha)x + \sin(\alpha)y)}_{\phi} + i\,\underbrace{U(\cos(\alpha)y - \sin(\alpha)x)}_{\psi}\,. \end{aligned} \tag{2.36}$$

The streamlines, $\psi = const.$, are then lines making an angle α with the horizontal, as desired. Fig. 2.1 shows the streamlines and equipotentials associated to this flow.

2.3.2 Source and Sink

A source (or sink) corresponds to a flow having the following velocity field:

$$\vec{v} = \frac{m}{2\pi r}\,\hat{r}\,, \tag{2.37}$$

where $\hat{r}$ is the unit vector in the radial direction and m is the intensity of the source ($m > 0$) or sink ($m < 0$), representing the amount of "fluid area" injected (removed) by the source (sink) per unit time. This velocity field (2.37) is obtained from the following potential

$$\phi = \frac{m}{2\pi}\log r\,, \tag{2.38}$$

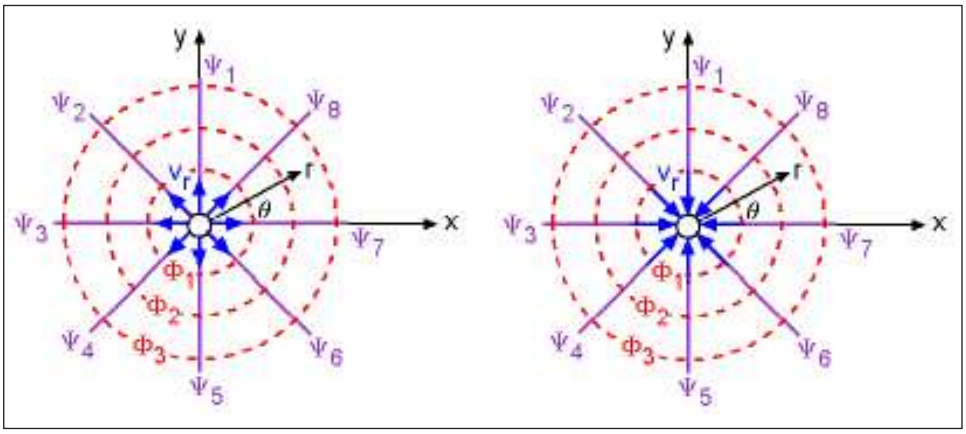

Figure 2.2 Streamlines (purple) and equipotential lines (red) for a source (left) or a sink (right).

which is the real part of the complex potential

$$w = \frac{m}{2\pi} \log z \, . \tag{2.39}$$

If instead of being located at the origin, the source (sink) is located at a different point $z = z_0$ of the complex plane, then the complex potential reads

$$w = \frac{m}{2\pi} \log (z - z_0) \, . \tag{2.40}$$

Fig. 2.2 shows the streamlines and equipotentials associated with this flow.

2.3.3 Dipole

A dipole (or doublet) is obtained in the limit that a source and a sink of equal intensity, $|m|$, "merge" in such a way that the product of the intensity m and the distance between source and sink is kept constant. To obtain the corresponding complex potential for a dipole, let us consider a source-sink pair in the x-axis, with the source at $x = -\epsilon$ and the sink at $x = +\epsilon$. The complex potential for this source-sink pair is

$$\begin{aligned} w &= \frac{m}{2\pi} \log (z + \epsilon) - \frac{m}{2\pi} \log (z - \epsilon) \\ &= \frac{m}{2\pi} \log \left(\frac{z + \epsilon}{z - \epsilon} \right) \\ &= \frac{m}{2\pi} \log \left(1 + \frac{2\epsilon}{z} + \cdots \right) \, . \end{aligned} \tag{2.41}$$

Ignoring the additive constant and terms or second order in ϵ and defining the limit $\mu = m\epsilon/\pi$ as $m \to \infty$ and $\epsilon \to 0$, we have

$$w = \frac{\mu}{z} \, . \tag{2.42}$$

The real and imaginary parts of this complex potential give

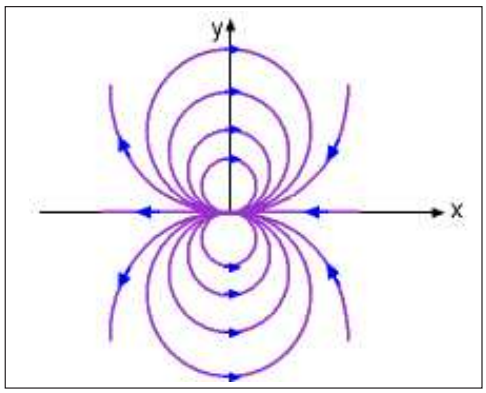

Figure 2.3 Streamlines for a dipole at the x-axis.

$$\phi = \frac{\mu x}{x^2 + y^2} \,, \tag{2.43}$$

$$\psi = -\frac{\mu y}{x^2 + y^2} \,. \tag{2.44}$$

The streamlines of this dipole are circles centered in the y-axis, as shown in Fig. 2.3.

2.3.4 Point Vortex

The complex potential for a point vortex can be generated from the complex potential for a source (or sink) by simply interchanging the roles of ϕ and ψ. This can be easily seen by noting that, as already discussed in Chapter 1, the streamlines for a point vortex should be circles around the vortex center. On the other hand the equipotential lines for a source are also circles, see Fig. 2.2. Thus, the velocity potential of a source plays the role of the streamfunction for the vortex. This interchange can be achieved by simply multiplying the complex potential Eq. (2.40) by $\pm i$. To respect the convention that a positive vortex circulation means counterclockwise flow, we pick the negative sign:

$$w = -i\frac{m}{2\pi} \log\left(z - z_0\right) \,. \tag{2.45}$$

Changing the nomenclature $m \to \Gamma$ to denote the vortex intensity, we have

$$w = \frac{\Gamma}{2\pi i} \log\left(z - z_0\right) \,. \tag{2.46}$$

The real and imaginary parts of this equation produce

$$\phi = \frac{\Gamma}{2\pi}\,\theta \,, \tag{2.47}$$

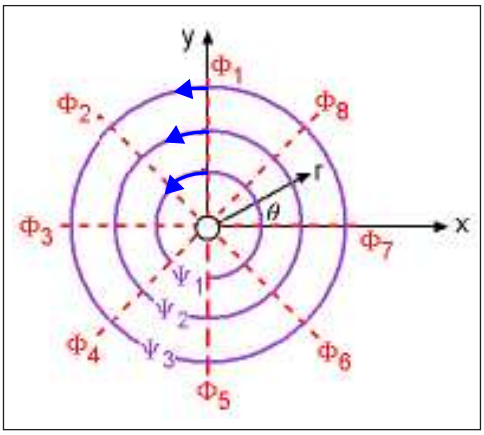

Figure 2.4 Streamlines (purple) and equipotential lines (red) for a vortex of positive circulation ($\Gamma > 0$).

$$\psi = -\frac{\Gamma}{2\pi} \log r \, . \tag{2.48}$$

Fig. 2.4 shows the streamlines and equipotential lines for a point vortex located at the origin.

By means of the superposition principle it is possible to use the complex potentials given above as building blocks to obtain new complex potentials, as we will discuss next.

2.3.5 Uniform Flow Past a Circular Cylinder

The complex potential for the flow consisting of a uniform stream of intensity U around a circular cylinder of radius a, located at the origin, can be constructed by superimposing the complex potential for a uniform stream, Eq. (2.35), with the complex potential for a dipole, Eq. (2.42), thus yielding

$$w(z) = Uz + \frac{\mu}{z} \, . \tag{2.49}$$

One now has to choose the dipole intensity μ so as to satisfy the boundary condition that the cylinder must be a streamline of the flow. This means that the imaginary part of the complex potential (2.49) must be constant at the cylinder surface, i.e., the function

$$w(ae^{i\theta}) = Uae^{i\theta} + \frac{\mu}{a} \, e^{-i\theta} \, , \tag{2.50}$$

must have a constant imaginary part for $0 < \theta < 2\pi$. If we make $\mu = Ua^2$,

$$\begin{aligned} w(ae^{i\theta}) &= Uae^{i\theta} + Uae^{-i\theta} \\ &= 2Ua \, \cos(\theta) \, , \end{aligned} \tag{2.51}$$

which is purely real, and so $\psi = 0$ at the cylinder, thus satisfying the desired boundary condition. So the complex potential reads

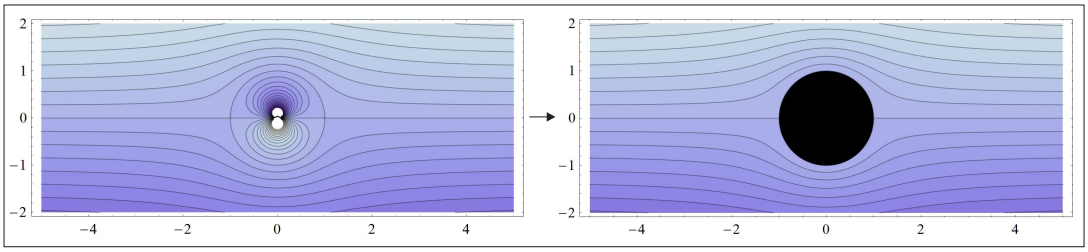

Figure 2.5 Streamline pattern for a uniform flow around a circular cylinder. The color code in this figure (and in similar figures in the following chapters) associates lighter colors to higher values of the streamfunction. If one follows the direction of the flow along a streamline, the streamfunction increases to the left, therefore, the colors to the left are lighter than the ones to the right.

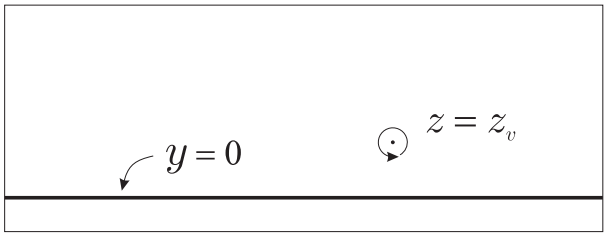

Figure 2.6 Diagram of the problem of one vortex near an infinite solid wall.

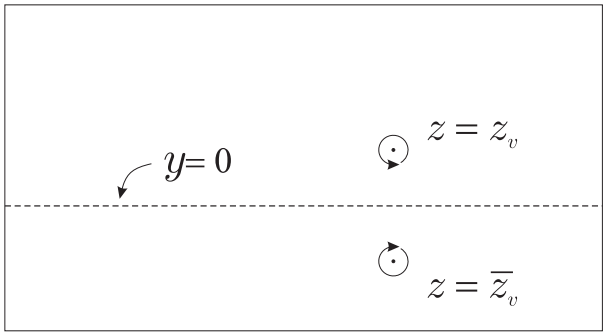

Figure 2.7 Image construction for the problem of one vortex near an infinite solid wall.

$$w(z) = U\left(z + \frac{a^2}{z}\right) . \tag{2.52}$$

The streamfunction associated with this flow is obtained by taking the imaginary part of this complex potential:

$$\psi(x, y) = Uy\left(1 - \frac{a^2}{x^2 + y^2}\right) . \tag{2.53}$$

Fig. 2.5 shows a streamline pattern produced by taking the contour plot $\psi(x, y) = k$ for several different values of the constant k. To produce this plot we used the parameters $U = 1$ and $a = 1$. As can be seen on the left side of the figure, the superposition of the dipole at the origin with a uniform stream produces a circular region where no fluid comes in and no fluid goes out. The boundary condition is then satisfied since the circle of radius $a = 1$ is a streamline. It is thus the desired flow describing the situation on the right side, where instead of the dipole there is a real solid boundary.

This example provides a first contact with the so-called *method of images*, which will be explained in more details in the next section. The dipole at the origin can be thought of as the image of the uniform stream by the cylinder, which acts like a "circular mirror".

2.4 METHOD OF IMAGES

The method of images consists of a technique to solve Laplace equation subject to a given set of boundary conditions. It is usually discussed in textbooks on Classical Electrodynamics, as a technique to calculate the electrostatic potential (which obeys Laplace

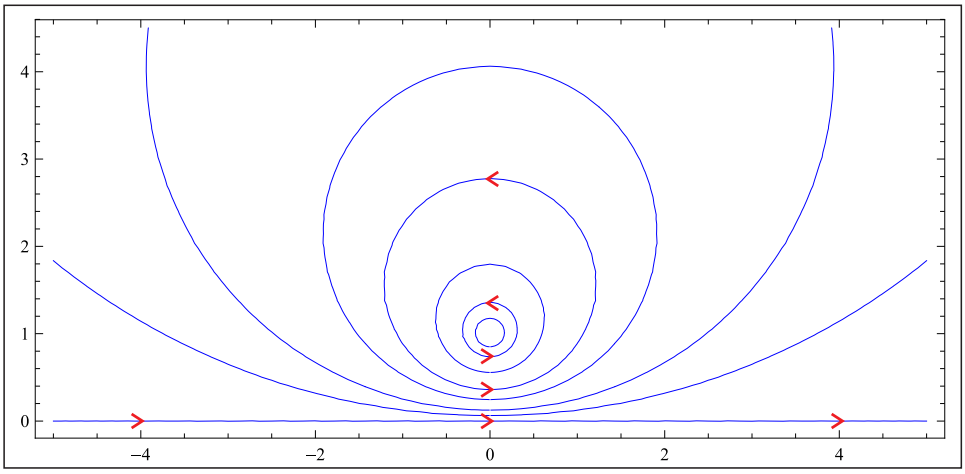

Figure 2.8 Streamline pattern for one vortex near a plane wall. The arrows indicate the direction of the flow.

equation in free space) in the presence of a grounded surface (where the electrostatic potential is held constant, say zero).

Let us use this method to solve the problem of a point vortex near an infinite wall. Let the vortex, of intensity Γ, be located at the position $z = z_v$ in the upper half-plane. The line $y = 0$ represents the solid wall. Fig. 2.6 shows the geometry of this problem.

The problem then consists of finding the complex potential satisfying the following boundary conditions: i) the line $y = 0$ is a streamline, ii) the potential must approach a constant value as $|z| \to \infty$ (with $y > 0$), and iii) it must have a logarithm singularity at the vortex position, i.e., near z_v the complex potential must tend to Eq. (2.46) with the substitution $z_0 \to z_v$. It is easily verified that all these conditions are satisfied if we introduce an image vortex with opposite circulation in the unphysical region ($y < 0$) at $z = \bar{z}_v$. Fig. 2.7 shows this construction. The line $y = 0$ is a streamline because the y-component of the velocity in this line induced by one vortex is precisely canceled by the other, so that the resulting velocity is always horizontal.

The complex potential produced by the vortex and its image is then given by

$$w(z, z_v) = \frac{\Gamma}{2\pi i} \log(z - z_v) - \frac{\Gamma}{2\pi i} \log(z - \bar{z}_v) \, . \tag{2.54}$$

The streamfunction for the flow can then be obtained by taking the imaginary part of the complex potential above. Fig. 2.8 shows a streamline patten for this problem, considering the parameters $\Gamma = 1$ and $z_v = i$.

2.4.1 Milne-Thomson Circle Theorem

When the solid boundary is an infinite plane, it is generally easy to find the images, for they are simple plane-mirror reflections of the actual flow elements. But when arbitrary boundaries are involved, the system of images is not easily guessed. Luckily, when the boundary is a single circle, there is a theorem due to Milne-Thomson that can be used

to automatically calculate the images necessary to satisfy the boundary condition on the circle.

Theorem 2.1 (Milne-Thomson Circle Theorem)**.** *Let $f(z)$ be the complex potential for a flow where all the singularities (vortices, sources, sinks...) are located in the region $|z| > a$, then*

$$w(z) = f(z) + \bar{f}\left(\frac{a^2}{z}\right) \tag{2.55}$$

is the complex potential for a flow having the same singularities as $f(z)$ in the region $|z| > a$ and having the circle of radius a as a streamline.

In this theorem, $\bar{f}(z)$ is the conjugate function of $f(z)$ defined as

$$\bar{f}(z) = \overline{f(\bar{z})} \tag{2.56}$$

To prove the theorem, first notice that since all singularities of $f(z)$ are outside the circle of radius a, the singularities of $\bar{f}\left(\frac{a^2}{z}\right)$ are all inside this circle. So the singularities outside the circle are the same for $w(z)$ and $f(z)$. Next, for any point on the circle, we have

$$w(ae^{i\theta}) = f(ae^{i\theta}) + \overline{f\left(\frac{a^2}{\overline{ae^{i\theta}}}\right)} = f(ae^{i\theta}) + \overline{f(ae^{i\theta})}\,, \tag{2.57}$$

which is purely real. So the circle is a streamline of the flow.

To exemplify the use of this theorem, let us obtain once again Eq. (2.52) for the complex potential of a uniform stream around a circular cylinder of radius a. The potential without the cylinder is simply due to the uniform flow. This will be the function $f(z)$:

$$f(z) = Uz\,. \tag{2.58}$$

The potential in the presence of the circle is then

$$\begin{aligned} w(z) &= f(z) + \overline{f\left(\frac{a^2}{\bar{z}}\right)} \\ &= Uz + U\left(\frac{a^2}{z}\right) \\ &= U\left(z + \frac{a^2}{z}\right)\,, \end{aligned} \tag{2.59}$$

thus reproducing Eq. (2.52), as desired. The circle theorem then automatically produces the image terms (in this case, the dipole term) necessary to satisfy the boundary condition on the cylinder surface.

Now let us move on to the second part of this chapter where we will state some basic theorems and results on the dynamics of vorticity.

2.5 VORTEX DYNAMICS

2.5.1 The Vorticity Equation

Let us consider once again Eq. (2.4), which is obtained from Euler equation (2.1) after considering that the flow is steady and making use of the fact that the gravity is a conservative force. After using the vector identity (2.5), Eq. (2.4) can be written in the form

$$\frac{\partial \vec{v}}{\partial t} + \vec{\omega} \times \vec{v} = -\vec{\nabla} H \, . \tag{2.60}$$

Taking the curl of this equation, we have

$$\frac{\partial \vec{\omega}}{\partial t} + \vec{\nabla} \times (\vec{\omega} \times \vec{v}) = 0 \, . \tag{2.61}$$

Using the vector identity

$$\vec{\nabla} \times (\vec{\omega} \times \vec{v}) = (\vec{v} \cdot \vec{\nabla})\vec{\omega} - (\vec{\omega} \cdot \vec{\nabla})\vec{v} + \vec{\omega}\, \vec{\nabla} \cdot \vec{v} - \vec{v}\, \vec{\nabla} \cdot \vec{\omega} \tag{2.62}$$

in the previous equation, we have

$$\frac{\partial \vec{\omega}}{\partial t} + (\vec{v} \cdot \vec{\nabla})\vec{\omega} - (\vec{\omega} \cdot \vec{\nabla})\vec{v} + \vec{\omega}\, \vec{\nabla} \cdot \vec{v} - \vec{v}\, \vec{\nabla} \cdot \vec{\omega} = 0 \, . \tag{2.63}$$

Now $\vec{\nabla} \cdot \vec{v} = 0$ because the flow is incompressible and $\vec{\nabla} \cdot \vec{\omega} = 0$ since $\vec{\nabla} \cdot (\vec{\nabla} \times \vec{v}) = 0$, so Eq. (2.63) becomes

$$\frac{\partial \vec{\omega}}{\partial t} + (\vec{v} \cdot \vec{\nabla})\vec{\omega} - (\vec{\omega} \cdot \vec{\nabla})\vec{v} = 0 \, , \tag{2.64}$$

which can be rewritten as

$$\frac{D\vec{\omega}}{Dt} = (\vec{\omega} \cdot \vec{\nabla})\vec{v} \, . \tag{2.65}$$

This is the so-called *vorticity equation*. Notice that the pressure field has been eliminated from this equation—it involves only $\vec{v}$ and $\vec{\omega}$. In the particular case of two-dimensional flows,

$$\vec{v} = (u(x, y), v(x, y), 0) \, , \tag{2.66}$$

we have

$$\vec{\omega} = (0, 0, \omega) \, , \tag{2.67}$$

which implies that $(\vec{\omega} \cdot \vec{\nabla})\vec{v} = 0$, and so the vorticity equation simplifies to

$$\frac{D\omega}{Dt} = 0 \, . \tag{2.68}$$

This means that in two dimensional ideal flows the vorticity of a particular fluid element does not change with the flow. In particular, if the flow is steady, Eq. (2.68) reduces to

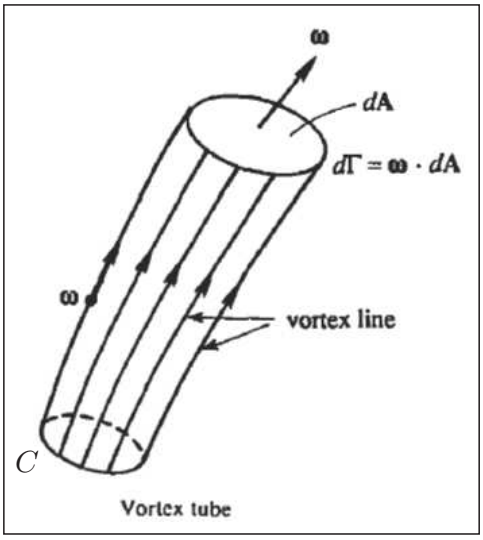

Figure 2.9 A vortex tube is formed by the vortex lines passing through the spatial closed curve C (figure adapted from Ref. [3]).

$$(\vec{v} \cdot \vec{\nabla})\omega = 0 \,, \tag{2.69}$$

i.e., *the vorticity is constant in each streamline of a steady two-dimensional flow of an ideal fluid, subjected only to conservative forces (like the gravity).*

For the sake of completeness, in the next subsection we shall state the main theorems of three-dimensional vortex dynamics, due to Helmholtz and Kelvin. We shall then use these theorems to justify the point-vortex model to be introduced subsequently.

2.5.2 The Vortex Dynamics Theorems

In the study of three dimensional flows, it is useful to introduce the concept of *vortex line*, which is a curve such that its tangent is always in the direction of the local vorticity vector $\vec{\omega}$. Since $\vec{\nabla} \cdot \vec{\omega} = 0$, a vortex line cannot start or end within the fluid domain, they have to be attached to a solid boundary, form a closed loop or extend to infinity. Consider now a closed curve C in the interior of the fluid flow domain, which is transported by the flow (one can think of this curve as if it were formed by dyed fluid particles). The vortex lines that pass through this curve define a surface in space which is the boundary of a *vortex tube*, see Fig. 2.9.

In his 1858 seminal paper, Helmholtz introduced the model of point vortices and vortex lines and proved the following theorems, valid for an inviscid incompressible fluid of constant density moving in the presence of conservative forces (like the gravity, for example).

Theorem 2.2 (Helmholtz first theorem)**.** *The fluid elements that lie on a vortex line at some instant will continue to lie on this vortex line, i.e, vortex lines move with the fluid.*

Theorem 2.3 (Helmholtz second theorem)**.** *The circulation around a vortex tube*

$$\Gamma = \int_C \vec{v} \cdot d\vec{x} = \int_A \vec{\omega} \cdot d\vec{A} \tag{2.70}$$

is the same for any cross-section of the vortex tube. This common value is called the strength of the vortex tube.

Another important theorem was proved by Kelvin in 1867.

Theorem 2.4 (Kelvin theorem)**.** *Let $C(t)$ be a closed curve made by fluid particles that is carried within the flow of an ideal irrotational fluid, subjected only to conservative forces. The circulation around $C(t)$*

$$\Gamma = \int_{C(t)} \vec{v} \cdot d\vec{x} \tag{2.71}$$

is constant in time.

Notice that C is not a fixed curve in space. It denotes a "dyed" circuit. Also, notice that it is not essential that the fluid domain inside the curve be simply connected, i.e., the curve could, for example, encircle a solid obstacle like an airfoil.

If one chooses the curve $C(t)$ in Kelvin theorem to be the curve around the vortex tube in Helmholtz theorem, one immediately concludes that the strength of a vortex tube is time independent. As a consequence, if a region of a vortex tube is stretched, its cross-section area is reduced and the vorticity in that region is then increased, in order to keep the circulation constant. Thus, the stretching of a vortex tube increases the angular velocity of the fluid particles. The proof of Kelvin and Helmholtz theorems can be found in many textbooks on fluid mechanics, such as [3] or [7].

In the next section we will explain in details the point-vortex model that will be employed to describe the dynamics of real vortices.

2.6 THE POINT VORTEX MODEL

From Helmholtz first theorem, we see that vortex lines move with the flow, that is to say, each portion of the vortex line will move with the velocity of the flow there. In two dimensional flows, the vorticity vector $\vec{\omega}$ is perpendicular to the plane of the flow; see Eq. (2.67). This means that the vorticity field can be treated as a scalar field $\omega(x, y)$. A case of particular interest is the so-called *vortex patch*, when the vorticity ω is constant inside a finite region and zero outside this region. The dynamics of this patch can be analyzed by considering that each point inside it moves with the velocity induced by the rest of the flow in that particular point, as prescribed by Helmholtz first theorem.

When the vorticity distribution is singular, as is the case of a point vortex where the vorticity is concentrated in a single point, see Eq. (1.4), it is not straightforward to deduce that the vortex motion will follow a similar dynamics and additional considerations must be made to handle the divergence in the velocity field at the vortex position. Using momentum conservation arguments (as discussed by Saffman in Section 2.3 of his textbook [8]), one concludes that the motion of point vortices actually follows the same

kind of dynamics as the vortex lines, in the sense that they will also move with the velocity induced by the rest of the flow at the vortex position. This will be the basic dynamical idea that will be extensively employed in this thesis to analyze the motion of vortices. This approach originated with Helmholtz's 1858 seminal paper on vortex dynamics, Ref. [9], and constitutes the so-called *point vortex model*. Let us now obtain the equations governing the motion of a system consisting of N point vortices, according to this model.

2.6.1 Equations of Motion

Let us consider a system of N point vortices in an unbounded two dimensional flow, having intensities Γ_k and located at the positions $z_k = x_k + iy_k$, $k = 1, 2, \cdots, N$. Each of the vortices will move with the velocity field induced by all the other $N-1$ vortices. Mathematically this means

$$u_j - iv_j = \sum_{\substack{k=1 \\ k\neq j}}^{N} \frac{\Gamma_k}{2\pi i} \frac{1}{z_j - z_k} \,, \tag{2.72}$$

where (u_j, v_j) is the velocity of the j-th vortex. Separating the real and imaginary parts of this equation and making use of the correspondence $(u_j, v_j) \to (\dot{x_j}, \dot{y_j})$, where the dot means differentiation with respect to the time, we have

$$\dot{x_j} = -\sum_{\substack{k=1 \\ k\neq j}}^{N} \frac{\Gamma_k}{2\pi} \frac{(y_j - y_k)}{(x_j - x_k)^2 + (y_j - y_k)^2} \tag{2.73}$$

$$\dot{y_j} = \sum_{\substack{k=1 \\ k\neq j}}^{N} \frac{\Gamma_k}{2\pi} \frac{(x_j - x_k)}{(x_j - x_k)^2 + (y_j - y_k)^2} \,. \tag{2.74}$$

Notice that the summation excludes the contribution of the particular vortex whose velocity is being calculated. If other contributions to the flow are present, such as incoming streams or dipoles, these can be thought of as limits taken over appropriate point vortex configurations. For example, the dipole was introduced in Sec. 2.3.3 as resulting from the "merging" procedure of a source and a sink in the real axis, but it can also be obtained by taking the limit corresponding to the "merging" of a pair of opposite point vortices in the imaginary axis, i.e., in a direction perpendicular to the source-sink case. To obtain a dipole in the negative horizontal direction, one would take the upper vortex to have negative circulation and the lower one to have positive circulation. Similarly, the incoming stream can be thought of as a dipole placed at infinity. Therefore, Eqs. (2.73) and (2.74) can also encompass these contributions.

To perform the analysis of the dynamics of vortices in a two dimensional ideal flow, it is useful to introduce the concept of an "effective potential" to account for the resulting interaction acting on each vortex. This will be explained in the next section.

2.6.2 The Effective Potential

Since a point vortex moves in a fluid with the velocity induced by all the other elements of the flow, it is useful to introduce a function, called the "effective potential", obtained from the complex potential for a given flow by removing the contribution due to the vortex itself, so that the vortex velocity can be readily obtained as a derivative of the "effective potential".

Let $w(z, z_0)$ denote the complex potential for a general flow, having a point vortex of intensity Γ located at the point $z = z_0$ in the complex plane. The "effective potential", w_{eff}, for the vortex at z_0 is defined as

$$w_{eff}(z, z_0) = w(z, z_0) - \frac{\Gamma}{2\pi i} \log(z - z_0) \,. \tag{2.75}$$

The vortex complex velocity, $u - iv$, is then obtained by calculating the derivative of the "effective potential" at the vortex position z_0,

$$u - iv = \frac{d}{dz}\, w_{eff}(z, z_0)\bigg|_{z=z_0} \,. \tag{2.76}$$

Let us apply this formalism to analyze the vortex dynamics of some simple examples.

2.6.2.1 Vortex in a uniform flow Let us start from the very simple case of a vortex of intensity Γ at $z = z_0$ in a uniform flow of intensity U parallel to the x-axis. It is immediate that this vortex will be carried by the incoming flow with velocity $u = U$, but let us obtain this result making use of the formalism explained above.

The complex potential for this situation is

$$w(z, z_0) = Uz + \frac{\Gamma}{2\pi i} \log(z - z_0) \,. \tag{2.77}$$

Therefore, the effective potential is

$$\begin{aligned} w_{eff}(z, z_0) &= w(z, z_0) - \frac{\Gamma}{2\pi i} \log(z - z_0) \\ &= Uz \,, \end{aligned} \tag{2.78}$$

which is given only by the contribution of the incoming stream. The complex velocity is calculated using Eq. (2.76),

$$u - iv = U \quad \Longrightarrow \quad u = U \,, \quad v = 0 \,. \tag{2.79}$$

Let us move to an example slightly more complicated where a boundary is involved, which is the case of a vortex near a plane wall.

2.6.2.2 Vortex near a plane wall The complex potential for this system was obtained using the method of images and is given in Eq. (2.54), where the notation z_v was used instead of z_0. The corresponding effective potential is

$$\begin{aligned} w_{eff}(z, z_v) &= w(z, z_v) - \frac{\Gamma}{2\pi i} \log(z - z_v) \\ &= -\frac{\Gamma}{2\pi i} \log(z - \bar{z_v}) \,, \end{aligned} \tag{2.80}$$

Using Eq. (2.76) to calculate the vortex complex velocity, we have

$$\begin{aligned} u - iv &= \frac{d}{dz}\, w_{eff}(z, z_v)\bigg|_{z=z_v} \\ &= -\frac{\Gamma}{2\pi i} \frac{1}{z_v - \bar{z_v}} \,. \end{aligned} \tag{2.81}$$

Making $z_v = x + iy$, one obtains

$$u - iv = \frac{\Gamma}{4\pi y} \quad \Longrightarrow \quad u = \frac{\Gamma}{4\pi y} \,, \quad v = 0 \,. \tag{2.82}$$

Therefore, a vortex near a plane wall will move parallel to it, and its speed will decrease with the inverse of the distance y to the wall.

If we superimpose to this system a uniform stream coming from the right, with velocity $U = -\frac{\Gamma}{4\pi y}$ it would be possible to maintain this vortex configuration stationary: the velocity induced by the image vortex would be exactly canceled by the velocity of the incoming stream and the vortex wold not move. In the next chapter we will be interested in this situation when instead of a vortex near a plane, we have a pair of counter-rotating vortices near a cylinder placed in a uniform stream. But before going into that, let us analyze the dynamics of a single vortex placed near a cylinder (without the incoming stream).

2.6.2.3 Vortex near a circular cylinder The potential for a point vortex of intensity Γ at $z = z_0$, near a circular cylinder of radius a and centered at the origin, can be calculated by means of the Milne-Thomson Circle Theorem, discussed in Sec. 2.4.1. In this case the complex potential is

$$w(z, z_0) = \frac{\Gamma}{2\pi i} \log(z - z_0) + \overline{\frac{\Gamma}{2\pi i} \log\left(\frac{a^2}{\bar{z}} - z_0\right)} \,. \tag{2.83}$$

After some algebraic manipulation and ignoring constant additive terms, the complex potential (2.83) can be written as

$$w(z, z_0) = \frac{\Gamma}{2\pi i} \log\left[\frac{z(z - z_0)}{z - \frac{a^2}{\bar{z}_0}}\right] \,, \tag{2.84}$$

from which the effective potential can be easily calculated,

$$w_{eff}(z, z_0) = \frac{\Gamma}{2\pi i} \log \left(\frac{z}{z - \frac{a^2}{\bar{z}_0}} \right) . \tag{2.85}$$

The vortex velocity is calculated using Eq. (2.76), and after some algebraic manipulation we obtain that the velocity of the vortex at $z = z_0$ outside the cylinder is

$$u + iv = \frac{\Gamma}{2\pi} \frac{a^2}{|z_0|^2 \left(|z_0|^2 - a^2\right)} (-iz_0) . \tag{2.86}$$

From this expression we see that the velocity of the vortex is always perpendicular to the vortex position vector and has the same modulus for fixed distance $|z_0|$ to the center of the cylinder. Therefore, the vortex will rotate around the cylinder at constant speed, maintaining the same distance to the origin. If the vortex circulation is anti-clockwise ($\Gamma > 0$), the vortex rotates around the cylinder clockwise. Conversely, a vortex of negative circulation ($\Gamma < 0$) rotates around the cylinder in anti-clockwise direction. Also, the closer the vortex is to the cylinder, the faster it rotates.

2.6.3 Hamiltonian Dynamics

In 1876 Kirchhoff showed (Ref. [10]) that the motion of point vortices in an unbounded domain follows a Hamiltonian dynamics. Let there be a set of N vortices of intensity Γ_k located at $z_k = x_k + iy_k$, $k = 1, 2, \cdots, N$. Each one of the vortices moves with the velocity induced by the other vortices, as given by Eqs. (2.73) and (2.74). Kirchhoff showed that the equations of motion correspond to a Hamiltonian system of the form

$$\Gamma_k \frac{dx_k}{dt} = \frac{\partial H}{\partial y_k} , \quad \Gamma_k \frac{dy_k}{dt} = -\frac{\partial H}{\partial x_k}, \tag{2.87}$$

where $H(x_1, y_1, \cdots, x_N, y_N)$ is the Hamiltonian, also known as the Kirchhoff-Routh path function, given by the following expression:

$$H(x_1, y_1, \cdots, x_N, y_N) = -\frac{1}{4\pi} \sum_{j=1}^{N} \sum_{\substack{k=1 \\ k \neq j}}^{N} \Gamma_j \Gamma_k \log |z_j - z_k| \tag{2.88}$$

Furthermore, Lin showed (Ref. [11]) that when solid obstacles are present, the motion of vortices also follows a Hamiltonian dynamics, but this time the Hamiltonian is different from Eq. (2.88). Therefore, the dynamics of vortices can be analyzed either by defining an effective potential, as was done in the previous section, or by calculating the system Hamiltonian. In the following chapters we will make use of both approaches according to our convenience. The Hamiltonian approach is particularly useful when one wants to obtain the vortex trajectories in the case when only one vortex is involved. In this case, to calculate the vortex trajectory with initial conditions (x_0, y_0), one only needs to calculate the level set $H(x, y) = H(x_0, y_0)$, since the Hamiltonian is a constant of motion. We will be using this approach extensively in the next chapters.

Let us now obtain the Hamiltonians governing the motion of the three simple examples given in the previous section.

2.6.3.1 Vortex in a uniform flow The Hamiltonian yielding the velocity field in Eq. (2.79) is simply

$$H(x, y) = \Gamma U y \,, \tag{2.89}$$

where the subscript from the coordinate (x, y) was dropped, since only one vortex is involved. By applying Hamilton equations (2.87), and identifying (u, v) with $(\dot{x}, \dot{y})$, it is immediate to see that this Hamiltonian produces the desired velocity field. Also, the vortex trajectories can be calculated by taking the level sets $H(x, y) = const.$, yielding the lines $y = const.$, as expected.

2.6.3.2 Vortex near a plane wall The velocity field for this case is given by Eq. (2.82). The associate Hamiltonian is then

$$H(x, y) = \frac{\Gamma^2}{4\pi} \log y \,. \tag{2.90}$$

Once again, the vortex trajectories $H(x, y) = const.$ are the lines $y = const.$, meaning that the vortex will move parallel to the wall, as expected.

2.6.3.3 Vortex near a circular cylinder The velocity field is expressed in Eq. (2.86). Making $z_0 = x + iy$, this equation can be written as

$$u + iv = \frac{\Gamma y}{2\pi}\left(\frac{1}{x^2 + y^2 - a^2} - \frac{1}{x^2 + y^2}\right) + i\frac{\Gamma x}{2\pi}\left(\frac{1}{x^2 + y^2} - \frac{1}{x^2 + y^2 - a^2}\right) . \tag{2.91}$$

The Hamiltonian that yields this velocity field is

$$H(x, y) = \frac{\Gamma^2}{4\pi} \log\left(\frac{x^2 + y^2 - a^2}{x^2 + y^2}\right) . \tag{2.92}$$

It is easy to verify that the curves defined by $H(x, y) = const.$ are circles centered at the origin of radius $r > a$. A vortex near a cylinder then tends to rotate around the cylinder, as already anticipated.

We are now in position to apply the formalism just presented to analyze some vortex configurations of more practical interest. In the next chapter we study the so-called Föppl system, a pair of counter-rotating vortices formed behind a circular cylinder in a uniform stream.

CHAPTER 3

VORTEX DYNAMICS AROUND A CYLINDER: THE FÖPPL SYSTEM

In this chapter we analyze the dynamics of the pair of counter-rotating vortices formed downstream of a circular cylinder placed in a uniform flow. The treatment of this problem by means of a point-vortex model was first done by Ludwig Föppl in 1913, and the system became known as the Föppl pair of vortices. We will revisit Föppl's original solution and show several new features of this system. Part of the analysis present in Föppl's original paper was in error. Here we will make the appropriate corrections and present some extensions of the problem. Initially, we calculate the stationary configurations of the vortex pair and perform the linear stability analysis of these configurations. Some dynamical features that went previously unnoticed will be clarified, including the existence of a fixed point at infinity that plays a crucial role in the elucidation of the system's phase portrait. The Hamiltonian governing the vortex motion restricted to the symmetrical subspace is obtained and the nonlinear dynamics of the pair of vortices restricted to this subspace will be studied. This case corresponds to the situation in which the vortices move symmetrically with respect to the middle plane, a restriction that can be experimentally imposed by placing a splitter plate in that plane. We will also analyze the motion resulting from antisymmetrical perturbations of the stationary position, which is believed to be responsible for the instability that leads to vortex shedding, and ultimately gives rise to the so-called von Karman vortex street. The main results of this chapter can be found in our recent (2011) publication, Ref. [12], enclosed in this thesis in Appendix A.

3.1 STATEMENT OF THE PROBLEM

The formation of recirculating eddies in the wake of solid bodies placed in a stream is a rather common fluid dynamical event. It can be seen for example in the flow surrounding a bridge structure in a river, near the cables of an oil platform in the ocean, or even, in a much smaller scale, in the surroundings of a spoon that is used to stir an espresso coffee. In a laboratory this experiment can be done in a controlled environment by placing an obstacle, for example, a circular cylinder, in a uniform stream. The experiment can be performed in an open channel or in a Hele-Shaw cell, which is a device made by placing two glass plates together, leaving only a small gap between them where the fluid can flow in an "almost two-dimensional" domain. In this chapter we will study the pair of vortices formed downstream of a circular cylinder, which was shown in Fig. 1.6 in Chapter 1, and is reproduced here, in Fig. 3.1, for convenience.

The Reynolds number Re is a dimensionless parameter that measures the ratio of inertial to viscous forces in a given flow. It is given by the expression

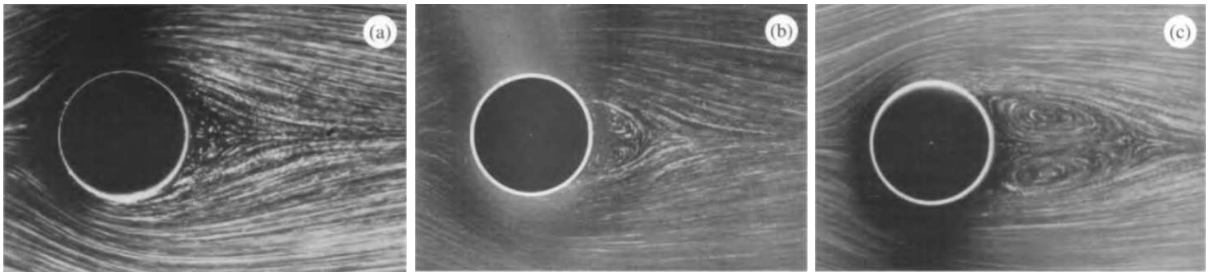

Figure 3.1 Pair of counter-rotating vortices formed downstream of a cylinder. The Reynolds number varies from left to right: a) $Re = 9.6$, b) $Re = 13.1$ and c) $Re = 26.0$ (figure from Ref. [2]).

$$Re = \frac{UL}{\nu} \tag{3.1}$$

where, U is a typical velocity, L is a typical length and ν is the kinematic viscosity of the fluid ($\nu = \mu/\rho$, where μ is the dynamic viscosity and ρ is the fluid density).

For the experiments shown in Fig. 3.1, the Reynolds number increases from left to right, as the speed of the incoming flow is increased. In a) $Re = 9.6$, b) $Re = 13.1$ and c) $Re = 26.0$. The pair of vortices formed downstream of the cylinder are observed in the range of $Re < 40$. If the Reynolds number is increased further, this pair of vortices becomes unstable and a new regime starts where vortices are alternately shed from both sides of the cylinder giving rise to the so-called von Karman vortex street, see Ref. [13]. This pattern occurs for Reynolds number in the range $40 < Re < 300$; see Fig. 1.7, which shows an experiment in which the Reynolds number is $Re = 140$. For $Re > 300$, the flow is turbulent and no vortical structure can be visually identified, although if one considers an average of the velocity field over time, a recirculating region in the near wake of the cylinder can still be found, see Ref. [14].

In this chapter, we focus our attention on a point vortex model introduced by Föppl in Ref. [15] to study the formation of stationary vortex configurations behind a cylinder. In this model the fluid is treated as inviscid and incompressible, and the vorticity is concentrated at isolated points, namely, at the positions of the vortices. In spite of these simplifications, the results obtained from this idealized model are in good qualitative agreement with experimental observations, as we will see later in this chapter. In the next section we start our analysis by defining the complex potential associated with the Föppl system.

3.2 THE COMPLEX POTENTIAL

Fig. 3.2 shows a diagram of the situation we want to treat. To define the complex potential in the presence of a circular cylinder, first we will find the complex potential without the cylinder (that we will call f) and then apply the circle theorem described in Sec. 2.4.1 to obtain the desired complex potential with the cylinder. The complex potential for a pair of counter-rotating vortices of intensities $\pm\Gamma$ located respectively at $z_1 = x_1 + iy_1$

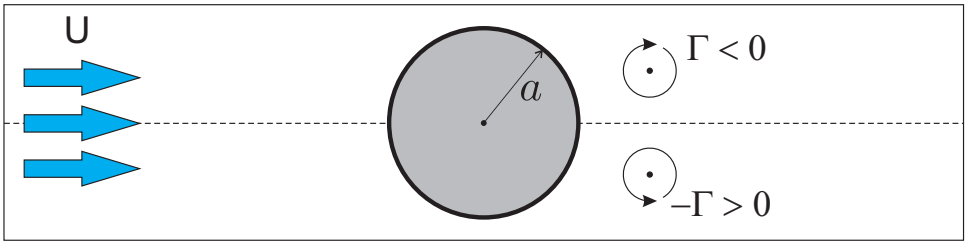

Figure 3.2 Diagram of the Föppl system. As can be seen from the experiments (Fig. 3.1), the upper (lower) vortex has negative (positive) circulation, as indicated in this diagram.

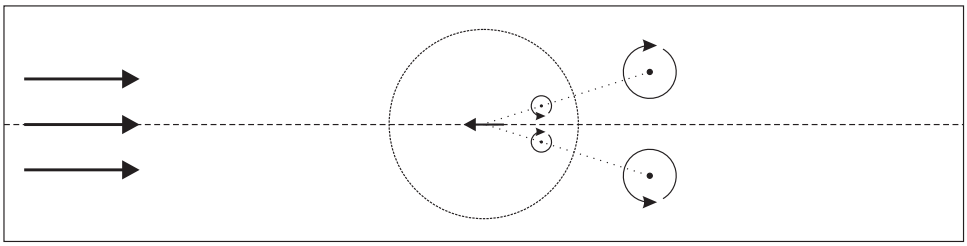

Figure 3.3 Diagram showing the images (inside the cylinder) for the Föppl system.

and $z_2 = x_2 + iy_2$ in an incident stream of intensify U is

$$f(z, z_1, z_2) = Uz + \frac{\Gamma}{2\pi i}\log(z - z_1) - \frac{\Gamma}{2\pi i}\log(z - z_2)\,. \tag{3.2}$$

Applying the circle theorem, we have,

$$w(z, z_1, z_2) = f\,(z, z_1, z_2) + \overline{f\left(\frac{a^2}{\bar{z}}, z_1, z_2\right)} \tag{3.3}$$

which, after some algebraic manipulation (including the neglect of some additive constants), yields

$$w(z, z_1, z_2) = U\left(z + \frac{a^2}{z}\right) + \frac{\Gamma}{2\pi i}\log\left(\frac{z - z_1}{z - \frac{a^2}{\bar{z}_1}}\right) - \frac{\Gamma}{2\pi i}\log\left(\frac{z - z_2}{z - \frac{a^2}{\bar{z}_2}}\right)\,. \tag{3.4}$$

The first two terms correspond to the incident stream and its image by the cylinder, a dipole at the origin, as explained before [see Eq. (2.59)]. The other two terms are the vortices at $z = z_1$ and $z = z_2$ (outside the cylinder) and their images at $z = a^2/\bar{z}_1$ and $z = a^2/\bar{z}_2$ (inside the cylinder), see Fig. 3.3.

It is convenient to introduce the dimensionless variables

$$z' = \frac{z}{a}, \quad t' = \frac{U}{a}t, \quad w' = \frac{w}{Ua}, \quad \kappa = -\frac{\Gamma}{2\pi Ua}\,, \tag{3.5}$$

where $\kappa > 0$ (see Fig. 3.2). With these new variables, the complex potential (3.4) reads

$$w(z,z_1,z_2) = z + \frac{1}{z} + i\kappa \log\left[\frac{(z-z_1)\left(z-\frac{1}{\bar{z}_2}\right)}{(z-z_2)\left(z-\frac{1}{\bar{z}_1}\right)}\right] , \tag{3.6}$$

where we have already dropped the prime notation, with the understanding that from now on the variables are dimensionless. We now define the effective potential acting on the vortex at $z = z_1$ by removing the term related to this vortex from Eq. (3.6):

$$w_{eff}(z,z_1,z_2) = z + \frac{1}{z} + i\kappa \log\left[\frac{\left(z-\frac{1}{\bar{z}_2}\right)}{(z-z_2)\left(z-\frac{1}{\bar{z}_1}\right)}\right] \tag{3.7}$$

Next we calculate the complex velocity of the vortex at $z = z_1$, by taking the derivative of the effective potential at the vortex position,

$$u_1 - iv_1 = \frac{d}{dz}\, w_{eff}(z,z_1,z_2)\Big|_{z=z_1} \tag{3.8}$$

$$u_1 - iv_1 = 1 - \frac{1}{z_1^2} - i\kappa\left(\frac{1}{z_1 - z_2} - \frac{\bar{z}_1}{1 - z_1\bar{z}_1} + \frac{\bar{z}_2}{1 - z_1\bar{z}_2}\right) . \tag{3.9}$$

Now, separating the real and imaginary parts of this equation we have,

$$u_1 = 1 - \frac{x_1^2 - y_1^2}{r_1^4} - \kappa\left[\frac{y_1 - y_2}{r_1^2 + r_2^2 - 2(x_1x_2 + y_1y_2)} + \frac{y_1}{r_1^2 - 1} - \frac{y_1 r_2^2 - y_2}{1 + r_1^2 r_2^2 - 2(x_1x_2 + y_1y_2)}\right] , \tag{3.10}$$

$$v_1 = -2\frac{x_1y_1}{r_1^4} + \kappa\left[\frac{x_1 - x_2}{r_1^2 + r_2^2 - 2(x_1x_2 + y_1y_2)} + \frac{x_1}{r_1^2 - 1} - \frac{x_1 r_2^2 - x_2}{1 + r_1^2 r_2^2 - 2(x_1x_2 + y_1y_2)}\right] , \tag{3.11}$$

where $r_i^2 = x_i^2 + y_i^2$. These are the equations governing the motion for the upper vortex. To obtain the equations for the lower vortex, a similar procedure can be taken, this time defining an effective potential acting on the vortex at $z = z_2$. But, from the symmetry of the system, we note that the equations for the lower vortex can be obtained by simply interchanging the indexes $1 \leftrightarrow 2$ and letting $\kappa \to -\kappa$ in Eqs. (3.10) and (3.11).

From the up-down symmetry of the problem (see Fig. 3.2), we find that a vortex configuration that is initially symmetrical with respect to the middle plane, will maintain this symmetry as time goes by. That is to say, if $x_1 = x_2$ and $y_1 = -y_2$ at $t = 0$, then $u_1 = u_2$, $v_1 = -v_2$ and therefore the system will evolve having $z_2(t) = \overline{z_1(t)}$ for any time $t > 0$. The up-down symmetry is thus preserved (or, saying it differently, the symmetric subspace is invariant under the dynamics).

The dynamics of the pair of counter-rotating vortices possesses another kind of symmetry, that we will call *conjugation symmetry*, which we now explain. Consider a pair of counter rotating vortices of intensities $\pm\Gamma$, with initial positions $z_{1,0}$ and $z_{2,0}$ respectively. The trajectories of the vortices are described by the functions $z_1(t; z_{1,0}, z_{2,0})$ and

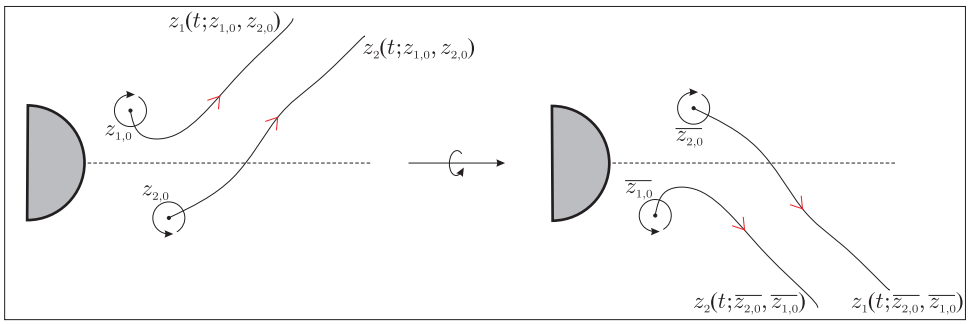

Figure 3.4 Diagram showing the physical origin of the vortex pair conjugation symmetry.

$z_2(t; z_{1,0}, z_{2,0})$. Let us suppose that the vortex trajectories are like the ones shown on the left side of Fig. 3.4. If we now rotate the system around the horizontal axis, the dynamics is of course symilar, and the trajectories are as shown on the right side of the figure. One can think that such a rotation may correspond simply to a change in the position of the observer in the laboratory. But the trajectories on the right, corresponds to the motion resulting from the initial conditions $\overline{z_{2,0}}$ and $\overline{z_{1,0}}$, for the vortices of intensity $\pm\Gamma$, respectively. Therefore, if we know the trajectory resulting from the pair of initial conditions $(z_{1,0}, z_{2,0})$, we automatically know the trajectory associated with the *conjugate* pair of initial conditions $(\overline{z_{2,0}}, \overline{z_{1,0}})$. Mathematically, this symmetry reads

$$z_1(t; \overline{z_{2,0}}, \overline{z_{1,0}}) = \overline{z_2(t; z_{1,0}, z_{2,0})}\,, \tag{3.12}$$

$$z_2(t; \overline{z_{2,0}}, \overline{z_{1,0}}) = \overline{z_1(t; z_{1,0}, z_{2,0})}\,. \tag{3.13}$$

A stationary configuration, or equilibrium position, of the dynamical system given in Eqs. (3.10) and (3.11) is obtained by making $u = 0$ and $v = 0$ for both vortices. It is reasonable to guess that such a configuration (if it exists at all) is symmetrical with respect to the middle plane. With this in mind, let us first calculate the vortex velocity subject to the symmetry condition $x_1 = x_2$ and $y_1 = -y_2$. Substituting this condition into Eqs. (3.10) and (3.11) for the motion of the upper vortex, we have

$$u = 1 - \frac{x^2 - y^2}{r^4} + \kappa y \left[\frac{r^2 + 1}{(r^2 - 1)^2 + 4y^2} - \frac{1}{r^2 - 1} - \frac{1}{2y^2} \right], \tag{3.14}$$

$$v = -2\frac{xy}{r^4} - \kappa x \left[\frac{r^2 - 1}{(r^2 - 1)^2 + 4y^2} - \frac{1}{r^2 - 1} \right], \tag{3.15}$$

where the subscripts have been dropped. Since we are considering now the symmetrical case, once the motion of the upper vortex is known, the motion of the lower one is obtained by simply considering it as the "mirror image" of the upper vortex.

To analyze the stationary configuration, we must solve Eqs. (3.14) and (3.15) for $u = v = 0$. This will be done in the next section.

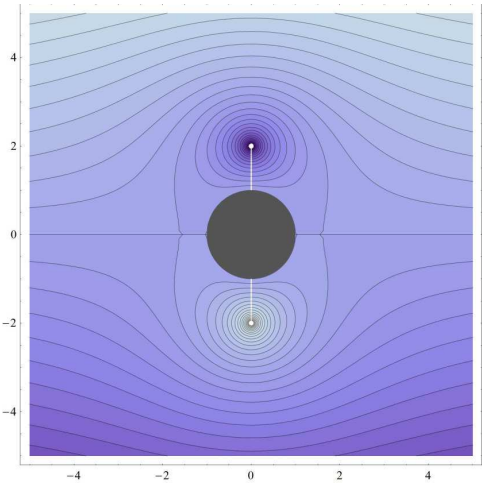

Figure 3.5 Streamline pattern of a vortex pair on the normal line. The incoming flow is $U = 1$ and the vortices are located at the points $(0, \pm 2)$. The dimensionless vortex intensity is $\kappa = 75/31$

3.3 STATIONARY CONFIGURATIONS

Three types of equilibria have been found for this system: equilibrium on the normal line, the Föppl equilibrium and equilibrium at infinity.

3.3.1 Equilibrium on the normal line

By inspection of Eq. (3.15), one immediately sees that $v = 0$ if the vortex is located at the normal line $x = 0$. It is still necessary to satisfy the condition $u = 0$ to have an equilibrium position. Making $x = 0$ and $y = b$ ($b > 1$, since the vortex is outside the cylinder) in Eq. (3.14), and solving it for $u = 0$, we have,

$$0 = 1 + \frac{b^2}{b^4} + \kappa b \left[\frac{b^2 + 1}{(b^2 - 1)^2 + 4b^2} - \frac{1}{b^2 - 1} - \frac{1}{2b^2} \right] . \tag{3.16}$$

Solving for κ in this equation, yields

$$\kappa = \frac{2(b^2 + 1)(b^4 - 1)}{b(b^4 + 4b^2 - 1)} . \tag{3.17}$$

Therefore, any point of the form $(0, b)$ with $b > 1$ can sustain a stationary vortex configuration with the condition that the dimensionless vortex intensity κ is given by Eq. (3.17). Fig. 3.5 shows the streamline pattern for a pair of vortices located at the points $(0, \pm 2)$. Fig. 3.6 shows the stationary positions curve (simply the normal line $x = 0$) and a plot of κ as a function of b.

Although this stationary configuration on the normal line does not appear on the experiments, the existence of this fixed point plays an important role in the understanding of the phase portrait of this system, as we will see later.

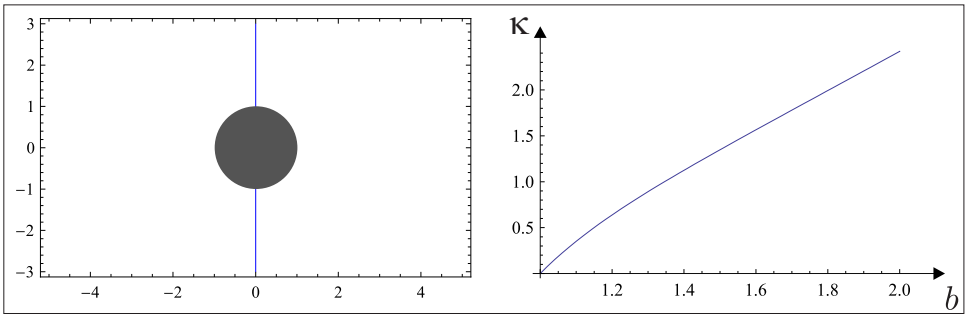

Figure 3.6 (left) Stationary positions on the normal line $x = 0$. (right) Plot of the dimensionless vortex intensity κ as a function of the position $y = b > 1$ on the normal line.

3.3.2 Föppl equilibrium

This is the equilibrium related to the experimental observations shown in Fig. 3.1, i.e., the pair of vortices downstream of the cylinder. If $x \neq 0$, the condition $v = 0$ is not immediately satisfied and we will have to work with both Eq. (3.14) and Eq. (3.15) in order to find a stationary condition (for which $u = v = 0$). Making $x^2 = r^2 - y^2$ on Eq. (3.14), we have, after some simplification,

$$u = 1 - \frac{r^2 - 2y^2}{r^4} - \kappa \frac{(r^2-1)^3 + 8y^4}{2y(r^2-1)\left[(r^2-1)^2 + 4y^2\right]} \,. \tag{3.18}$$

The condition $u = 0$ then gives

$$\frac{r^2(r^2-1) + 2y^2}{r^4} = \kappa \frac{(r^2-1)^3 + 8y^4}{2y(r^2-1)[(r^2-1)^2 + 4y^2]} \,. \tag{3.19}$$

Similarly, after some simplification, Eq. (3.15) reads

$$v = -2\frac{xy}{r^4} + \kappa \frac{4xy^2}{(r^2-1)\left[(r^2-1)^2 + 4y^2\right]} \,, \tag{3.20}$$

and the condition $v = 0$, implies

$$\frac{1}{r^4} = \kappa \frac{2y}{(r^2-1)\left[(r^2-1)^2 + 4y^2\right]} \,. \tag{3.21}$$

Now, solving for κ in Eq. (3.21) and substituting the result into Eq. (3.19), we obtain after some algebra:

$$r^2 - 1 = \pm 2ry \,. \tag{3.22}$$

This expression defines a curve, the so-called Föppl curve, which corresponds to the positions where a stationary vortex configuration can be found. Substituting y from Eq. (3.22) into Eq. (3.21) and solving for κ, we obtain

$$\kappa = \frac{(r^2-1)(r^4-1)}{r^5} \tag{3.23}$$

Fig. 3.7 shows the streamline pattern of a Föppl pair located at a distance $r = 2$ to the origin. Fig. 3.8 shows the Föppl curve (left) and a three-dimensional plot of the vortex intensity κ for points on that curve (right). Since κ is a function of the vortex distance r only, we could visualize it by making a simple two-dimensional plot, but we find it helpful here to introduce this kind of three-dimensional plot because plots like this are going to appear again later in this thesis, in situations where a simple two-dimensional plot is not very suitable. In Fig. 3.9 we show a visual comparison between an experiment and a streamline pattern produced using the point vortex approximation to the flow.

We observe that the x dependence on the Föppl curve, Eq. (3.22), is only by means of the term $r = \sqrt{x^2 + y^2}$ and, therefore, we can have stationary positions both for $x > 0$ (downstream of the cylinder) and for $x < 0$ (upstream of the cylinder). Nevertheless, because of the mechanisms involved in the creation of vorticity in a flow around an obstacle, only the configuration downstream of the cylinder appears in the experiments. A case in which a vortex configuration upstream of the cylinder is observed will be treated in Chapter 5. There, in addition to the cylinder, there will be also a secondary boundary, a plane wall, placed below the cylinder.

3.3.3 Equilibrium at infinity

Very far from the origin, the "perturbation" induced by the cylinder in the uniform flow is negligible and the situation is like if there were only a pair of counter rotating vortices in a uniform stream. This situation is identical to the case treated in Sec. 2.6.2, concerning the motion of a vortex near a plane wall. As we saw there, an equilibrium configuration can be achieved if the incoming stream has velocity $U = -\frac{\Gamma}{4\pi y}$, or, saying it differently, the configuration is stationary if the distance y from the vortex to the middle plane is $y = -\frac{\Gamma}{4\pi U}$. In terms of the dimensionless variables, this means that the equilibrium positions are

$$x = \pm\infty\,, \quad y = \frac{\kappa}{2}\,. \tag{3.24}$$

Plugging these values for x and y into Eqs. (3.14) and (3.15) one can easily verify that this is indeed a stationary configuration. As far as we know, this equilibrium point at infinity was not noted before. This equilibrium position, together with the equilibrium position on the normal line, plays a very important role in the characterization of the nonlinear dynamics of the vortex pair in the particular case in which the vortex trajectories are symmetrical with respect to the middle plane, as we will see later in this chapter.

Now that we have calculated the stationary configurations associated with this system, let us move on to the analysis of the stability of these configurations under small displacements.

3.4 LINEAR STABILITY ANALYSIS

In this section we will perform the linear stability analysis of the stationary configurations studied, under symmetrical and antisymmetrical perturbations. First of all, let us clarify what we mean by these two types of perturbations.

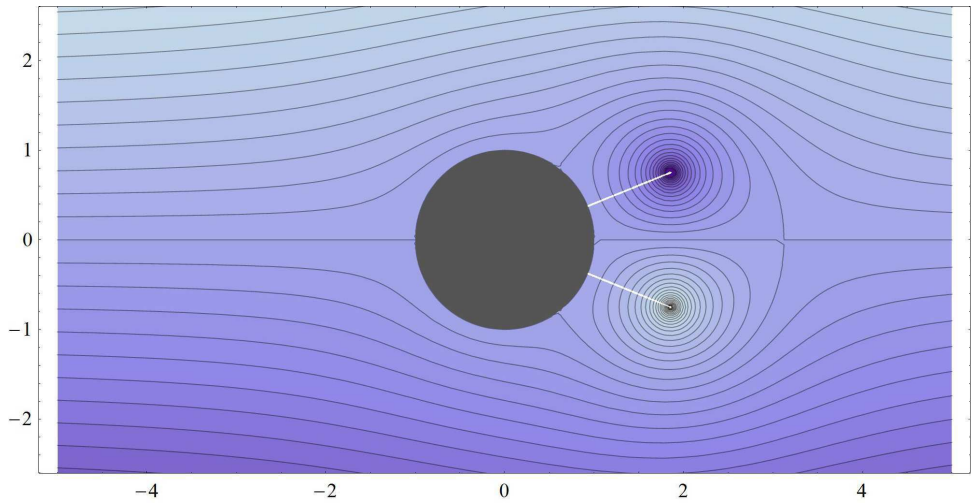

Figure 3.7 Streamline pattern of a Föppl pair. The incoming flow is $U = 1$ and the vortices are located at a distance $r = 2$ to the origin. The dimensionless vortex intensity is $\kappa = 45/32$.

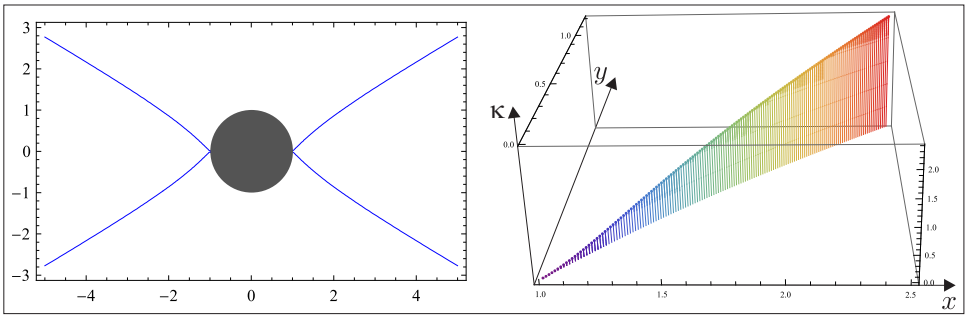

Figure 3.8 (left) Föppl curve for stationary vortex configurations. (right) Three-dimensional plot of the dimensionless vortex intensity κ as a function of the position for points on the Föppl curve.

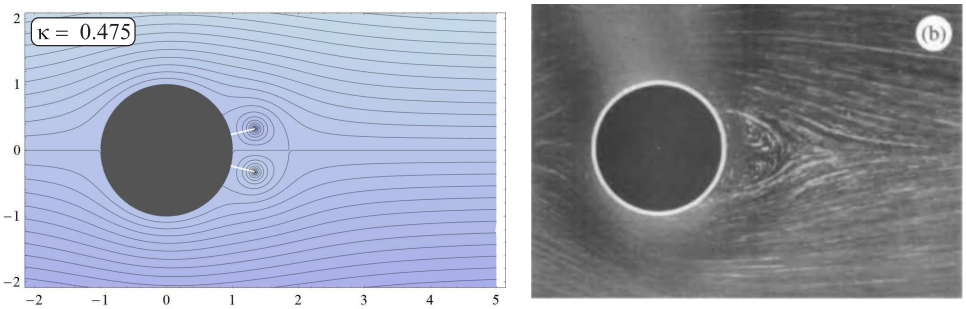

Figure 3.9 Comparison between the experimental measurement obtained for the Reynolds number $Re = 13.1$ and a streamline pattern produced with the point vortex approximation to the flow.

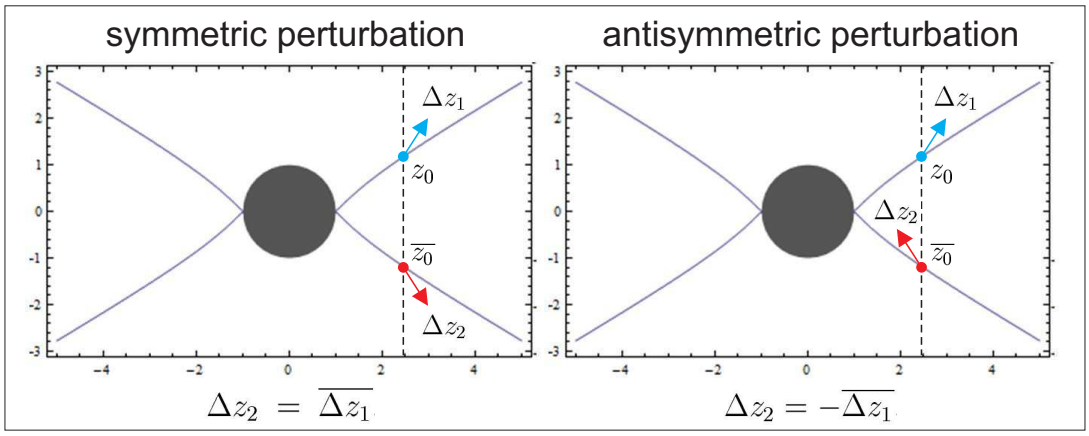

Figure 3.10 Scheme for the symmetrical (left) and antisymmetrical (right) perturbations, shown exaggerated in the figure. The blue and red dots on the Föppl curve are the stationary positions z_0 and $\bar{z}_0$.

Let z_0 and $\bar{z}_0$ be, respectively, the stationary positions for the upper and lower vortices. Let $\Delta z_1 = \xi_1 + i\eta_1$ and $\Delta z_2 = \xi_2 + i\eta_2$ be the (small) perturbations from the equilibrium position. If $\Delta z_2 = \overline{\Delta z_1}$ the perturbation is said to be symmetric. If, otherwise, $\Delta z_2 = -\overline{\Delta z_1}$, then the perturbation is called antisymmetric. Fig. 3.10 exemplifies these two types of perturbations.

Since a generic perturbation can always be written in terms of a symmetric and an antisymmetric components, it suffices to consider these two types of perturbations separately

3.4.1 Stability under symmetrical perturbations

To study the stability of vortex configurations in the symmetric subspace we will make use of Eqs. (3.14) and (3.15) for the motion of the upper vortex. Let $z_0 = x_0 + iy_0$ denote a stationary position. The velocity (u, v) at a position $z_0 + \Delta z$, where $\Delta z = \xi + i\eta$ is a small perturbation, can be obtained by a linearization of the velocity field around the stationary position,

$$u(x_0 + \xi, y_0 + \eta) = u(x_0, y_0) + \left.\frac{\partial u}{\partial x}\right|_0 \xi + \left.\frac{\partial u}{\partial y}\right|_0 \eta \tag{3.25}$$

$$v(x_0 + \xi, y_0 + \eta) = v(x_0, y_0) + \left.\frac{\partial v}{\partial x}\right|_0 \xi + \left.\frac{\partial v}{\partial y}\right|_0 \eta\,, \tag{3.26}$$

where the subscript 0 means that the derivatives must be evaluated at the stationary position (x_0, y_0). Since $u(x_0, y_0) = v(x_0, y_0) = 0$ it is useful to write this pair of equations in matricial form. Identifying (u, v) with $(\dot{\xi}, \dot{\eta})$, we have

$$\begin{pmatrix} \dot{\xi} \\ \dot{\eta} \end{pmatrix} = A \begin{pmatrix} \xi \\ \eta \end{pmatrix}\,, \tag{3.27}$$

where the matrix A reads

$$A = \begin{pmatrix} A_{11} & A_{12} \\ A_{21} & A_{22} \end{pmatrix} = \left. \begin{pmatrix} \frac{\partial u}{\partial x} & \frac{\partial u}{\partial y} \\ \frac{\partial v}{\partial x} & \frac{\partial v}{\partial y} \end{pmatrix} \right|_0 . \tag{3.28}$$

Note that, since the motion of vortices follows a Hamiltonian dynamics, the trace of the matrix A always vanishes because

$$A_{11} = \frac{\partial u}{\partial x} = \frac{\partial}{\partial x}\frac{1}{\Gamma}\frac{\partial H}{\partial y} = \frac{\partial}{\partial y}\frac{1}{\Gamma}\frac{\partial H}{\partial x} = -\frac{\partial v}{\partial y} = -A_{22} . \tag{3.29}$$

This is also expected from Liouville theorem: in a Hamiltonian system a finite element of volume in the phase space is always preserved by the dynamics. We will now perform the linear stability analysis under symmetric perturbations of the three types of equilibria calculated in the previous section.

3.4.1.1 Equilibrium on the normal line The elements of the matrix A for points of the form $(x_0, y_0) = (0, b)$, are given by

$$A_{11} = -A_{22} = 0 , \tag{3.30}$$

$$A_{12} = \frac{b^8 + 10b^6 - 8b^4 + 14b^2 - 1}{b^3(b^2-1)(b^4+4b^2-1)} , \tag{3.31}$$

$$A_{21} = \frac{2(b^2-1)(3b^2-1)}{b^3(b^4+4b^2-1)} . \tag{3.32}$$

The eigenvalues λ of this matrix are

$$\lambda^2 = \frac{2\,(3b^2-1)\,(b^8+10b^6-8b^4+14b^2-1)}{b^6(b^4+4b^2-1)^2} > 0 , \tag{3.33}$$

for $b > 1$. This matrix then yields a pair of real eigenvalues with opposite signs $\lambda_\pm = \pm\sqrt{\lambda^2}$. Therefore this fixed point is a *saddle*, having a stable and an unstable direction. It is easy to verify that the eigenvectors $\vec{w}_\pm$ associated with the eigenvalues $\lambda_\pm$ are respectively,

$$\vec{w}_\pm = \begin{pmatrix} \pm\sqrt{A_{12}/A_{21}} \\ 1 \end{pmatrix} . \tag{3.34}$$

Fig. 3.11 shows an example of motion resulting from a symmetrical perturbation of the pair of vortices at stationary positions $(0, \pm 2)$. To generate this figure, we numerically integrated the equations of motion given in Eqs. (3.14) and (3.15), after making $\dot{x} = u$ and $\dot{y} = v$. To integrate this system of ODEs, we used the NDSolve routine of *Mathematica*. According to the *Mathematica* documentation, "for ordinary differential equations, NDSolve by default uses an LSODA approach, switching between a non-stiff Adams method and a stiff Gear backward differentiation formula method", see Refs. [16] and [17] for additional information concerning these methods. This procedure was used to perform all integrations of ODEs in this thesis.

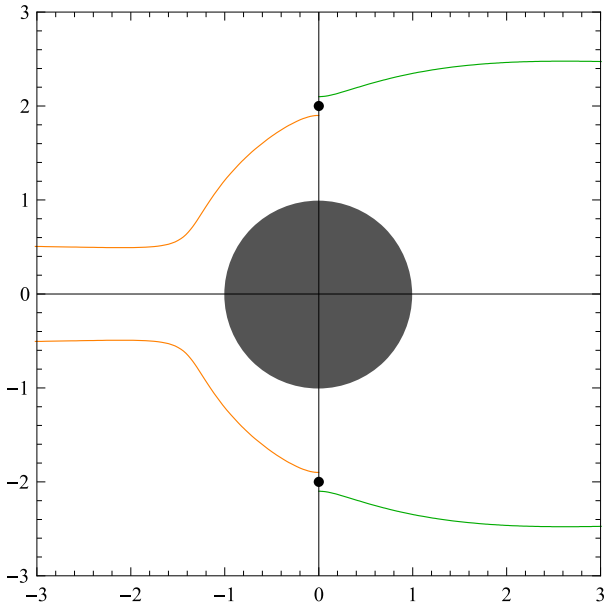

Figure 3.11 Motion of the vortex pair symmetrically displaced from the equilibrium position on the normal curve. The trajectories are obtained by the numerical integration of Eqs. (3.14) and (3.15). The stationary positions are $(0, \pm 2)$ and the dimensionless vortex intensity is $\kappa = 75/31$. The green curves are the trajectories resulting from a displacement $\Delta z = i0.1$ and the orange curves are for $\Delta z = -i0.1$.

3.4.1.2 Föppl equilibrium We compute now the elements of the matrix A for points (x_0, y_0) on the Föppl curve, Eq. (3.22). After taking the appropriate derivatives, see Eq. (3.28), one obtains the following matrix elements:

$$A_{11} = -A_{22} = -\frac{x_0(r_0^4 - 3r_0^2 + 2)}{r_0^8}\,, \tag{3.35}$$

$$A_{12} = \frac{4r_0^8 + 5r_0^6 + 2r_0^4 - 5r_0^2 + 2}{2r_0^9}\,, \tag{3.36}$$

$$A_{21} = -\frac{2x_0^2(r_0^4 + r_0^2 + 2)}{r_0^7(r_0^2 + 1)}\,. \tag{3.37}$$

The eigenvalues λ of this matrix are

$$\lambda^2 = -\frac{3r_0^6 + 5r_0^4 + 13r_0^2 - 5}{r_0^{10}} < 0\,. \tag{3.38}$$

The eigenvalues are then a pair of conjugate purely imaginary numbers, which means that the Föppl equilibrium is a center. Therefore, if the vortex pair is displaced symmetrically from the equilibrium position downstream of the cylinder, the vortices continuously rotate around the respective equilibrium positions. The upper (lower) vortex rotates clockwisely (anticlockwisely), see Fig. 3.12. This result is at variance with the one obtained by Föppl himself in his 1913 paper (Ref. [15]), where he mistakenly found that the eigenvalues were

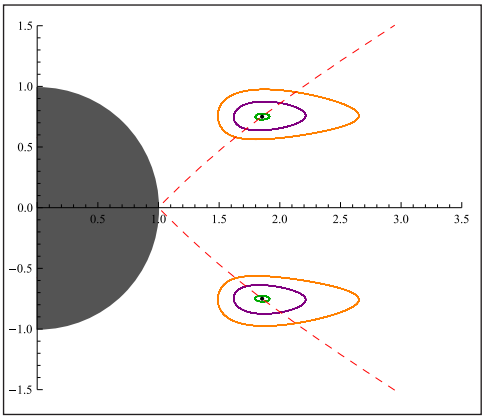

Figure 3.12 Motion of the vortex pair symmetrically displaced from the equilibrium position (black dot on the Föppl curve). The trajectories are obtained by the numerical integration of Eqs. (3.14) and (3.15). The equilibrium position is at the distance $r = 2$ to the origin. The vortex dimensionless intensity is $\kappa = 45/32$. The trajectories are the orange, purple and green curves respectively, for three separate perturbations. The closer the vortex is to the stationary position, the faster it rotates.

a pair of conjugate complex numbers having a negative real part, which would correspond to a stable focus. Such a fixed point, of course, could not occur in a 2D Hamiltonian system, because in such a system, the sum of the two eigenvalues must vanish. (A focus in the phase portrait would act as a "sink of phase portrait volume", which is not allowed by Liouville theorem.) In other words, in a 2D Hamiltonian system, only centers and saddles are possible. Therefore, in the light of the Liouville's theorem, the Hamiltonian approach allows a fast identification of Föppl's mistake.

3.4.1.3 Equilibrium at infinity To linearize the equations of motion around the fixed point at $x = \infty$, $y = \frac{\kappa}{2}$, we introduce the following perturbations:

$$\xi = x_c - x\,, \quad x_c = \infty\,, \tag{3.39}$$

$$\eta = y - y_c\,, \quad y_c = \frac{\kappa}{2}\,. \tag{3.40}$$

The elements of the linearized matrix A for the point at infinity are given by

$$A_{11} = -A_{22} = 0\,, \tag{3.41}$$

$$A_{12} = -\frac{2}{\kappa}\,, \tag{3.42}$$

$$A_{21} = 0\,, \tag{3.43}$$

as can be easily checked. The matrix A is then of the form

$$A = -\frac{2}{\kappa}\begin{pmatrix} 0 & 1 \\ 0 & 0 \end{pmatrix}\,. \tag{3.44}$$

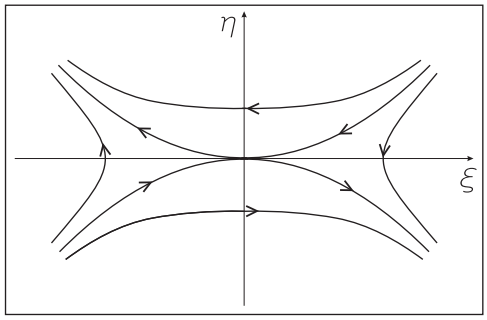

Figure 3.13 Typical trajectories near a generic nilpotent saddle point.

In this case, A is a nilpotent matrix of degree 2, which means that A^2 is the zero matrix. It has, therefore, zero eigenvalues and to study the dynamics around the fixed point at infinity, one has to analyze the contributions of the nonlinear terms in the expansion of the velocity around this equilibrium position. In the limit $(x, y) \to (\infty, \frac{\kappa}{2})$, the first relevant term for the y component of the velocity is

$$\dot{y} = -\frac{\kappa}{x^3} \tag{3.45}$$

From the theory of ordinary differential equations (Ref. [18]), it follows that the fixed point at infinity is a *degenerate or nilpotent saddle*, for which the two eigenvectors are the same. Fig. 3.13 shows an example of the trajectories near a generic nilpotent saddle. Physically, the vortex motion around the nilpotent fixed point is as follows: if the vortex is placed very far downstream ($|x| \gg 1$) and above the line $y = \kappa/2$, the vortex moves downstream, thus approaching the fixed point at infinity. Conversely, if it is released below the line $y = \kappa/2$, it will move in the other direction, against the flow, towards the cylinder. A similar analysis can be done for the case in which the vortex is placed very far upstream of the cylinder. In this case, if the vortex is placed above the line $y = \kappa/2$, it moves towards the cylinder and if it is below it, the motion will be to the left, against the incoming flow.

Let us move on now to the second part of this instability analysis that concerns the motion resulting from antisymmetric perturbations of the equilibrium positions.

3.4.2 Stability under antisymmetrical perturbations

To study antisymmetrical perturbations, we can no longer make use of Eqs. (3.14) and (3.15) to calculate the vortex velocity, since these equations already include the fact that the vortices move symmetrically with respect to the middle plane. We must, therefore, use the full set of Eqs. (3.10) and (3.11) for the velocities (u_1, v_1) and (u_2, v_2) of the upper and lower vortices, respectively. Nevertheless, since the antisymmetric subspace is also invariant under the linear dynamics (although not under the general nonlinear dynamics), we can proceed with the linear stability analysis focusing only on the upper vortex.

Let $u_i(x_1, x_2, y_1, y_2)$ and $v_i(x_1, x_2, y_1, y_2)$ denote respectively the horizontal and vertical components of the velocity of the vortex i, $i = 1, 2$. Let once again $z_0 = x_0 + iy_0$ and

$\bar{z}_0 = x_0 - iy_0$ denote the stationary positions of the upper and lower vortex. Since the perturbation is antisymmetric, the vortex positions after the perturbation will be $z_1 = z_0 + \Delta z$ and $z_2 = \bar{z}_0 - \overline{\Delta z}$, where $\Delta z = \xi + i\eta$. Recalling that $u = v = 0$ at the stationary positions, the linearization of the velocity field near this equilibrium is

$$u_1(x_0+\xi, x_0+\xi, y_0+\eta, y_0-\eta) = \left[\frac{du_1}{dx_1} + \frac{du_1}{dx_2}\right]_0 \xi + \left[\frac{du_1}{dy_1} - \frac{du_1}{dy_2}\right]_0 \eta \quad (3.46)$$

$$v_1(x_0+\xi, x_0+\xi, y_0+\eta, y_0-\eta) = \left[\frac{dv_1}{dx_1} + \frac{dv_1}{dx_2}\right]_0 \xi + \left[\frac{dv_1}{dy_1} - \frac{dv_1}{dy_2}\right]_0 \eta\,, \quad (3.47)$$

where the subscript 0 means that the derivatives must be evaluated at the stationary position $(x_0, x_0, y_0, -y_0)$. Writing these equations in matricial form, we have

$$\begin{pmatrix} \dot{\xi} \\ \dot{\eta} \end{pmatrix} = B \begin{pmatrix} \xi \\ \eta \end{pmatrix}\,, \quad (3.48)$$

where

$$B = \begin{pmatrix} B_{11} & B_{12} \\ B_{21} & B_{22} \end{pmatrix} = \left.\begin{pmatrix} \frac{du_1}{dx_1} + \frac{du_1}{dx_2} & \frac{du_1}{dy_1} - \frac{du_1}{dy_2} \\ \frac{dv_1}{dx_1} + \frac{dv_1}{dx_2} & \frac{dv_1}{dy_1} - \frac{dv_1}{dy_2} \end{pmatrix}\right|_0 . \quad (3.49)$$

We will now analyze the equilibrium properties under antisymmetric perturbation for the stationary positions on the normal line and on the Föppl curve.

3.4.2.1 Equilibria on the normal line The elements of the matrix B for the equilibrium on the normal line $(x_0, y_0) = (0, b)$, are

$$B_{11} = B_{22} = 0\,, \quad (3.50)$$

$$B_{12} = \frac{2\,(3b^6 + b^4 + 5b^2 - 1)}{b^3(b^2-1)\,(b^4 + 4b^2 - 1)}\,, \quad (3.51)$$

$$B_{21} = \frac{b^2 - 1}{b^3}\,. \quad (3.52)$$

The eigenvalues, λ, of this matrix are given by

$$\lambda^2 = \frac{2\,(3b^6 + b^4 + 5b^2 - 1)}{b^6\,(b^4 + 4b^2 - 1)} > 0\,. \quad (3.53)$$

The eigenvalues are a pair of real numbers with opposite signs, $\lambda_\pm = \pm\sqrt{\lambda^2}$. Therefore, as in the case of symmetric perturbations, the equilibrium position on the normal line is also a saddle point with respect to antisymmetric perturbations. The eigenvectors are respectively

$$\vec{w}_\pm = \begin{pmatrix} \pm\sqrt{B_{12}/B_{21}} \\ 1 \end{pmatrix}\,. \quad (3.54)$$

Fig. 3.14 shows an example of motion resulting from an antisymmetrical perturbation of the pair of vortices at stationary positions $(0, \pm 2)$. To obtain this trajectory, we integrated the full set of equations of motion for u_1, v_1, u_2, v_2, since the antisymmetry between the upper and lower vortices is broken in the nonlinear regime.

3.4.2.2 Föppl equilibrium Now let us compute the elements of the matrix B for points (x_0, y_0) on the Föppl curve, Eq. (3.22). In this case, one obtains

$$B_{11} = -B_{22} = \frac{x_0\,(r_0^4 + 3r_0^2 - 2)}{r_0^8}\,, \tag{3.55}$$

$$B_{12} = \frac{3r_0^6 - 5r_0^2 + 2}{2r_0^9}\,, \tag{3.56}$$

$$B_{21} = \frac{4r_0^8 + 3r_0^6 - 4r_0^4 - 5r_0^2 + 2}{2r_0^9}\,. \tag{3.57}$$

Computing the eigenvalues of this matrix, we obtain

$$\lambda^2 = \frac{3r_0^6 + 3r_0^4 - 3r_0^2 + 1}{r_0^{10}} > 0\,. \tag{3.58}$$

Differently from the symmetric case, the eigenvalues of the Föppl equilibrium for an antisymmetric perturbation are a pair of real numbers with opposite signs, $\lambda_\pm = \pm\sqrt{\lambda^2}$. The fixed point is, thus, a saddle. Eq. (3.58) is also at variance with the results obtained by Föppl in Ref. [15]. Although Föppl obtained a pair of real eigenvalues for this case, his original expressions are in error. In fact, upon comparison of our matrix B above with the equivalent expressions given in Eq. (17) of Ref. [15], we identified an error in Föppl's formula for the matrix element X', which in our notation corresponds to B_{21}. To allow a more direct comparison between Föppl's formulae and our expressions, let us mention that in Eq. (17) of Ref. [15] the symbols ξ and η correspond, in our notation, to the coordinates x_0 and y_0 of the fixed point. One can then verify that there is an extra factor of η in the last term of Föppl's expression for the matrix element X'.

The eigenvectors associated with the saddle point are respectively given by

$$\vec{w}_\pm = \begin{pmatrix} (\lambda_\pm + B_{11})/B_{21} \\ 1 \end{pmatrix}\,. \tag{3.59}$$

Fig. 3.15 shows an example of trajectory resulting from an antisymmetric perturbation of the stationary position on the Föppl curve. On the left side, both vortices are displaced by an amount $\Delta z = 0.045i$ from the equilibrium position, and on the right side, $\Delta z = -0.045i$. Analyzing the trajectory on the left, we see that the upper vortex moves downstream all the time, while the lower vortex initially moves upstream, until a moment when it turns, and then goes downstream. The situation is interchanged on the right side, the lower vortex goes downstream while the upper one initially goes upstream. We notice that the trajectory on the right is a reflection of the one on the left. This is expected, because of the conjugation symmetry of this system, since the initial conditions

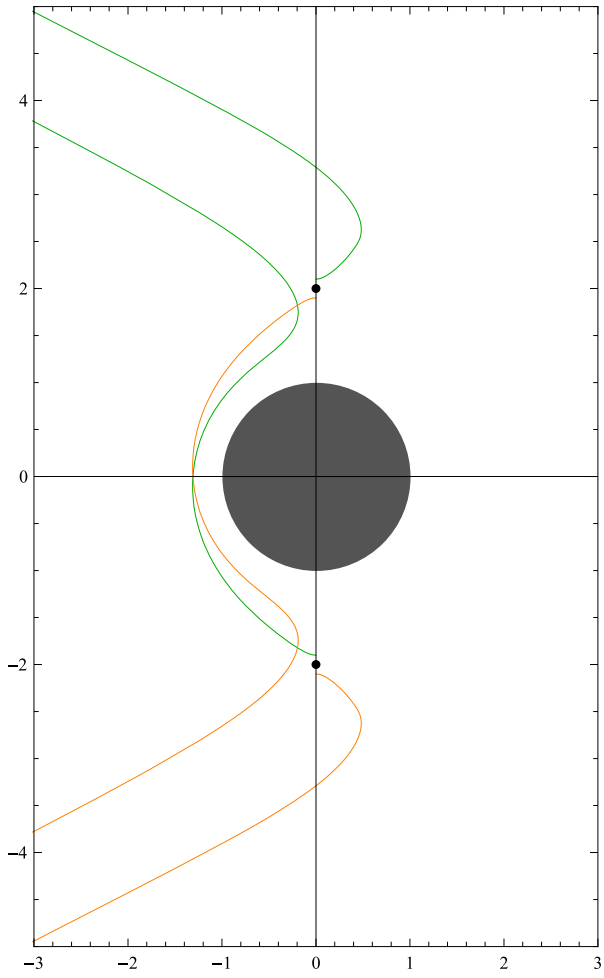

Figure 3.14 Motion of the vortex pair antisymmetrically displaced from the equilibrium position on the normal curve. The trajectories are obtained by the numerical integration of Eqs. (3.10) and (3.11) and their respective counterparts for the lower vortex. The stationary positions are $(0, \pm 2)$ and the dimensionless vortex intensity is $\kappa = 75/31$. The green curves are the trajectories resulting from a displacement $\Delta z = i0.1$ and the orange curves are for $\Delta z = -i0.1$.

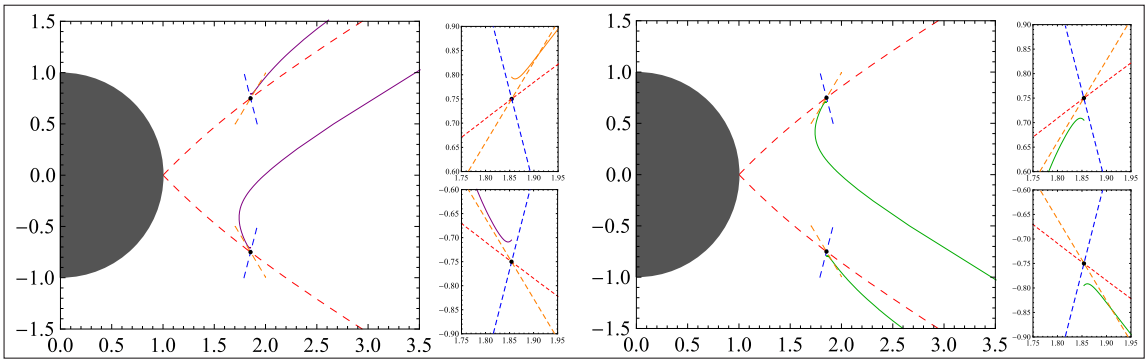

Figure 3.15 Motion of the vortex pair antisymmetrically displaced from the equilibrium position (black dot on the Föppl curve). The trajectories are obtained by the numerical integration of Eqs. (3.10) and (3.11) and their respective counterparts for the lower vortex. The equilibrium position is at the distance $r = 2$ to the origin. The vortex dimensionless intensity is $\kappa = 45/32$. On the detail we show a zoom in the region around the upper and lower stationary position. The orange and blue dashed lines are, respectively, the unstable and stable directions.

for the vortices on the right are conjugated (in the sense explained in Sec. 3.2) to the initial conditions for the vortices on the left. Notice also that far from the cylinder the vortex trajectories become parallel, with one of the vortices (the upper one in the left panel, lower one in the right panel) moving a little bit ahead of the other.

If a generic perturbation is given to a Föppl pair, it can be decomposed into a symmetric and an antisymmetric component. The symmetric component tend to rotate around the fixed point (a center for symmetric perturbations) while the antisymmetric component will eventually move away from the fixed point (a saddle for antisymmetric perturbations). For larger times, the antisymmetric component associated with the positive eigenvalue dominates the dynamics and the vortices will move away from the equilibrium position, see Fig. 3.16.

We will now analyze the Hamiltonian dynamics of the pair of vortices in the symmetrical subspace, in which the vortices move symmetrically with respect to the middle plane. As mentioned previously in this chapter, this situation can be achieved experimentally by placing a splitter plate in the middle of the flow and considering the motion of the upper vortex only. Finally, we will produce the phase portrait of this system and verify many of the characteristics already anticipated regarding the stability properties of the fixed points.

3.5 HAMILTONIAN DYNAMICS

As discussed previously in Chapter 2, the motion of point vortices in the vicinity of solid obstacles follows a Hamiltonian dynamics. In the present case, we are considering the motion of a pair of point vortices in the vicinity of a circular cylinder in a uniform flow. When restricted to the symmetric subspace, in which the two vortices move like “mirror images” of each other, we can think of this system as being formed by a single vortex, moving in the upper half-plane having a half cylinder placed at the origin, see Fig. 3.17.

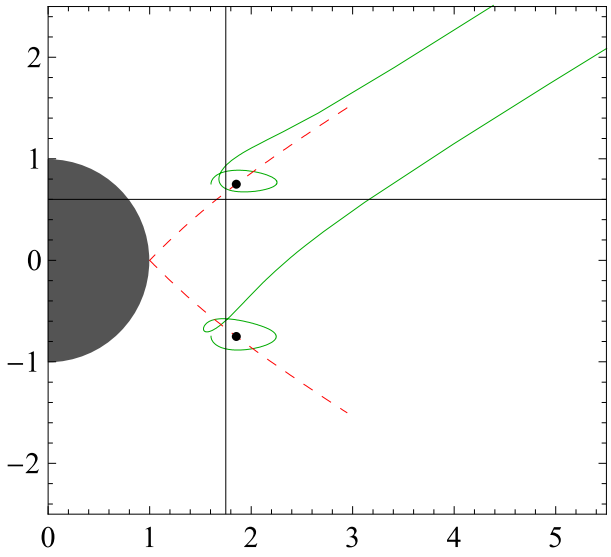

Figure 3.16 Motion resulting from the perturbation $\Delta z_1 = \Delta z_2 = -0.25 + 0.0015i$ from the equilibrium position. This perturbation is almost symmetric, but the existence of the very small antisymmetric component makes the trajectories to move away from the equilibrium positions for larger times. The trajectories are obtained by the numerical integration of Eqs. (3.10) and (3.11) and their respective counterparts for the lower vortex.

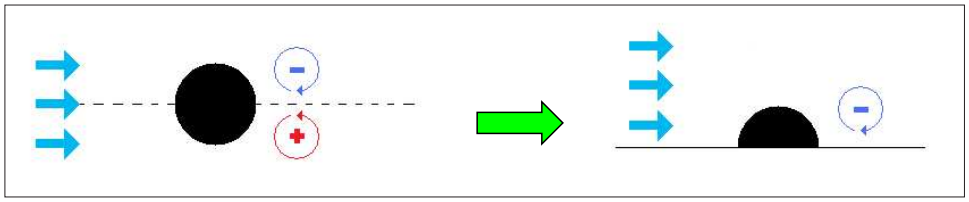

Figure 3.17 The restriction of the vortex motion to the symmetric subspace can be achieved by placing a splitter plate in the middle plane of the flow and then considering only the upper vortex motion.

As stated before, the motion in this symmetric subspace is governed by Eqs. (3.14) and (3.15). These equations can be obtained from Hamilton equations

$$\dot{x} = \frac{\partial H}{\partial y}\,, \quad \dot{y} = -\frac{\partial H}{\partial x}\,, \tag{3.60}$$

with the following Hamiltonian:

$$H(x,y) = y\left(1 - \frac{1}{r^2}\right) - \frac{\kappa}{2}\log\frac{y\left(r^2-1\right)}{\sqrt{\left(r^2-1\right)^2 + 4y^2}}\,. \tag{3.61}$$

Notice that, since we are using dimensionless variables, Hamilton equations do not include the vortex intensity Γ.

Since this is a two dimensional system, it is possible to compute its phase portrait by simply calculating the level sets $H(x,y) = k$, for several different values of the constant k,

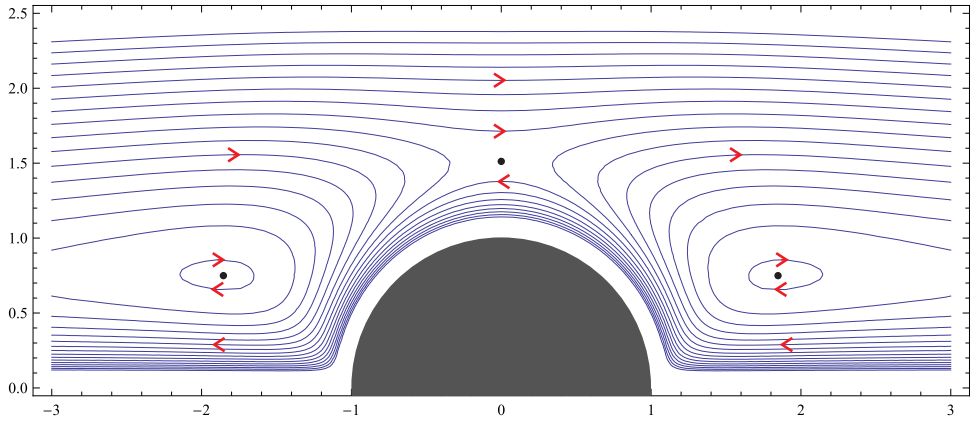

Figure 3.18 Phase portrait for the symmetric Föppl pair obtained by making a contour plot of the Hamiltonian (3.61) with $\kappa = 45/32$. The blue curves are the vortex trajectories and the arrows indicate the direction of the motion. In this Figure one can easily see the centers upstream and downstream the cylinder and the saddle point on the normal line.

see Fig. 3.18. The analysis of this figure immediately shows the centers upstream and downstream of the cylinder, at the Föppl equilibrium, and the saddle point on the y-axis, the normal line equilibrium. The analysis also suggests that the trajectories arising from the stable and unstable branches associated with the saddle point on the normal line, and with the nilpotent saddle at infinity, act as separatrices of the vortex dynamics.

To calculate the separatrices associated with the saddle point on the normal line, we will look for the level set $H(x, y) = H(0, b)$, where $(0, b)$ is the stationary point on the normal line for the particular value of κ we are treating (in the case of Fig. 3.18, $\kappa = 45/32$). The value of b is calculated by numerically inverting Eq. (3.17), which yields $b = 1.52679$ for $\kappa = 45/32$. Therefore, the separatrices associated with the normal line saddle point are obtained by computing the level set $H(x, y) = H(0, 1.52679)$. Similarly, to obtain the separatrices related to the nilpotent saddle point at infinity, we must look for the level set $H(x, y) = H(x_0, y_0)$, where (x_0, y_0) is the fixed point at infinity given by Eq. 3.24. Computationally, we can take a very large value for x_0, for example, $x_0 = 10^5$. So, to calculate this separatrix for $\kappa = 45/32$, we take the level set $H(x, y) = H(10^5, 45/64)$, since the equilibrium occurs at $y_0 = \kappa/2$.

Fig. 3.19 shows a superposition of the separatrices just computed with some of the trajectories of Fig. 3.18. Although not seen in the figure, the branches associated with the nilpotent saddle point at infinity get together to form a homoclinic loop (thick solid line in the figure), which defines the region of nonlinear stability of the Föppl pair under symmetric disturbances. This means that any initial condition inside these loops yields periodic trajectories, with the vortex circulating around the Föppl equilibrium position.

In addition to the trajectories rotating around the Föppl fixed point inside the nilpotent homoclinic loops, several other types of trajectories can be identified in Fig. 3.19. If a vortex is placed above the upper dashed separatrix, it is simply carried away by the incoming stream, since it is very far from the cylinder and the plane to feel their influence. If placed upstream the cylinder, in the region below the dashed curve and above

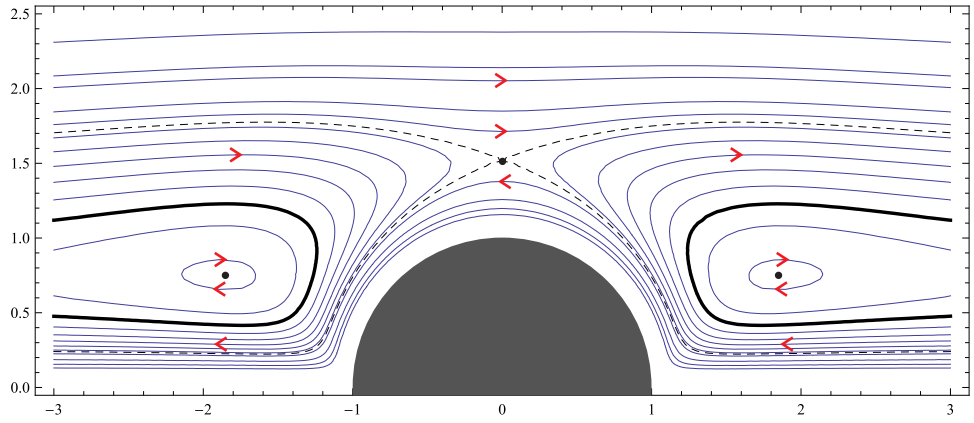

Figure 3.19 Phase portrait including separatrices. The dashed line denotes the separatrices associated with the fixed point at the normal line. The thick solid line is the nilpotent saddle loop which defines the region of nonlinear stability of the Föppl equilibrium.

the thick solid line, the vortex will move along towards the cylinder until it is "reflected back", first by its image inside the cylinder and then by the image by the plane which will make the vortex move upstream. Another curious trajectory occurs if the vortex is placed far downstream of the cylinder, and very close to the plane, below the lower dashed separatrix. In this case, the vortex moves upstream along the plane, then it overcomes the cylinder and finally move off to upstream infinity, against the incoming flow.

3.6 DISCUSSION

In this chapter we have investigated the dynamics of the Föppl system: a pair of counter-rotating point vortices placed in the vicinity of a circular cylinder, in a uniform stream. We have obtained the stationary configurations for the vortices and analyzed the stability properties of the fixed points.

In real flows, governed by the Navier-Stokes equations, the vortex pair is formed at Reynolds numbers in the range $Re < 40$. As the Reynolds numbers increases, the configuration loses its symmetry and becomes unstable. New vortices are alternately shed from each side of the cylinder and the system evolves to the formation of the von Karman vortex street ($40 < Re < 300$). The point vortex model studied in this chapter can shed some light into this process. The two basic unstable modes $\pm\vec{w}_+$, see Eq. (3.59), associated with antisymmetric perturbations of the Föppl equilibrium (Fig. 3.15), are consistent with the early stages of the vortex shedding phenomenon. This scenario is also supported by Tang and Aubry (Ref. [19]), which showed, using direct numerical simulations (DNS), that the stable and unstable directions calculated from the point vortex model, Eq. (3.59), are in qualitative agreement with the motion observed in numerical experiments. It is also known that the vortex shedding can be suppressed by placing a splitter plate in the middle plane of the flow (Ref. [20]). This fact is also in agreement with the point vortex results, since the splitter plate forces the system to stay in the symmetric subspace (see Fig. 3.17), where the Föppl equilibrium is a center. The suppression of vortex shedding

by a splitter plate is thus consistent with the scenario where the antisymmetric modes are responsible for the development of the instability, which ultimately gives rise to the von Karman vortex street.

The problem of vortex flows around a circular cylinder with patches of constant vorticity was addressed numerically by Elcrat et al. in Ref. [21]. The stationary positions for the vortex patches in the vicinity of the cylinder found by the authors are the same of the equivalent point vortex model, namely the normal line and Föppl equilibria presented in Secs. 3.3.1 and 3.3.2.

With this we conclude the study of the Föppl system. We will now move to the analysis of vortex dynamics in domains with more than one boundary, called multiply-connected domains. In the next chapter, we will present the mathematical apparatus that will be necessary to treat vortex dynamics in multiply-connected domains. This apparatus will be employed in Chapter 5 to study the dynamics of vortices around a cylinder that is placed above an infinite plane wall.

CHAPTER 4

VORTEX DYNAMICS IN MULTIPLY CONNECTED DOMAINS: FORMALISM

In this chapter we will introduce the basic mathematical formalism that is used to treat the dynamics of vortices in multiply connected domains. This formalism will be applied in Chapter 5 to analyze the dynamics of a point vortex in the vicinity of a circular cylinder in a uniform stream placed above a plane wall.

In the systems treated so far we have considered the motion of vortices in domains with a single boundary, namely, only one cylinder. The complex potential produced by the vortex configuration was then easily calculated by means of the Milne-Thomson circle theorem which provides the appropriate images in the unphysical domain (interior of the cylinder) in order to satisfy the boundary conditions.

When more than one boundary is involved the circle theorem is no longer helpful to find the vortex images, and other techniques are needed. Our approach to this problem will be based on the method devised by Crowdy and Marshall in Ref. [22] that makes use of the so-called *Schottky-Klein prime function* to produce the appropriate images.

In applying this method, we are going to make use of a circular domain in an auxiliary complex ζ-plane on which the complex potential and the Hamiltonian (the Kirchhoff-Routh path function) are calculated first. These functions are then translated into the physical domain in the z-plane by means of an appropriate conformal mapping. The complex potential is invariant by this conformal mapping but the Hamiltonian must be appropriately corrected, as will be discussed later.

To better understand the basic steps that will be used hereafter, we will consider first the simple case when there is only one vortex in the vicinity of a single cylinder. This case was discussed in Chapter 2, but we study it again using an alternative approach that will be generalized later to the case of multiple boundaries.

4.1 ONE VORTEX NEAR A CYLINDER

As we have seen in Chapter 2, the complex potential for a vortex of intensity Γ at $z = z_1$ near a cylinder of radius a, with vanishing circulation around the cylinder is given by Eq. (2.84), rewritten below with the change in notation $z_0 \to z_1$:

$$w(z) = \frac{\Gamma}{2\pi i} \log \left[\frac{z(z - z_1)}{z - \frac{a^2}{\bar{z}_1}} \right] . \tag{4.1}$$

Let us now introduce a conformal mapping, $z(\zeta)$, from the domain D_ζ corresponding to the interior of the unit circle in the complex ζ-plane onto the fluid region D_z, i.e., the exterior of the disk of radius a, in the physical complex z-plane. The location of the

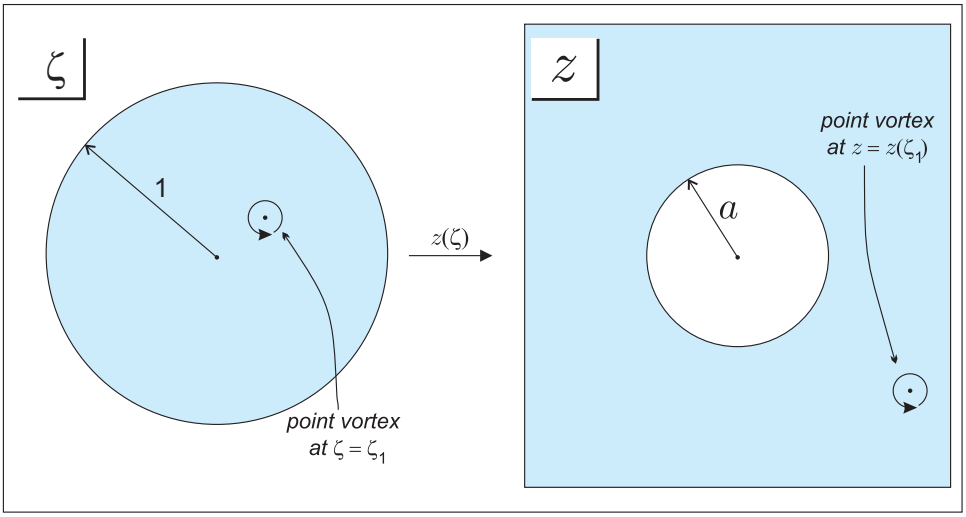

Figure 4.1 Auxiliary complex ζ-plane and physical complex z-plane.

vortex in the ζ-plane is denoted by ζ_1, so that the corresponding position of the vortex in the z-plane is $z(\zeta_1)$; see Fig. 4.1.

The complex potential, $w(\zeta)$, in the ζ-plane, produced by one vortex at $\zeta = \zeta_1$ can be calculated by applying the circle theorem,

$$w(\zeta) = \frac{\Gamma}{2\pi i} \log \left[\frac{\zeta(\zeta - \zeta_1)}{\left(\zeta - \frac{1}{\zeta_1}\right)} \right] . \tag{4.2}$$

The potential (4.2) satisfies the boundary condition at the unit circle $|\zeta| = 1$ but, since the vortex image at the origin has the same sign of the vortex itself, the circulation around the unit circle is $+2$. It is then necessary to change the sign of the vortex at the origin to make the circulation vanish,

$$w(\zeta) = \frac{\Gamma}{2\pi i} \log \left[\frac{(\zeta - \zeta_1)}{\zeta\left(\zeta - \frac{1}{\zeta_1}\right)} \right] . \tag{4.3}$$

Now let us transpose the solution to the physical complex z-plane. The conformal map from the interior of the unit circle in the ζ-plane onto the exterior of the disc of radius a in the z-plane is

$$z(\zeta) = \frac{a}{\zeta} . \tag{4.4}$$

The complex potential is invariant by conformal mapping, so the complex potential in the z-plane is simply given by

$$w(z) = w(\zeta(z)) . \tag{4.5}$$

Here, in an abuse of notation, we are using the same symbol w to denote the complex potential in the z-plane. Substituting Eqs. (4.3) and (4.4) into Eq. (4.5) yields:

$$
\begin{aligned}
w(z) &= \frac{\Gamma}{2\pi i}\log\left[\frac{\frac{a}{z}-\frac{a}{z_1}}{\frac{a}{z}\left(\frac{a}{z}-\frac{\bar{z}_1}{a}\right)}\right] \\
&= \frac{\Gamma}{2\pi i}\log\left[\frac{1-\frac{z}{z_1}}{\frac{a^2-z\bar{z}_1}{za}}\right] \\
&= \frac{\Gamma}{2\pi i}\log\left[\frac{z(z-z_1)}{z-\frac{a^2}{\bar{z}_1}}\frac{a}{z_1\bar{z}_1}\right] . \qquad (4.6)
\end{aligned}
$$

Neglecting the constant term (independent of z), we get:

$$
w(z) = \frac{\Gamma}{2\pi i}\log\left[\frac{z(z-z_1)}{z-\frac{a^2}{\bar{z}_1}}\right] , \qquad (4.7)
$$

recovering thus Eq. (4.1).

We also want to obtain once again the Hamiltonian (2.92) using this auxiliary-plane approach, but differently from the complex potential the hamiltonian is not invariant under conformal mapping, so we will postpone this discussion to a later section.

The use of an auxiliary ζ-plane to calculate the complex potential $w(z)$ was not necessary for the analyses of the systems treated in the previous chapters, because there we had only a single solid boundary and so the analysis could be carried out directly in the physical plane. It turns out, however, that for the study of systems with multiple boundaries, such as the dynamics of a vortex in the vicinity of many disconnected obstacles, it will be essential to make use of the auxiliary ζ-plane to compute the complex potential (and also the Hamiltonian, as we will see later). To analyze the motion of a vortex outside a collection of solid obstacles, we must find first the conformal mapping from a special circular domain D_ζ in the complex ζ-plane onto the physical domain D_z in the complex z-plane. Such mappings will be discussed in the next section.

4.2 CONFORMAL MAPPING BETWEEN MULTIPLY CONNECTED DOMAINS

The Riemann mapping theorem for simply connected domains was generalized by Koebe [23] to include the case of multiply connected domains: any multiply connected domain D_z having $M+1$ boundaries is conformally equivalent to a multiply connected circular domain D_ζ with M inner boundaries. The circular domain D_ζ consists of the unit circle with M inner circles excised from it. Let C_j, for $j = 1, \ldots, M$, denote the boundaries of the M inner circles in the circular domain D_ζ. Also let C_0 denote the boundary of the unit circle. The circular domain D_ζ is completely specified by the set of parameters δ_j and q_j, called *conformal moduli*, corresponding respectively to the centers and radii of the M excised circles.

To exemplify the procedure, let us consider an example taken from Ref. [4] with three cylinders. In this case, the fluid region corresponds to the outside of three circular cylinders of radii s whose centers are located at 0, $-d$ and $+d$ on the x-axis, see Fig. 4.2.

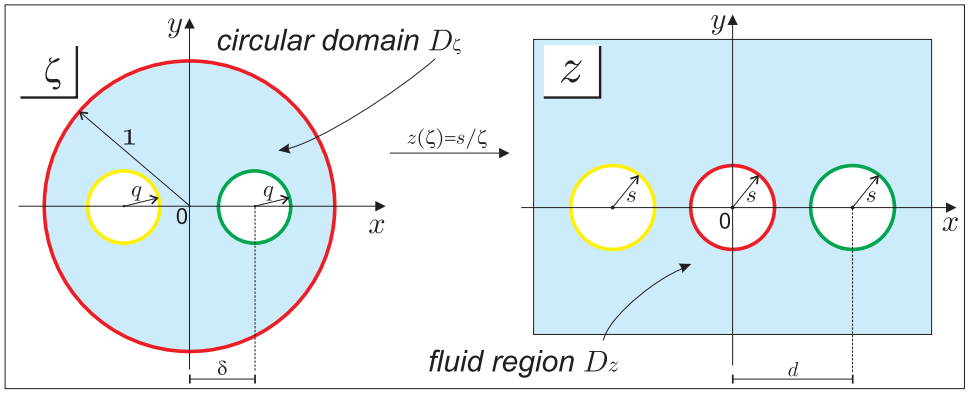

Figure 4.2 Map from the auxiliary ζ-plane to the physical z-plane (figure adapted from Ref. [4]).

The circular domain must then be the unit circle with 2 circles excised from it. The conformal map

$$z(\zeta) = \frac{s}{\zeta} \tag{4.8}$$

takes the unit disc C_0 to the disc at the origin on the z-plane. It also maps $\zeta = 0$ to $z = \infty$. In order to make the discs in the ζ-plane to be mapped into the discs at $\pm d$, we must choose:

$$q = \frac{s^2}{d^2 - s^2}\,, \qquad \delta = \frac{sd}{d^2 - s^2}\,. \tag{4.9}$$

The conformal moduli are then specified by the geometrical parameters of the physical system.

For each excised disc from the ζ-plane one defines a Möbius transformation by

$$\theta_j(\zeta) = \delta_j + \frac{q_j^2 \zeta}{1 - \bar{\delta}_j \zeta}\,. \tag{4.10}$$

This set of transformations will be used later in the definition of the Schottky-Klein prime function.

In the next section we explain the method, based on the Schottky-Klein prime function, that will be used in this chapter to compute the complex potential for a vortex in the presence of multiple solid boundaries. We anticipate here that in order to apply this method it will be necessary to know:

The circular domain D_ζ (unit circle with M inner circles excised from it);

The conformal map from D_ζ onto the physical domain D_z (where $M+1$ boundaries are present in D_z);

The set of M Möbius transformations $\theta_j(\zeta)$.

4.3 THE SCHOTTKY-KLEIN PRIME FUNCTION

To analyze the dynamics of vortices in multiply connected domains, it is necessary first to find the complex potential that satisfies the appropriate boundary conditions, namely, that each solid boundary is a streamline of the flow. The potential due to a single vortex of unit circulation close to one cylinder is given in the auxiliary ζ-plane by Eq. (4.3), with $\Gamma = 1$. This yields a flow without circulation around the cylinder. In fact, any potential of the form

$$w(\zeta) = \frac{1}{2\pi i} \log \left[\frac{(\zeta - \zeta_1)}{|\bar{\zeta_1}| \left(\zeta - \frac{1}{\bar{\zeta_1}} \right)} \right] + \frac{\gamma}{2\pi i} \log(\zeta) + \text{constant} \tag{4.11}$$

satisfies the boundary condition on the cylinder, namely, that the cylinder is a streamline of the flow: $\mathrm{Im}[w(\zeta)] = const.$ on the cylinder. After mapping this region to the physical domain in the z-plane, this potential gives a total circulation of $-\gamma - 1$ around the cylinder. The reason why the potential was written in this way will become clear later.

Let us now denote by G_0 the first function in the Eq. (4.11), that is (making the change $\zeta_1 \to \alpha$),

$$G_0(\zeta, \alpha) = \frac{1}{2\pi i} \log \left[\frac{(\zeta - \alpha)}{|\bar{\alpha}| \left(\zeta - \frac{1}{\bar{\alpha}} \right)} \right] . \tag{4.12}$$

Introducing the notation

$$\omega(\zeta, \alpha) = (\zeta - \alpha) , \tag{4.13}$$

Eq. (4.12) can be rewritten as

$$G_0(\zeta, \alpha) = \frac{1}{2\pi i} \log \left[\frac{\omega(\zeta, \alpha)}{|\bar{\alpha}| \, \omega \left(\zeta, \frac{1}{\bar{\alpha}} \right)} \right] . \tag{4.14}$$

Recall that this is the complex potential in the ζ-plane due to a vortex of intensity $\Gamma = 1$ at $\zeta = \alpha$ (inside the unit disk) and its image (outside the disk). After the conformal mapping $z(\zeta)$ from the ζ-plane to the outside of the disk (or any other object) in the z-plane, this will yield the potential of a vortex, with intensity $\Gamma = 1$ located at $z(\alpha)$, and its image(s). The flow thus generated has circulation -1 around the obstacle.

We would like to obtain an expression equivalent to Eq. (4.14) valid for the multiply connected case. The remarkable fact proved by Crowdy and Marshall in Ref. [22] is that this expression is exactly the same as Eq. (4.14), with the only difference that $\omega(\zeta, \alpha)$ will now be given by a special function, the so-called Schottky-Klein prime function. This function contains the infinite vortex images necessary to satisfy the boundary conditions on the surface of the obstacles, i.e., all boundaries are streamlines of the flow.

After the conformal mapping from D_ζ to the physical domain D_z, the function G_0 gives the complex potential of a vortex of unit intensity in the vicinity of a given set of obstacles, with circulation -1 around the obstacle C_0', whose pre-image in the ζ-plane is the unit circle C_0, and vanishing circulation around all of the other obstacles, see Fig. 4.3.

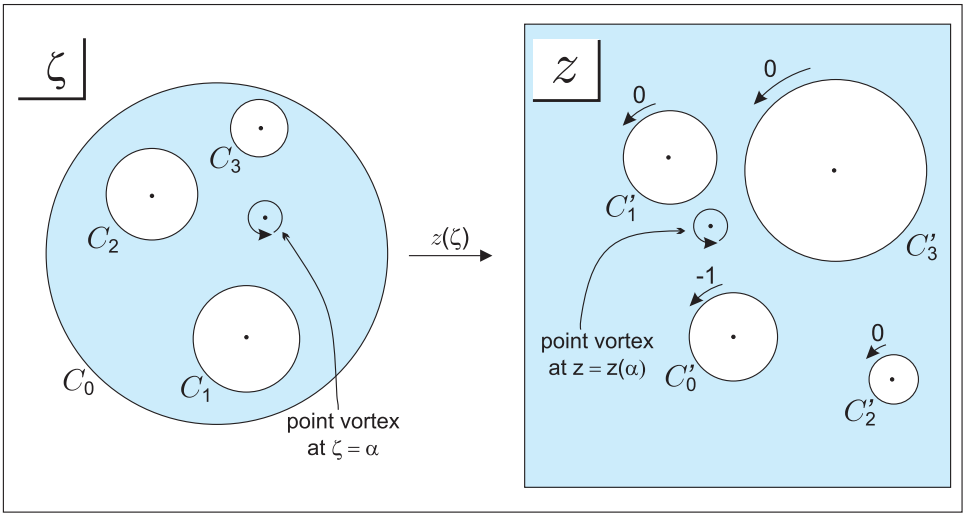

Figure 4.3 Scheme for the potential G_0. The arrows close to each circle on the z-plane denote the value of the circulation around each obstacle.

In order to make the circulation around C'_0 vanish, it is necessary to add a term equivalent to a point vortex of opposite circulation at infinity in the physical plane. The potential due to such a vortex of unit circulation at infinity in the auxiliary ζ-plane is given by

$$G_0(\zeta,\beta) = \frac{1}{2\pi i}\log\left[\frac{\omega(\zeta,\beta)}{|\bar{\beta}|\,\omega\left(\zeta,\frac{1}{\beta}\right)}\right], \tag{4.15}$$

where β is the point such that $z(\beta)=\infty$. To find, for example, the potential for a vortex located at $z=z_v$, having intensity Γ and zero circulation around all the obstacles, one would compute the following function:

$$\Gamma\left(G_0\left(\zeta\left(z\right),\zeta\left(z_v\right)\right) - G_0\left(\zeta\left(z\right),\beta\right)\right). \tag{4.16}$$

By superimposing expressions like the one above one can generate the complex potential due to a collection of point vortices with arbitrary intensities and positions.

It is also possible to add circulation around any of the other obstacles. According to Ref. [4], to add circulation γ_j around the object whose pre-image is the inner circle C_j, $j=0,\ldots,M$, in the ζ-plane, it suffices to add to Eq. (4.16) a term of the form

$$-\gamma_j G_j(\zeta,\beta), \tag{4.17}$$

where

$$G_j(\zeta,\beta) = \frac{1}{2\pi i}\log\left[\frac{\omega(\zeta,\beta)}{|\bar{\beta}|\,\omega\left(\zeta,\theta_j\left(\frac{1}{\bar{\beta}}\right)\right)}\right]. \tag{4.18}$$

Here θ_j, $j=0,\ldots,M$, are the Möbius transformations defined by Eq. (4.10), with θ_0 being the identity map.

From the preceding discussion we thus conclude that in order to obtain the complex potential for a given vortex configuration with a given set of obstacles, all we have to do is to compute the corresponding Schottky-Klein (SK) prime function $\omega(\zeta, \alpha)$. With the knowledge of $\omega(\zeta, \alpha)$, it is possible to find the *complex potential for any number of vortices outside the collection of obstacles.* It is also possible to control the circulation around these obstacles.

For example, consider the case of a system of 2 vortices in the vicinity of 3 circles, having intensities Γ_i, and positions ζ_i, $i = 1, 2$, in the ζ-plane and circulation γ_j around the circle whose pre-image is C_j, $j = 0, 1, 2$. The complex potential $w(\zeta)$ for this case is given by

$$w(\zeta) = \underbrace{\sum_{i=1}^{2} \Gamma_i G_0(\zeta, \zeta_i))}_{\text{vortices}} \overbrace{-\sum_{i=1}^{2} \Gamma_i G_0(\zeta, \beta)}^{\substack{\text{cancel circulation} \\ \text{around } C_0}} \underbrace{-\sum_{j=0}^{2} \gamma_j G_j(\zeta, \beta)}_{\text{add circulations}}. \tag{4.19}$$

The dependence on the geometrical parameters (conformal moduli) is not explicitly indicated in the expression above. These parameters only enter in the definition of the SK prime function, as we will see next.

4.3.1 Computing the SK Prime Function

For each circle C_j, $j = 1, \ldots, M$, in the interior of the unit circle C_0 in the ζ-plane, we define a Möbius map θ_j by Eq. (4.10). With these basic maps one can define a group Θ, called the Schottky group, including all compositions of the M basic maps, their inverses and the identity map. Some examples of elements of this group are $\theta_1(\zeta)$, $\theta_2(\theta_1(\zeta))$, $\theta_1^{-1}(\theta_2^{-1}(\zeta))$, $\theta_1(\theta_2(\theta_5(\zeta)))$. A map $\theta_j(\zeta)$ is called a level 1 map because it involves only one of the basic maps, while $\theta_i(\theta_j(\zeta))$ is a level 2 map, and so on. Let us define a special subset Θ'' of the Schottky group formed by excluding from Θ the identity and all inverse maps. For example if we choose to include the element $\theta_2(\theta_1(\zeta))$ in Θ'', then $\theta_1^{-1}(\theta_2^{-1}(\zeta))$ shall not be included.

The Schottky-Klein prime function is defined by

$$\omega(\zeta, \gamma) = (\zeta - \gamma)\omega'(\zeta, \gamma), \tag{4.20}$$

where the function $\omega'(\zeta, \gamma)$ is given by

$$\omega'(\zeta, \gamma) = \prod_{\theta_i \in \Theta''} \frac{(\theta_i(\zeta) - \gamma)(\theta_i(\gamma) - \zeta)}{(\theta_i(\zeta) - \zeta)(\theta_i(\gamma) - \gamma)}. \tag{4.21}$$

Notice that here the prime does not indicate derivatives.

When computing the SK prime function one has to truncate the infinite product in Eq. (4.21). A natural way to do this is to choose the maps in Θ'' up to a certain level, as we will discuss later.

Notice that the SK prime function encompasses all the geometrical features of the domain D_ζ, since the conformal moduli, namely, the parameters δ_j and q_j corresponding to the centers and radii of the circles C_j, are included in the definition of each θ_j.

Summarizing our procedure thus far, one must carry out the following routine in order to find the complex potential for a vortex configuration in a multiply connected domain:

1. Determine the circular domain, D_ζ, in the auxiliary complex ζ-plane and a conformal mapping $z(\zeta)$ taking this domain onto the physical domain, D_z, in the complex z-plane. If D_z has a number $M+1$ of obstacles, D_ζ must consist of the unit disk with M inner circles excised from it. The centers δ_j and radii q_j of the M inner circles will form the conformal moduli. Each of the circles (including the unit disk) in the auxiliary ζ-plane must be conformally mapped into one of the obstacles in the z-plane.

2. After determining the conformal moduli of the domain D_ζ, define the set of M Möbius transformations θ_j via Eq. (4.10).

3. Compute the SK prime function via (4.20) and (4.21), choosing a proper level to truncate the series.

4. The complex potential for a point vortex of unit intensity in D_ζ, having circulation -1 around the obstacle whose pre-image is the circle C_0, is then given by (4.14).

5. Multiply this complex potential by the desired vortex intensity Γ and superimpose as many terms as necessary to form the complex potential $w(\zeta)$ for the number of vortices in question. Manipulate, as desired, the value of the circulation around the obstacles as in (4.19).

6. From $w(\zeta)$, obtain the complex potential $w(z)$ in the physical domain D_z via the conformal mapping determined in step 1, as shown in Eq. (4.5).

In the next section we will explain how to construct the Hamiltonian governing the motion of point vortices in a multiply connected domain.

4.4 HAMILTONIAN DYNAMICS

4.4.1 The Hydrodynamic Green's Function

As we have seen before (Sec. 2.6.3), the equations of motion for N point vortices in an unbounded domain can be formulated as a Hamiltonian system, as first shown by Kirchhoff in 1876 (Ref. [10]). In 1941 Lin showed that the motion of N point vortices in a multiply connected domain also follows a Hamiltonian dynamics (Ref. [11]). To prove this he introduced a certain *hydrodynamic Green's function* $G(x, y, x_0, y_0)$ with respect to two points (x, y) and (x_0, y_0), possessing a specific set of properties. He then showed that G, defined in accordance with those given properties, existed uniquely and obeyed a reciprocity condition:

$$G(x, y, x_0, y_0) = G(x_0, y_0, x, y)\,. \tag{4.22}$$

He also showed this important Lemma:

Lemma 4.1. *If N vortices of intensities Γ_k are present in an incompressible fluid at positions (x_k, y_k), $k = 1, \ldots, N$, in a general region D consisting of fixed boundaries, the streamfunction of the flow is given by*

$$\psi(x, y, x_1, y_1, \ldots, x_N, y_N) = \psi_0(x, y) + \sum_{k=1}^{N} \Gamma_k G\left(x, y, x_k, y_k\right), \tag{4.23}$$

where $\psi_0(x, y)$ is a streamfunction due to outside agents, such as incoming streams or vortices placed at infinity (to add circulation around obstacles).

The function $G(x, y, x_0, y_0)$ thus defined has a logarithmic singularity at (x_0, y_0, x_0, y_0). Let us consider the function $g(x, y, x_0, y_0)$ which is the "regular part" of $G(x, y, x_0, y_0)$,

$$g(x, y, x_0, y_0) = -G(x, y, x_0, y_0) - \frac{1}{2\pi} \log r_0\,, \tag{4.24}$$

where $r_0 = \sqrt{(x - x_0)^2 + (y - y_0)^2}$. We define now the so-called Robin function as the above function taken at the singularity position:

$$R(x_0, y_0) = g(x_0, y_0, x_0, y_0)\,. \tag{4.25}$$

With knowledge of $G(x, y, x_0, y_0)$ and $R(x_0, y_0)$, it is possible to find the Hamiltonian governing the motion of the point vortices in this multiply connected domain. The following theorem, due to Lin, shows how to compute the Hamiltonian:

Theorem 4.1. *For the motion of vortices of intensities Γ_k, $k = 1, \ldots, N$, in a general multiply connected domain D, with fixed boundaries, there exists a function $H(x_1, y_1, \ldots, x_N, y_N)$ such that,*

$$\Gamma_k \frac{dx_k}{dt} = \frac{\partial H}{\partial y_k}\,, \quad \Gamma_k \frac{dy_k}{dt} = -\frac{\partial H}{\partial x_k}, \tag{4.26}$$

where $H(x_1, y_1, \ldots, x_N, y_N)$ is given by

$$\begin{aligned} H(x_1, y_1, \ldots, x_N, y_N) \;=\; & \sum_{k=1}^{N} \Gamma_k \psi_0(x_k, y_k) + \sum_{\substack{k_1, k_2 = 1 \\ k_1 > k_2}}^{N} \Gamma_{k_1} \Gamma_{k_2} G(x_{k_1}, y_{k_1}, x_{k_2}, y_{k_2}) \\ & - \frac{1}{2} \sum_{k=1}^{N} \Gamma_k^2 R(x_k, y_k). \end{aligned} \tag{4.27}$$

If we define the rescaled variables $x'_k = \sqrt{\Gamma_k} x_k$ and $y'_k = \sqrt{\Gamma_k} y_k$, Eq. (4.26) can be cast in the canonical Hamiltonian form. The physical interpretation of the three terms in the Hamiltonian (4.27) is the following: the first term is responsible for the interaction of a vortex with outside agents, such as an incoming stream or vortices placed at infinity (to add circulation around obstacles). The second term is responsible for the interaction between one vortex and the other vortices (including their images). Finally, the third term is due to the interaction of one vortex with its own images.

To compute the Hamiltonian, it is necessary first to calculate the *hydrodynamic Green's function* $G(x, y, x_0, y_0)$. For convenience, let us make use of complex notation and denote it as $G(\zeta, \alpha)$, where $\zeta = x + iy$ and $\alpha = x_0 + iy_0$. Although Lin [11] proved the existence of such function, he did not provide any mechanism to actually compute this function. Using the SK prime function technique, Crowdy and Marshall gave in [22] an explicit mechanism to calculate $G(\zeta, \alpha)$: the hydrodynamic Green's function is the imaginary part of the complex potential, i.e., the streamfunction, associated with a point vortex of unit intensity:

$$G(\zeta, \alpha) = \mathrm{Im}[G_0(\zeta, \alpha)] \, . \tag{4.28}$$

G_0 was already computed in (4.14), with the SK prime function $\omega(\zeta, \alpha)$ being calculated via (4.20) and (4.21).

Making use of the SK prime function technique together with theorem 4.1, it is then possible to compute the Hamiltonian $H^{(\zeta)}$ governing the vortex dynamics in a multiply connected circular domain D_ζ in the ζ-plane. We show next how to use the Hamiltonian $H^{(\zeta)}$ to obtain the desired Hamiltonian $H^{(z)}$ in the physical domain D_z. For convenience we will keep using the complex notation on a first moment: instead of writing $H^{(\zeta)}(\xi_1, \eta_1, \ldots, \xi_n, \eta_n)$ and $H^{(z)}(x_1, y_1, \ldots, x_n, y_n)$ we will write $H^{(\zeta)}(\zeta_1, \bar{\zeta}_1, ..., \zeta_n, \bar{\zeta}_n)$ and $H^{(z)}(z_1, \bar{z}_1, ..., z_n, \bar{z}_n)$.

4.4.2 Transformation of the Hamiltonian under Conformal Mappings

Differently from the complex potential, the Hamiltonian is not invariant under conformal mappings, i.e.,

$$H^{(z)}(z_1, \bar{z}_1, ..., z_n, \bar{z}_n) \neq H^{(\zeta)}(\zeta_1(z_1), \overline{\zeta_1(z_1)}, ..., \zeta_n(z_n), \overline{\zeta_n(z_n)}) \tag{4.29}$$

It is thus necessary to add an extra term in order to make Hamilton equations still valid in the new domain D_z. Lin showed (Ref. [24]) that under a conformal mapping $z(\zeta)$, the Hamiltonian transforms as

$$H^{(z)}(z_1, \bar{z}_1, ..., z_n, \bar{z}_n) = H^{(\zeta)}(\zeta_1, \bar{\zeta}_1, ..., \zeta_n, \bar{\zeta}_n) + \sum_{k=1}^{N} \frac{\Gamma_k^2}{4\pi} \log \left| \frac{dz}{d\zeta}(\zeta_k) \right| , \tag{4.30}$$

where the sum is over all the k vortices present and z_k and ζ_k are the vortex positions on the z and ζ-plane, respectively.

By using this result it is possible to calculate the Hamiltonian $H^{(z)}$ in any domain D_z conformally equivalent to the circular domain D_ζ for which we already know how to compute $H^{(\zeta)}$.

In summary, the steps one must follow in order to produce the Hamiltonian governing the dynamics of a set of N point vortices outside a collection of obstacles are:

1. Follow steps 1-4 stated in the final of Sec. 4.3.1 to compute SK and obtain the complex potential $G_0(\zeta, \alpha)$ for a point vortex located at $\zeta = \alpha$ in the auxiliary domain D_ζ.

2. Compute the hydrodynamic Green function $G(x, y, x_0, y_0)$ by taking the imaginary part of $G_0(\zeta, \alpha)$, Eq. (4.28), where $\zeta = x + iy$ and $\alpha = x_0 + iy_0$.

3. Compute the Robin function $R(x_0, y_0)$ using Eqs. (4.24) and (4.25).

4. Use Eq. (4.27) to calculate the Hamiltonian $H^{(\zeta)}(\xi_1, \eta_1, \ldots, \xi_N, \eta_N)$ in the auxiliary complex ζ-plane.

5. Convert the Hamiltonian $H^{(\zeta)}$ in the auxiliary ζ-plane into the Hamiltonian $H^{(z)}$ in the physical z-plane by adding Lin's correction term, via Eq. (4.30).

In the next chapter we will explicitly apply this method to analyze the dynamics of a point vortex near a circular cylinder in a uniform stream, placed above a plane wall. But before going into that, let us return to the example discussed in Sec. 4.1, i.e., a vortex near a single cylinder (without the plane) and see how Lin's correction term is used to obtain the desired Hamiltonian $H^{(z)}$ in the physical z-plane from the Hamiltonian $H^{(\zeta)}$ in the auxiliary ζ-plane.

4.4.2.1 Example: One Vortex near a Cylinder In Chapter 2, we obtained the Hamiltonian governing the motion of one point vortex of intensity Γ at $z = x + iy$, near a circular cylinder of radius a, Eq. (2.92). For convenience we rewrite this equation below

$$H(x, y) = \frac{\Gamma^2}{4\pi} \log\left(\frac{x^2 + y^2 - a^2}{x^2 + y^2}\right). \tag{4.31}$$

Our goal in this section is to obtain this result again by first computing the Hamiltonian in the auxiliary ζ-plane and then transposing it to the physical z-plane using Eq. (4.30). From the complex potential in the ζ-plane, Eq. (4.3), the effective potential $w_{eff}(\zeta)$ is calculated:

$$\begin{aligned} w_{eff}(\zeta)(\zeta) &= w(\zeta) - \frac{\Gamma}{2\pi i} \log(\zeta - \zeta_1) \\ &= \frac{\Gamma}{2\pi i} \log\left[\frac{1}{\zeta\left(\zeta - \frac{1}{\zeta_1}\right)}\right], \end{aligned} \tag{4.32}$$

where, we recall, $\zeta = \zeta_1$ is the vortex position. The complex velocity in the ζ-plane is then

$$\begin{aligned} u - iv &= \left[\frac{d}{d\zeta} w_{eff}(\zeta)\right]_{\zeta=\zeta_1} \\ &= -\frac{\Gamma}{2\pi i}\frac{1}{\zeta_1} - \frac{\Gamma}{2\pi i}\frac{1}{\zeta_1 - \frac{1}{\bar{\zeta}_1}}. \end{aligned} \tag{4.33}$$

Making $\zeta_1 = \xi_1 + i\eta_1$ in Eq. (4.32) and separating the real and imaginary parts of the velocity, we have

$$\frac{d\xi}{dt} = \frac{\Gamma}{2\pi i}\left(\frac{\eta}{\xi^2+\eta^2} + \frac{\eta}{\xi^2+\eta^2-1}\right), \tag{4.34}$$

$$\frac{d\eta}{dt} = -\frac{\Gamma}{2\pi i}\left(\frac{\xi}{\xi^2+\eta^2} + \frac{\xi}{\xi^2+\eta^2-1}\right), \tag{4.35}$$

where the subscripts have been dropped for convenience. The Hamiltonian yielding these equations of motion in the ζ-plane is

$$H^{(\zeta)}(\xi,\eta) = \frac{\Gamma^2}{4\pi}\log\left[(\xi^2+\eta^2-1)(\xi^2+\eta^2)\right], \tag{4.36}$$

as can be readily verified. Eq. (4.36) can be rewritten in terms of the variable $\zeta = \xi + i\eta$ as

$$H^{(\zeta)}(\zeta,\bar{\zeta}) = \frac{\Gamma^2}{4\pi}\log\left[(\zeta\bar{\zeta}-1)(\zeta\bar{\zeta})\right], \tag{4.37}$$

To transpose this Hamiltonian to the physical z-plane it is necessary to add Lin's correction via Eq. (4.30)

$$H^{(z)}(z,\bar{z}) = H^{(\zeta)}(\zeta,\bar{\zeta}) + \frac{\Gamma^2}{4\pi}\log\left|\frac{dz}{d\zeta}\right|. \tag{4.38}$$

Using the conformal map $z(\zeta)$ given in Eq. (4.4) we have

$$\begin{aligned} H^{(z)}(z,\bar{z}) &= \frac{\Gamma^2}{4\pi}\log\left[\left(\frac{a^2}{z\bar{z}}-1\right)\left(\frac{a^2}{z\bar{z}}\right)\right] + \frac{\Gamma^2}{4\pi}\log\left|-\frac{z^2}{a}\right| \\ &= \frac{\Gamma^2}{4\pi}\log\left[\left(\frac{z\bar{z}-a^2}{z\bar{z}}\right)\left(\frac{-a^2}{z\bar{z}}\right)\left(\frac{z\bar{z}}{a}\right)\right]. \end{aligned} \tag{4.39}$$

Ignoring additive constants (unimportant to the dynamics) and writing $z = x + iy$, we have

$$H^{(z)}(z,\bar{z}) = \frac{\Gamma^2}{4\pi}\log\left(\frac{x^2+y^2-a^2}{x^2+y^2}\right), \tag{4.40}$$

thus obtaining once again Eq. (4.31).

CHAPTER 5

VORTEX DYNAMICS AROUND A CYLINDER NEAR A PLANE BOUNDARY

This chapter is devoted to the analysis of the dynamics of a point vortex near a circular cylinder placed above a plane wall. Since more than one boundary is involved, it will be necessary to employ the formalism presented in the previous chapter to perform the study.

Our motivation to study this system comes from a 2009 paper by Wei-Jung Lin et al. [5] on which a vortex configuration *upstream* of the cylinder was observed using particle trajectory photography, a technique in which a fine powder (in this case aluminum powder) is used as a tracer to make the fluid particles observable, see Fig. 5.1. Such a configuration is not usually observed in experiments with only one cylinder, so the plane boundary is decisive in its formation upstream of the cylinder. Flows around a cylinder placed near a plane boundary were studied previously by several other authors, including Bearman and Zdravkovich in 1978 (Ref. [25]) and Price et al. in 2002 (Ref. [26]).

As done in the case of the Föppl pair in Chapter 3, our study starts by the definition of the complex potential associated with the flow, which is the topic of the following section.

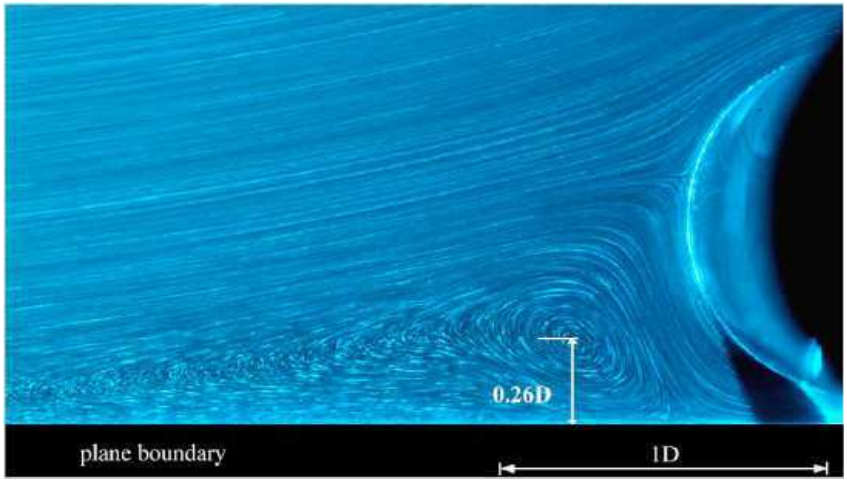

Figure 5.1 Vortex formation upstream of the cylinder. The ratio between the gap and the diameter of the cylinder is $G/D = 0.1$ (figure from Ref. [5]).

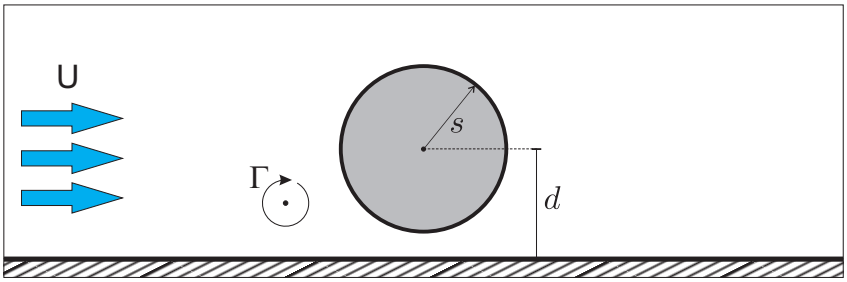

Figure 5.2 Scheme of one vortex close to cylinder and wall under a constant incident flux.

5.1 COMPLEX POTENTIAL

In this section we analyze the problem of one vortex of intensity $\Gamma < 0$ located at $z = z_v$ close to a cylinder and a plane boundary. The cylinder is not touching the plane so that there is a small gap between the cylinder and the plane through which water can flow. A uniform stream of velocity U passes by the cylinder, above the plane. Let s be the radius of the cylinder and d the vertical distance from its center to the plane. A scheme for this problem is shown in Fig. 5.2. Note that, similarly to what we have done in Fig. 3.17 for the Föppl case, this problem could also be studied considering it as a flow passing by two identical cylinders, with a pair of counter-rotating vortices with up-down symmetry imposed. However, this time we prefer to avoid this alternative approach, because now the imposition of up-down symmetry could lead to some complications later (additional terms would be necessary during the calculation of the Hamiltonian).

Our goal is to use the formalism devised in the previous section to analyze a point-vortex model for the system shown in 5.2 and test if a stationary configuration similar to the one observed in the experiments can be predicted by the model. First we consider the case without the incident flux, i.e., $U = 0$.

Since the physical domain consists of two boundaries, namely, the plane and the cylinder, the domain D_ζ in the auxiliary ζ-plane will be the unitary disk with only one disk excised from it. Let us then consider D_ζ to be the annulus $r_0 \leq |\zeta| \leq 1$. From the geometry of the boundaries (lines and circles) the conformal map $z(\zeta)$ from the annulus D_ζ onto the physical domain D_z must be a Möbius transformation of the form

$$z(\zeta) = A\frac{\zeta + B}{\zeta + C}\,. \tag{5.1}$$

We take the outer circle, $|\zeta| = 1$, of the annulus to be mapped onto the plane boundary, $y = 0$, while the inner circle, $|\zeta| = r_0$, is mapped into the cylinder, see Fig. 5.3. We also map the point $\zeta = i$ to the origin, i.e., $z(i) = 0$, and the point $\zeta = -i$ to infinity, i.e., $z(-i) = \infty$. These conditions determine the constants B and C in Eq. (5.1):

$$z(i) = 0 \quad \Longrightarrow \quad B = -i\,, \tag{5.2}$$

$$z(-i) = \infty \quad \Longrightarrow \quad C = i\,. \tag{5.3}$$

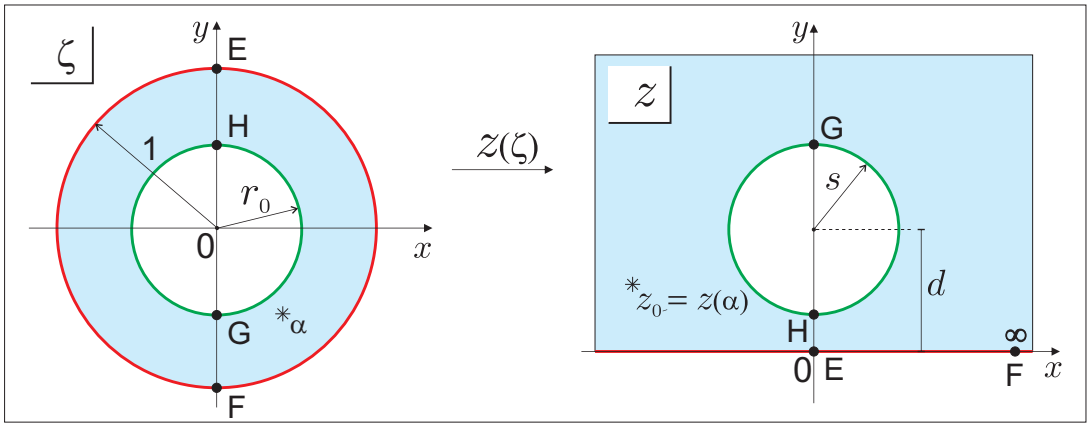

Figure 5.3 Auxiliary domain D_ζ and physical domain D_z.

To determine the constant A and the radius r_0 of the inner circle of the annulus, we choose to map the points $\zeta = \pm i r_0$ to the points $z = i(d \mp s)$. These conditions give

$$\left.\begin{array}{rcl} z(ir_0) & = & i(d-s) \\ z(-ir_0) & = & i(d+s) \end{array}\right\} \quad \Rightarrow \quad \left\{\begin{array}{rcl} A & = & -i\sqrt{d^2-s^2} \\ r_0 & = & \frac{1-\sqrt{\frac{d-s}{d+s}}}{1+\sqrt{\frac{d-s}{d+s}}} \end{array}\right. . \tag{5.4}$$

The map finally reads

$$z(\zeta) = -i\sqrt{d^2-s^2}\,\frac{\zeta - i}{\zeta + i}\,, \tag{5.5}$$

and its inverse is

$$\zeta(z) = -i\frac{z - i\sqrt{d^2-s^2}}{z + i\sqrt{d^2-s^2}}\,. \tag{5.6}$$

A plot showing the action of such a map is shown in Fig. 5.4. The gap between the cylinder and the plane is chosen to be 0.3 and the cylinder radius is $s = 1$.

From our choice for the domain D_ζ (annulus), it is clear that the conformal moduli are:

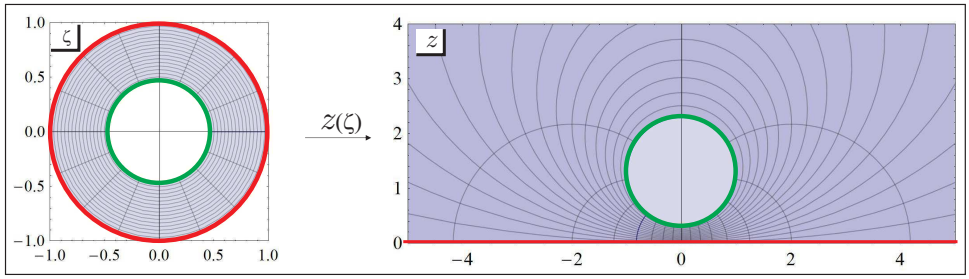

Figure 5.4 Plot of the conformal map $z(\zeta)$ given in Eq. (5.5).

$$\delta_1 = 0 \ , \qquad q_1 = r_0 = \frac{1 - \sqrt{\frac{d-s}{d+s}}}{1 + \sqrt{\frac{d-s}{d+s}}}. \tag{5.7}$$

Since the domain D_ζ has only one inner circle, there is only one basic Möbius map:

$$\theta_1(\zeta) = q_1^2 \zeta = r_0^2 \zeta. \tag{5.8}$$

To compute the SK prime function via Eqs. (4.20) and (4.21), let us first obtain the elements of the subset Θ'' of the Schottky group Θ to be used. Since there is only one Möbius map for this problem, the elements of the subset Θ'' are:

$$\begin{aligned} \theta_1(\zeta) &= r_0^2 \zeta \\ \theta_1 \circ \theta_1(\zeta) &= r_0^4 \zeta \\ &\vdots \\ \underbrace{\theta_1 \circ \cdots \circ \theta_1(\zeta)}_{n \text{ times}} &= r_0^{2n} \zeta \\ &\vdots \end{aligned} \tag{5.9}$$

The infinite product in (4.21) then reads

$$\omega'(\zeta, \alpha) = \prod_{n=1}^{\infty} \frac{(r_0^{2n}\zeta - \alpha)(r_0^{2n}\alpha - \zeta)}{(r_0^{2n}\zeta - \zeta)(r_0^{2n}\alpha - \alpha)}, \tag{5.10}$$

or more conveniently,

$$\omega'(\zeta, \alpha) = \frac{1}{\prod_{n=1}^{\infty}(r_0^{2n} - 1)^2} \prod_{n=1}^{\infty} \left[1 - r_0^{2n}\left(\frac{\zeta}{\alpha}\right)\right] \left[1 - r_0^{2n}\left(\frac{\zeta}{\alpha}\right)^{-1}\right]. \tag{5.11}$$

Finally, using Eq. (4.20) to compute the SK prime function, we obtain

$$\omega(\zeta, \alpha) = \frac{(\zeta - \alpha)}{\prod_{n=1}^{\infty}(r_0^{2n} - 1)^2} \prod_{n=1}^{\infty} \left[1 - r_0^{2n}\left(\frac{\zeta}{\alpha}\right)\right] \left[1 - r_0^{2n}\left(\frac{\zeta}{\alpha}\right)^{-1}\right], \tag{5.12}$$

which can be rewritten as

$$\omega(\zeta, \alpha) = -\frac{\alpha}{C} P\left(\frac{\zeta}{\alpha}, r_0\right), \tag{5.13}$$

where

$$C = \prod_{n=1}^{\infty} \left(1 - r_0^{2n}\right) \tag{5.14}$$

is a constant, and the function $P(x, y)$ is defined by

$$P(x, y) = (1 - x) \prod_{n=1}^{\infty} \left(1 - y^{2n}x\right)\left(1 - y^{2n}x^{-1}\right). \tag{5.15}$$

We note here that the problem of vortex dynamics around two obstacles (without the incoming stream) was solved before by a different approach, using elliptical functions (see, for example, Ref. [27]). The reason why the solution (5.12) was written in Eq. (5.13) in terms of the P function defined in Eq. (5.15) is because this function is closely related to the first Jacobi theta function Θ_1 that appears in the previous solutions. The method based on the SK prime function formalism thus presented recovers the results obtained before for the doubly connected case, as was previously shown in Ref. [28].

For computational purposes, the infinite product in the SK function defined in Eq. (5.12) must be truncated, as discussed before. In all computations in this chapter, we will consider products up to $n = 5$. This corresponds to taking up to level 5 Möbius maps in the set Θ'' used in the definition of SK. Calculations of the P function defined in Eq. (5.15) using $n = 5$ and $n = 6$ differ by less than 10^{-4}, so we are safe to use $n = 5$.

The complex potential due to this single vortex is then given by Eq. (4.14) multiplied by the vortex intensity Γ, with $\omega(\zeta, \alpha)$ given by Eq. (5.13). Using the map in (5.5) to transpose the solution to the physical plane, we have

$$\Gamma G_0(\zeta(z), \zeta(z_v)) = \frac{\Gamma}{2\pi i} \log \left[\frac{\omega(\zeta(z), \zeta(z_v))}{\left|\overline{\zeta(z_v)}\right| \omega\left(\zeta(z), \frac{1}{\overline{\zeta(z_v)}}\right)} \right], \tag{5.16}$$

where z_v is the vortex position in the physical domain D_z, ω is the SK prime function, given by Eq. (5.12), and $\zeta(z)$ is the inverse of the map $z(\zeta)$ given by Eq. (5.6).

Since the obstacle whose pre-image is C_0 is the infinite plane we do not need to worry about the circulation around this particular boundary. A contour plot of the streamline function ψ (imaginary part of the potential G_0) for a $\Gamma = -10$ vortex at $z_v = -1.5 + 0.5i$ is shown in Fig. 5.5. The cylinder radius is 1 and the gap between cylinder and wall is 0.3. The arrows indicate the flow direction. Notice that the boundary condition is satisfied both in the cylinder and in the plane.

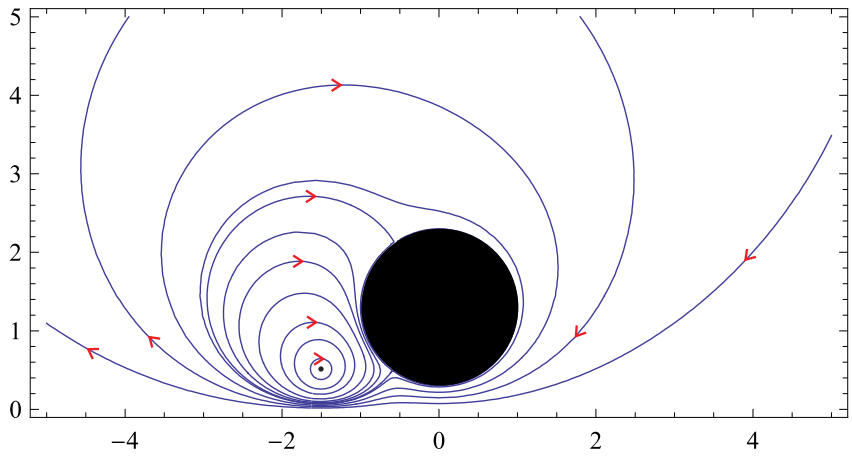

Figure 5.5 Streamline pattern for one vortex without the incident flux.

Let us now include the incoming flux. Crowdy shows in Ref. [4] that the complex potential, $w_U(\zeta)$, in the ζ-plane due to a uniform stream of velocity U in the presence of

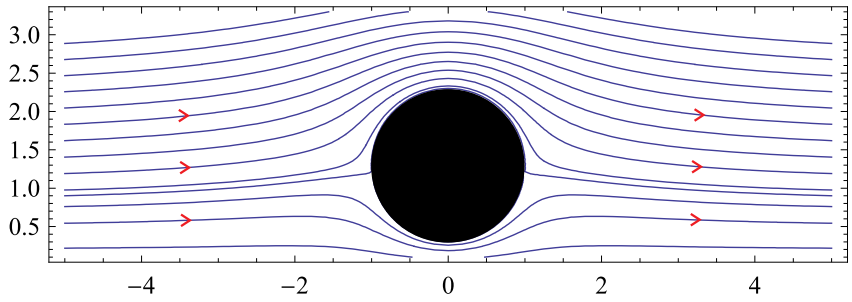

Figure 5.6 Streamline pattern for the incident flux.

a given set of boundaries (in this case, the cylinder and the plane) is given by

$$w_U(\zeta) = 2\pi U a\, i \left(\frac{\partial G_0}{\partial \bar{\alpha}} - \frac{\partial G_0}{\partial \alpha} \right) \Bigg|_{\alpha=\beta} , \tag{5.17}$$

where β is the point that satisfies $z(\beta) = \infty$ and a is the residue of the conformal map $z(\zeta)$ at $\zeta = \beta$, i.e., a is a constant such that close to β, the conformal map behaves as

$$z(\zeta) = \frac{a}{\zeta - \beta} + \text{analytic function} . \tag{5.18}$$

In our case, $U = 1$ and $a = -2\sqrt{d^2 - s^2}$, as can be easily checked from Eq. (5.5). Moreover, $\beta = -i$, which lies on the boundary of the outer circle (mapped to the plane). Due to the fact that β lies on the boundary of the circular domain, the factor of 2 in the potential w_U, Eq. (5.17), is not present, resulting in

$$w_U(\zeta) = -2\pi i \sqrt{d^2 - s^2} \left(\frac{\partial G_0}{\partial \bar{\alpha}} - \frac{\partial G_0}{\partial \alpha} \right) \Bigg|_{\alpha=-i} . \tag{5.19}$$

Fig. 5.6 shows a streamline pattern for this uniform flow.

It is worth noticing that in the ζ-plane the complex potential $w_U(\zeta)$ looks like a dipole placed in the point that is mapped to infinity ($\zeta = \beta$), just as in the case of a uniform stream around a single cylinder, where the image of the incident flux is a dipole placed at the origin. Fig. 5.7 shows the streamline pattern for the complex potential $w_U(\zeta)$ in the ζ-plane.

Now, by superimposing the complex potential given in Eq. (5.17), for the incident flux, with the complex potential given in Eq. (5.16), for the vortex, we obtain the full complex potential for this problem:

$$w(z, z_v) = w_U(\zeta(z)) + \Gamma G_0(\zeta(z), \zeta(z_v)) . \tag{5.20}$$

A streamline pattern of the flow with $\Gamma = -10$, $z_v = -1.5 + 0.5i$ and $U = 1$ is shown in Fig. 5.8.

The problem of finding the complex potential (and then the streamline pattern) for one vortex in the presence of a circular cylinder and a plane in a uniform stream is thus solved. Our next step is to deal with the dynamics involved, i.e., compute the Hamiltonian

(Kirchhoff-Routh path function) and then obtain a phase portrait depicting some vortex trajectories and the stationary positions.

5.2 HAMILTONIAN

5.2.1 Computing the Hamiltonian $H^{(\zeta)}$

Let us now compute the Hamiltonian governing the motion of a single vortex in the presence of a cylinder and a plane wall in a uniform stream, making use of theorem 4.1. First, notice that since there is only one vortex involved ($N = 1$), the second term in Eq. (4.27) will not be present. The dynamics is generated by the interaction of the vortex with the incoming flow and the infinite set of vortex images by the boundaries (cylinder and plane). The Hamiltonian then reads

$$H^{(\zeta)}(\zeta_1, \bar{\zeta}_1) = \Gamma \psi_0(\zeta_1, \bar{\zeta}_1) - \frac{1}{2}\Gamma^2 R(\zeta_1, \bar{\zeta}_1) \,, \tag{5.21}$$

where the Robin function R in the second term is responsible for the vortex infinite images and ψ_0 is the streamfunction associated with the outside agents, such as the incoming streams or vortices placed at infinity to control the circulation around the obstacles. For the moment, let us consider just the case in which the circulation around the cylinder is zero. Therefore, ψ_0 just accounts for the streamfunction associated with the incoming stream, which is given by the imaginary part of Eq. (5.17):

$$\psi_0(\zeta, \bar{\zeta}) = \mathrm{Im}\left[w_U(\zeta)\right] \,. \tag{5.22}$$

To compute the Robin function, we must first calculate the hydrodynamic Green's function $G(\zeta, \zeta_1)$. Making $\alpha \to \zeta_1$ in Eq. (4.28) and using Eq. (4.14) we have

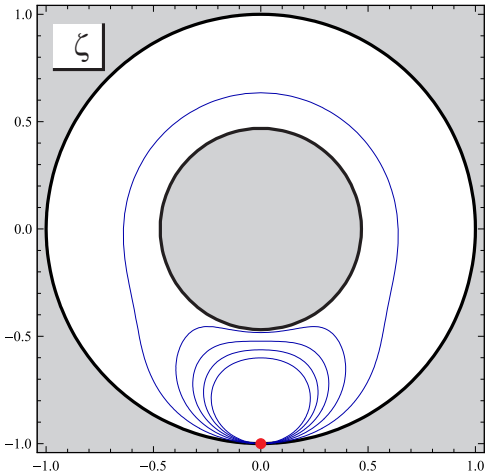

Figure 5.7 Streamline pattern of the uniform flow potential in the ζ-plane. The point marked in red is mapped to infinity by the conformal map.

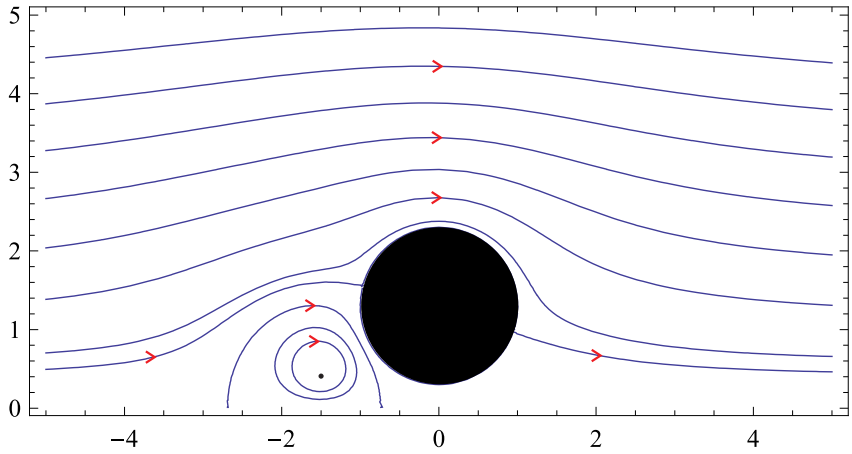

Figure 5.8 Streamlines pattern of the full potential, for a point vortex ($\Gamma = -10$) and an incident flux ($U = 1$).

$$\begin{aligned} G(\zeta,\zeta_1) &= \mathrm{Im}[G_0(\zeta,\zeta_1)] \\ &= \mathrm{Im}\left[\frac{1}{2\pi i}\log\left(\frac{\omega(\zeta,\zeta_1)}{|\bar{\zeta}_1|\,\omega\left(\zeta,\frac{1}{\bar{\zeta}_1}\right)}\right)\right] \\ &= -\frac{1}{2\pi}\log\left|\frac{\omega(\zeta,\zeta_1)}{|\bar{\zeta}_1|\,\omega\left(\zeta,\frac{1}{\bar{\zeta}_1}\right)}\right| . \end{aligned} \tag{5.23}$$

Next we need to compute the g function, corresponding to the regular part of $G(\zeta,\zeta_1)$. Using Eqs. (4.20), (4.24) and (5.23), we obtain

$$\begin{aligned} g(\zeta,\zeta_1) &= -G(\zeta,\zeta_1) - \frac{1}{2\pi}\log|\zeta-\zeta_1| \\ &= \frac{1}{2\pi}\log\left|\frac{(\zeta-\zeta_1)\,\omega'(\zeta,\zeta_1)}{|\bar{\zeta}_1|\,\omega\left(\zeta,\frac{1}{\bar{\zeta}_1}\right)}\right| - \frac{1}{2\pi}\log|\zeta-\zeta_1| \\ &= \frac{1}{2\pi}\log\left|\frac{\omega'(\zeta,\zeta_1)}{|\bar{\zeta}_1|\,\omega\left(\zeta,\frac{1}{\bar{\zeta}_1}\right)}\right| . \end{aligned} \tag{5.24}$$

For the specific problem in consideration (in which the boundaries are the cylinder and the plane), the SK prime function is given by Eq. (5.13). Defining the function $P'(x,y)$ as

$$P'(x,y) = \prod_{n=1}^{\infty}\left(1-y^{2n}x\right)\left(1-y^{2n}x^{-1}\right) , \tag{5.25}$$

we see, considering Eq. (5.12) that

$$\omega'(\zeta,\zeta_1) = \frac{1}{C}\,P'\left(\frac{\zeta}{\zeta_1}, r_0\right)\,, \tag{5.26}$$

where C is the constant given in Eq. (5.14). Eq. (5.24) can then be rewritten as

$$\begin{aligned} g(\zeta,\zeta_1) &= \frac{1}{2\pi}\log\left|\frac{\frac{1}{C}\,P'\left(\frac{\zeta}{\zeta_1}, r_0\right)}{\left|\bar{\zeta_1}\right|\left(-\frac{1}{C\bar{\zeta_1}}\right)\,P\left(\zeta\bar{\zeta_1}, r_0\right)}\right| \\ &= \frac{1}{2\pi}\log\left|\frac{P'\left(\frac{\zeta}{\zeta_1}, r_0\right)}{P\left(\zeta\bar{\zeta_1}, r_0\right)}\right|\,. \end{aligned} \tag{5.27}$$

Using (4.25) to compute the Robin function,

$$R\left(\zeta_1,\bar{\zeta_1}\right) = \frac{1}{2\pi}\log\left|\frac{P'\left(1, r_0\right)}{P\left(\zeta_1\bar{\zeta_1}, r_0\right)}\right|\,, \tag{5.28}$$

and inserting this result into Eq. (5.21), we obtain

$$H^{(\zeta)}\left(\zeta_1,\bar{\zeta_1}\right) = \Gamma\,\psi_0\left(\zeta_1,\bar{\zeta_1}\right) - \frac{\Gamma^2}{4\pi}\log\left|\frac{P'\left(1, r_0\right)}{P\left(\zeta_1\bar{\zeta_1}, r_0\right)}\right|\,. \tag{5.29}$$

This is the Hamiltonian $H^{(\zeta)}$ calculated in the circular domain D_ζ, which consists in this case of the annulus $r_0 < |\zeta| < 1$. Next we shall add Lin's correction term via Eq. (4.30) to obtain the desired Hamiltonian $H^{(z)}$ in the physical domain D_z.

5.2.2 Computing the Hamiltonian $H^{(z)}$

By using the transformation rule (4.30) we can obtain the Hamiltonian $H^{(z)}$ in the physical domain D_z. The conformal map from D_ζ to D_z is, according to Eq. (5.5), given by

$$z(\zeta) = -i\sqrt{d^2 - s^2}\,\frac{\zeta - i}{\zeta + i}\,. \tag{5.30}$$

The additional correction term in Eq.(4.30) reads

$$\frac{\Gamma^2}{4\pi}\log\left|\frac{dz}{d\zeta}\right|_{\zeta=\zeta_1} = \frac{\Gamma^2}{4\pi}\log\left|\frac{2\sqrt{d^2 - s^2}}{(\zeta_1 + i)^2}\right|\,, \tag{5.31}$$

thus the Hamiltonian $H^{(z)}$ is

$$H^{(z)}\left(z_1,\bar{z}_1\right) = \Gamma\,\psi_0\left(\zeta(z_1),\,\overline{\zeta(z_1)}\right) - \frac{\Gamma^2}{4\pi}\log\left|\frac{P'\left(1, r_0\right)}{P\left(\zeta(z_1)\,\overline{\zeta(z_1)}\,, r_0\right)}\right| + \frac{\Gamma^2}{4\pi}\log\left|\frac{2\sqrt{d^2 - s^2}}{(\zeta(z_1) + i)^2}\right|\,. \tag{5.32}$$

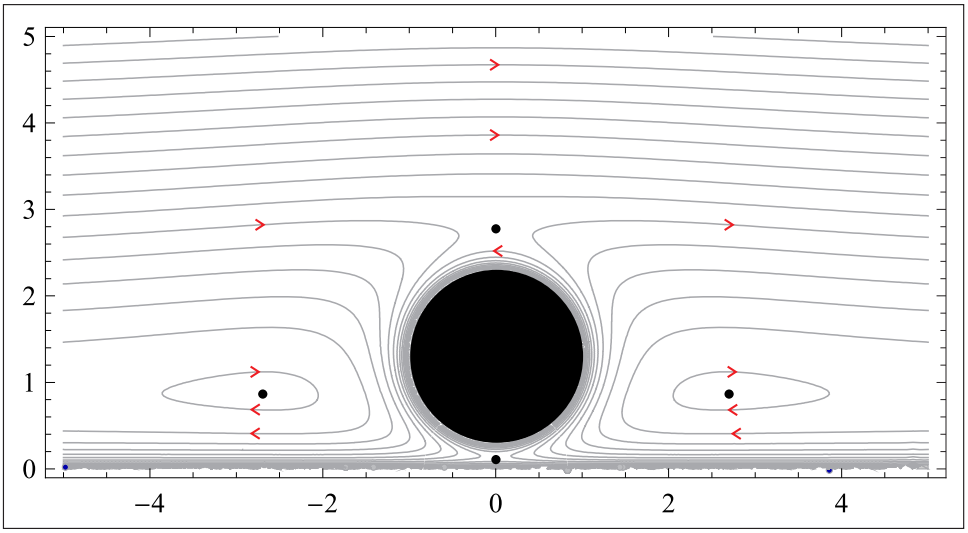

Figure 5.9 Phase portrait for $\Gamma = -10$ generated by a contour plot of the Hamiltonian.

where the inverse map $\zeta(z)$ is given by Eq. (5.6). Making $z_1 = x + iy$ in the equation above, we obtain the desired Hamiltonian in terms of the Cartesian coordinates of the vortex, to be used in connection with Hamilton equations (4.26) to generate the dynamics.

Since $H(x, y)$ is conserved in the dynamics, one way to obtain a phase portrait of this system is to take a contour plot $H(x, y) = c$ for various values of the constant c. An example of such a plot is shown in Fig. 5.9 for $\Gamma = -10$. In this figure, we notice the existence of four fixed points: two centers (upstream and downstream the cylinder) and two saddle points (above and below the cylinder). There must also be a nilpotent saddle point at infinity, just as in the Föppl case, which will be responsible for defining the nonlinear stability region of the centers. Notice also that trajectories close to the cylinder tend to circle around it, as expected, since the first image inside the cylinder is very close to the vortex and consequently gives the dominant contribution in comparison with all other images.

Although this approach to compute the phase portrait, based on contour plots, produces good results, it is computationally ineffective, taking several minutes to generate the desired portrait. It is then preferable to take a different approach, by defining an effective potential and numerically integrating the resulting equations of motion.

5.3 EFFECTIVE POTENTIAL

To obtain the desired equations of motion for the vortex, we must first define the effective potential acting on it, by removing from the full complex potential, Eq. (5.20), the contribution of the vortex itself. The resulting effective potential then accounts for the interaction of the vortex with all its images and with the incoming flow:

$$\begin{aligned} w_{eff}(z, z_v) &= w(z, z_v) - \frac{\Gamma}{2\pi i} \log(z - z_v) \\ &= w_U(\zeta(z)) + \Gamma \left[G_0(\zeta(z), \zeta(z_v)) - \frac{1}{2\pi i} \log(z - z_v) \right] . \end{aligned} \tag{5.33}$$

Since the complex potential is invariant by a conformal mapping, $G_0(\zeta(z), \zeta(z_v)) = G_0(z, z_v)$ and the term inside the square brackets in Eq. (5.33) represents the effective potential acting on a vortex of unit intensity at z_v, due only to its images by the boundaries. Let us denote this term by G_{0eff},

$$G_{0eff}(z, z_v) = G_0(z, z_v) - \frac{1}{2\pi i} \log(z - z_v) . \tag{5.34}$$

Then, the equation for the effective potential acting on the vortex of intensity Γ at z_v reads,

$$w_{eff}(z, z_v) = w_U(\zeta(z)) + \Gamma G_{0eff}(z, z_v) . \tag{5.35}$$

The handling of the singularity at $z = z_v$ in the right side of Eq. (5.34) is not straightforward. To deal with it, it is preferable to work in the auxiliary ζ-plane and then transform the result back to the z-plane. Let α be the point in the auxiliary ζ-plane that is mapped into z_v, in the z-plane, that is, $z_v = z(\alpha)$. Eq. (5.34) then reads,

$$G_{0eff}(z, z_v) = G_0(z(\zeta), z(\alpha)) - \frac{1}{2\pi i} \log \left[z(\zeta) - z(\alpha) \right] . \tag{5.36}$$

Using Eq. (5.5), the term under the log in Eq. (5.36) can be written as

$$z(\zeta) - z(\alpha) = (\zeta - \alpha) \frac{2Ai}{(\zeta + i)(\alpha + i)} , \tag{5.37}$$

where A is the constant given by Eq. (5.4). Plugging Eq. (5.37) into Eq. (5.36), and recalling that $G_0(z(\zeta), z(\alpha)) = G_0(\zeta, \alpha)$, we have

$$\begin{aligned} G_{0eff}(z, z_v) &= G_0(\zeta, \alpha) - \frac{1}{2\pi i} \log \left[(\zeta - \alpha) \frac{2Ai}{(\zeta + i)(\alpha + i)} \right] \\ &= G_0(\zeta, \alpha) - \frac{1}{2\pi i} \log(\zeta - \alpha) - \frac{1}{2\pi i} \log \left[\frac{2Ai}{(\zeta + i)(\alpha + i)} \right] . \end{aligned} \tag{5.38}$$

writing the last term as a function of z and z_v, we have,

$$G_{0eff}(z, z_v) = G_0(\zeta, \alpha) - \frac{1}{2\pi i} \log(\zeta - \alpha) + \frac{1}{2\pi i} \log \left[\frac{2Ai}{(z - A)(z_v - A)} \right] . \tag{5.39}$$

The first two terms on the right side define the effective potential in the ζ-plane acting on a vortex of unit intensity at $\zeta = \alpha$,

$$G_{0eff}(z, z_v) = G_{0eff}(\zeta, \alpha) + \frac{1}{2\pi i} \log \left[\frac{2Ai}{(z - A)(z_v - A)} \right] , \tag{5.40}$$

where,

$$G_{0eff}(\zeta, \alpha) = G_0(\zeta, \alpha) - \frac{1}{2\pi i} \log(\zeta - \alpha) . \tag{5.41}$$

Differently from Eq. (5.34), the singularity at $\zeta = \alpha$ in Eq. (5.41) is easy to handle. Recall that, in the auxiliary ζ-plane, G_0 is calculated in terms of the Schottky-Klein prime function, and is given by Eq. (4.14). Plugging this equation into Eq. (5.41), we have

$$G_{0eff}(\zeta, \alpha) = \frac{1}{2\pi i} \log \left(\frac{\omega(\zeta, \alpha)}{|\bar{\alpha}|\, \omega\left(\zeta, \frac{1}{\bar{\alpha}}\right)} \right) - \frac{1}{2\pi i} \log(\zeta - \alpha) . \tag{5.42}$$

The SK prime function can be factored as $\omega(\zeta, \alpha) = (\zeta - \alpha)\omega'(\zeta, \alpha)$, see Eq. (4.20). Using this in Eq. (5.42), we have

$$G_{0eff}(\zeta, \alpha) = \frac{1}{2\pi i} \log \left(\frac{\omega'(\zeta, \alpha)}{|\bar{\alpha}|\, \omega\left(\zeta, \frac{1}{\bar{\alpha}}\right)} \right) , \tag{5.43}$$

where ω' and ω are given respectively by Eqs. (5.11) and (5.12). Using Eqs. (5.40) and (5.43) we finally conclude that the effective potential on the z-plane acting on a vortex of unit intensity at $z = z_v$ is given by

$$G_{0eff}(z, z_v) = G_{0eff}(\zeta(z), \zeta(z_v)) + \frac{1}{2\pi i} \log \left[\frac{2Ai}{(z - A)(z_v - A)} \right] . \tag{5.44}$$

Thus, $G_{0eff}(z, z_v)$ has no singularity in $z = z_v$ anymore. The total effective potential acting on a vortex of intensity Γ at $z = z_v$ in the z-plane, due to the superposition of the incoming stream and the vortex images is given by Eq. (5.35), with $G_{0eff}(z, z_v)$ given by Eq. (5.44). Differently from the complex potential $G_0^{(\zeta)}$, for which

$$G_0(z, z_v)) = G_0(\zeta(z), \zeta(z_v)) , \tag{5.45}$$

the effective potential due to the vortex images does not conformally transform to the z-plane, that is,

$$G_{0eff}(z, z_v) \neq G_{0eff}(\zeta(z), \zeta(z_v)) . \tag{5.46}$$

It is necessary then to add an appropriate correction term: this correction term guarantees that the vortex complex velocity in the z-plane can be obtained by simply differentiating $G_{0eff}(z, z_v)$ and evaluating the derivative at the vortex position $z = z_v$, i.e.,

$$u - iv = \frac{d}{dz}\, w_{eff}(z, z_v)\Big|_{z=z_v} . \tag{5.47}$$

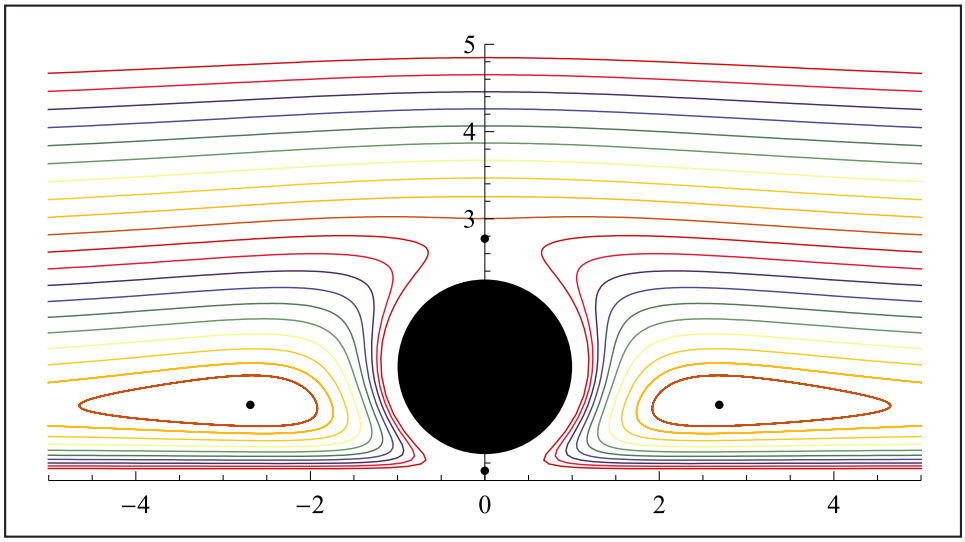

Figure 5.10 Phase portrait for $\Gamma = -10$ generated by the numerical integration of the equations of motion.

Making $z_v = x + iy$ after the differentiation and identifying $\dot{x} = u$ and $\dot{y} = v$, one obtains two nonlinear differential equations [real and imaginary parts of Eq. (5.47)] governing the vortex dynamics. This system of equations can now be numerically integrated to generate the vortex trajectories.

Fig. 5.10 shows a phase portrait analogous to the one shown in Fig. 5.9, which was obtained via a contour plot of the Hamiltonian. In Fig. 5.10, on the other hand, we numerically integrated the system of equations consisting of the real and imaginary parts of Eq. (5.47) to generate the vortex trajectories. This approach is computationally much faster than the one based on a contour plot of the Hamiltonian, taking only a few seconds to produce the desired phase portrait. To produce these trajectories, the initial conditions were $x(0) = \pm 2$ and $y(0) = 0.8 + 0.2j$, $j = 1, \ldots, 20$, and the time interval in the integration is $-100 \leq t \leq 100$.

Now, having the knowledge of the complex potential (5.20), the effective complex potential (5.35) and the Hamiltonian (5.32) associated with the problem of a single vortex in the vicinity of a circular cylinder near a plane wall in a uniform stream, we are in position to complete the analysis of this problem, which will be carried on in the next section. This time the analysis will be entirely based on numerical computations since the expressions involved are too complicated to be treated analytically.

5.4 ANALYSIS AND DISCUSSION

5.4.1 Stationary Positions

To calculate a stationary configuration, we must find the roots of Eq. (5.47). This can be done using the FindRoot routine of the software *Wolfram Mathematica*, but we preferred to take an alternative approach which proved to be computationally faster. Since this is a Hamiltonian system, the dynamics obeys Hamilton equations (4.26), so the stationary

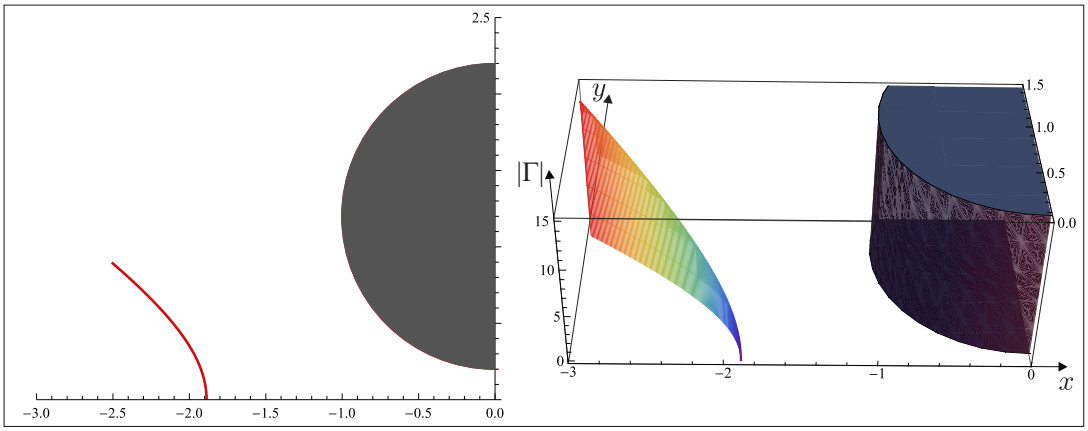

Figure 5.11 (left) Stationary positions curve upstream of the cylinder for $gap = 0.2$. The vortex intensity varies along the curve from $\Gamma = -0.1$ (closer to the plane) to $\Gamma = -10$ (away from the plane). The stationary positions curve for the fixed point downstream of the cylinder is just a reflexion of this one. (right) Three-dimensional plot of the vortex intensity $|\Gamma|$ for points on the stationary positions curve.

position is an extremum of the Hamiltonian (in this case a maximum):

$$\frac{\partial H^{(z)}}{\partial x} = 0\,, \tag{5.48}$$

$$\frac{\partial H^{(z)}}{\partial y} = 0\,. \tag{5.49}$$

We then used Mathematica's routine NMaximize to numerically find the points (x, y) that maximizes the Hamiltonian (5.32). To make sure this numerical method produces the correct results, we calculated a few points using the FindRoot routine and compared the results, the difference being of the order of 10^{-5} which is irrelevant for plot visualizations.

Fig. 5.11 shows on the left a plot of the stationary positions curve for the fixed point upstream of the cylinder (center) for the gap value of 0.2. On the right side of Fig. 5.11 is shown a 3D plot of the vortex intensity $|\Gamma|$ that makes the vortex configuration stationary (in analogy to Fig. 3.8 for the Föppl pair). If the cylinder-plane gap is increased (decreased), the stationary positions curve is shifted to the left (right), see Fig. 5.12. If the cylinder touches the plane (i.e., the gap is zero), the fluid domain becomes simply connected. In this case, the problem could be in principle analyzed by considering a conformal mapping from the fluid domain to, say, the upper half-plane, where the calculations can be easily performed. However, such a conformal map is not trivially obtained, since there is a cusp at the point where the cylinder touches the plane.

Fig. 5.13 shows the dependence of the vortex intensity $|\Gamma|$ with the position of the fixed point above the cylinder (right curve) and below the cylinder (left curve) for the gap value of 0.2. We see that, differently from the centers, these fixed points change their positions very little with an increase in $|\Gamma|$. This is because close to the cylinder the velocity induced by the first image inside the cylinder dominates. Moreover, the saddle

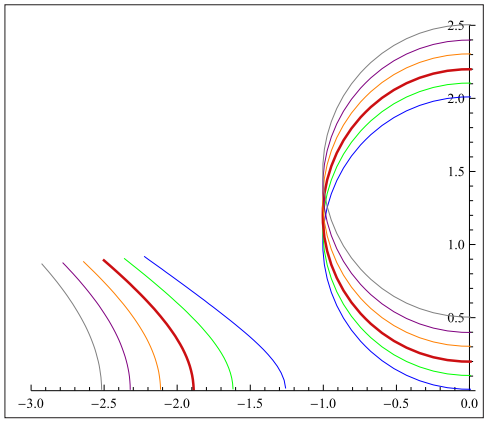

Figure 5.12 Stationary positions curve upstream of the cylinder for *gap* values of 0.01, 0.1, 0.2, 0.3, 0.4 and 0.5. The vortex intensity varies along the curve from $\Gamma = -0.1$ (closer to the plane) to $\Gamma = -10$ (away from the plane). The thick red curve corresponds to the one shown in Fig. 5.11.

point located below the cylinder is constrained to stay within the gap even for very large Γ. Numerically we check that for $\Gamma \to \infty$, the stationary position goes to the middle point between the cylinder and the wall. This is because in this regime the incident flux is negligible and the vortex is balanced between the first images by the cylinder and the plane which act in opposite directions.

Now that we can calculate the fixed points of this system, let us compute the separatrices of the phase portrait. Having these it will be possible to characterize all the regions of the phase portrait with respect to the type of trajectory in it.

5.4.2 Separatrices

In the case of the Föppl pair of vortices restricted to the symmetrical subspace studied in Chapter 3, there were separatrices from the saddle point above the cylinder and from the degenerate saddle point at infinity. Now, in addition to these, there are also separatrices from the saddle point below the cylinder. Since the Hamiltonian is a constant of motion, one way of calculating these curves is by plotting the following contour of the Hamiltonian:

$$H^{(z)}(x, y) = H^{(z)}(x_0, y_0) \,, \tag{5.50}$$

where (x_0, y_0) is the fixed point (saddles) for given values of the gap and vortex intensity. Although this produces the correct results, in this multiply connected system this method is computationally inefficient, as we discussed before, taking several minutes to determine the set of points (x, y) satisfying this equation. We take then an alternative approach: since the separatrices are themselves vortex trajectories in the phase portrait, we proceed a direct integration of the equations of motion resulting from the effective potential, i.e., we integrate the complex velocity, Eq. (5.47), just as we did before in the production of Fig. 5.10, but this time we choose the appropriate initial conditions to reconstruct precisely the separatrices.

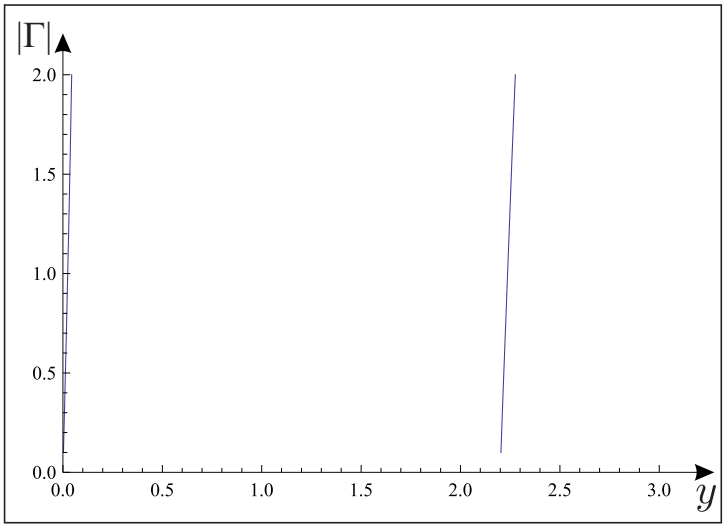

Figure 5.13 Dependence of the vortex intensity $|\Gamma|$ with the position for the saddle points below the cylinder (left curve) and above the cylinder (right curve), for $gap = 0.2$.

To calculate the separatrices from the saddle points above and below the cylinder, we must choose initial conditions in the eigendirections determined by the eigenvectors of the linearized vortex velocity field in the vicinity of each fixed point. The linearized equations of motion around a fixed point (x_0, y_0) are:

$$\begin{pmatrix} \dot{\xi} \\ \dot{\eta} \end{pmatrix} = A \begin{pmatrix} \xi \\ \eta \end{pmatrix} , \tag{5.51}$$

where $\xi = x - x_0$ and $\eta = y - y_0$ are the coordinates relative to the fixed point (x_0, y_0) and the matrix A is

$$A = \left(\begin{array}{cc} \frac{\partial u}{\partial x} & \frac{\partial u}{\partial y} \\ \frac{\partial v}{\partial x} & \frac{\partial v}{\partial y} \end{array} \right) \Bigg|_0 , \tag{5.52}$$

evaluated at the point (x_0, y_0). Using Hamilton equations (4.26) to evaluate u and v, we get

$$A = \left(\begin{array}{cc} \frac{1}{\Gamma}\frac{\partial^2 H}{\partial x \partial y} & \frac{1}{\Gamma}\frac{\partial^2 H}{\partial y^2} \\ -\frac{1}{\Gamma}\frac{\partial^2 H}{\partial x^2} & -\frac{1}{\Gamma}\frac{\partial^2 H}{\partial x \partial y} \end{array} \right) \Bigg|_0 , \tag{5.53}$$

This matrix has a vanishing trace, as expected. From the left-right symmetry of the problem, we see that on the y-axis (where the saddle points are), the vortex velocity is always horizontal, so

$$v(0, y_0) = 0 \quad \Rightarrow \quad \frac{\partial v}{\partial y}(0, y_0) = 0 \quad \Rightarrow \quad \frac{\partial^2 H}{\partial x \partial y}(0, y_0) = 0 \, , \tag{5.54}$$

and the matrix A reads:

$$A = \left(\begin{array}{cc} 0 & B \\ C & 0 \end{array} \right) \Bigg|_0 , \tag{5.55}$$

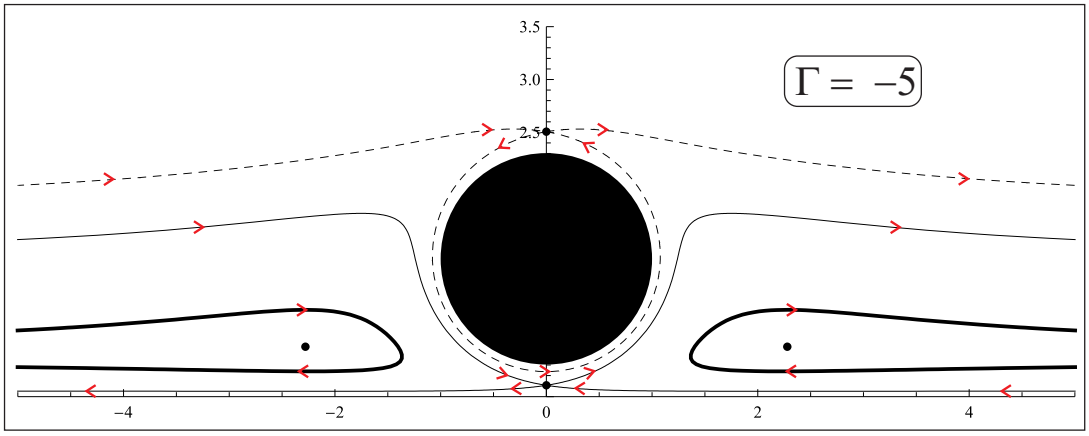

Figure 5.14 Separatrices associated with this system. The vortex intensity is $\Gamma = -5$ and the gap is 0.3.

where,

$$B = \frac{1}{\Gamma}\frac{\partial^2 H}{\partial y^2}\,, \quad C = -\frac{1}{\Gamma}\frac{\partial^2 H}{\partial x^2}\,. \tag{5.56}$$

It is easy to check that the directions of the eigenvectors are

$$\frac{\nu}{\xi} = \pm\sqrt{\frac{C}{B}}\,. \tag{5.57}$$

So, to integrate the equations of motion along the separatrices from the saddle points, we must choose initial conditions of the form

$$x(0) = x_0 \pm \epsilon\,, \quad y(0) = y_0 \pm \epsilon\sqrt{\frac{C}{B}}\,. \tag{5.58}$$

where ϵ is a small number. In the computations performed, we used $\epsilon = 10^{-3}$.

For the trajectory associated with the positive eigenvalue the integration interval is $0 < t < t_{\max}$. For the trajectory associated with the negative eigenvalue, the integration must be performed "backwards" and the integration interval is $t_{\min} < t < 0$. We used $t_{\max} = -t_{\min} = 50$.

It is still necessary to calculate the separatrix associated with the (degenerate) saddle point at infinity. Just like in the Föppl case, these separatrices will determine the region of nonlinear stability of the centers. To calculate the separatrix downstream (upstream) we take an initial condition very far from the cylinder in the x-axis and slightly below (above) the line $y = |\Gamma|/4\pi$. In the calculations performed we used:

$$x(0) = \pm 1000\,, \quad y(0) = \frac{|\Gamma|}{4\pi} \mp 10^{-3}\,. \tag{5.59}$$

This time the integration must be performed over a very long interval, for the vortex to have time to come from very far downstream, close to the cylinder, and back again to far downstream. To make sure the time interval was large enough, we used $t_{\max} = 500000$.

An example of phase portrait showing only the separatrices is shown in Fig. 5.14. The arrows show the velocity direction and the black dots mark the stationary positions. The thin lines are the separatrices from the saddle points above the cylinder (dashed lines) and below the cylinder (solid lines). The thick line is the separatrix from the degenerate saddle point at infinity. There are some interesting features of this phase portrait to be highlighted. First notice that, just like in the Föppl case, the separatrix from the degenerate saddle point at infinity (thick line) defines the nonlinear stability region of the centers. Also, notice that trajectories very close to the cylinder tend to circle around it anti-clockwisely and trajectories very close to the plane tend to follow parallel to it, going to the left. This is expected to happen because very close to these boundaries, the first image of the vortex by the boundaries dominates the dynamics and the effect of the other images is negligible. The trajectories are then the same of the single boundary systems analyzed in Chapter 2.

Notice also that, for this choice of parameters, the saddle point above the cylinder produces a homoclinic loop that encloses all closed trajectories around the cylinder. In this case, a vortex coming from far upstream can either go to infinite downstream passing above the cylinder, if it is located above the upper dashed separatrix, or below it, if it is located between the upper dashed separatrix and the upper solid thin separatrix. It is also possible that the vortex comes close to the gap but instead of passing through it, is "reflected" back to infinity upstream. This happens if the initial condition lies between the upper thin solid line and the thick line. Other trajectories can be deduced by looking at the arrows in the figure.

5.4.3 Topological Transitions

If we change the vortex intensity, the fixed points will move as we have seen in the last subsection. The saddle points positions do not change much, as discussed earlier, but the centers do: they follow the curve of Fig. 5.11. As the vortex intensity grows larger, the centers move away and the upper separatrix from the lower saddle (solid thin line) gets closer and closer to the upper saddle separatrices (dashed lines), see Fig. 5.15 a and b, and then, at a certain critical value of the vortex intensity (numerically estimated to be approximately $\Gamma_c = -7.763428$), the separatrices come together and a heteroclinic loop is formed connecting the two saddle points (Fig. 5.15 c). At this point, it is not possible anymore to have a vortex trajectory starting upstream, going below the cylinder and finally moving downstream. As the vortex intensity increases past the critical value, the heteroclinic loop breaks up and a new homoclinic loop is formed, but this time associated with the saddle point below the cylinder (Fig. 5.15 d and e). In this case a very unusual trajectory occurs: for initial positions lying downstream the cylinder in the narrow space between the two thin separatrices close to the plane, the vortex moves left under the effect of its image by the plane, until a moment when it gets close enough to the cylinder, after which it circles the cylinder almost completely, and then finally goes off to infinity upstream, moving closely to the plane.

The topology of the phase portrait can also undergo a similar transition if, instead of the vortex intensity, we vary the cylinder-plane gap. The qualitative behavior is that

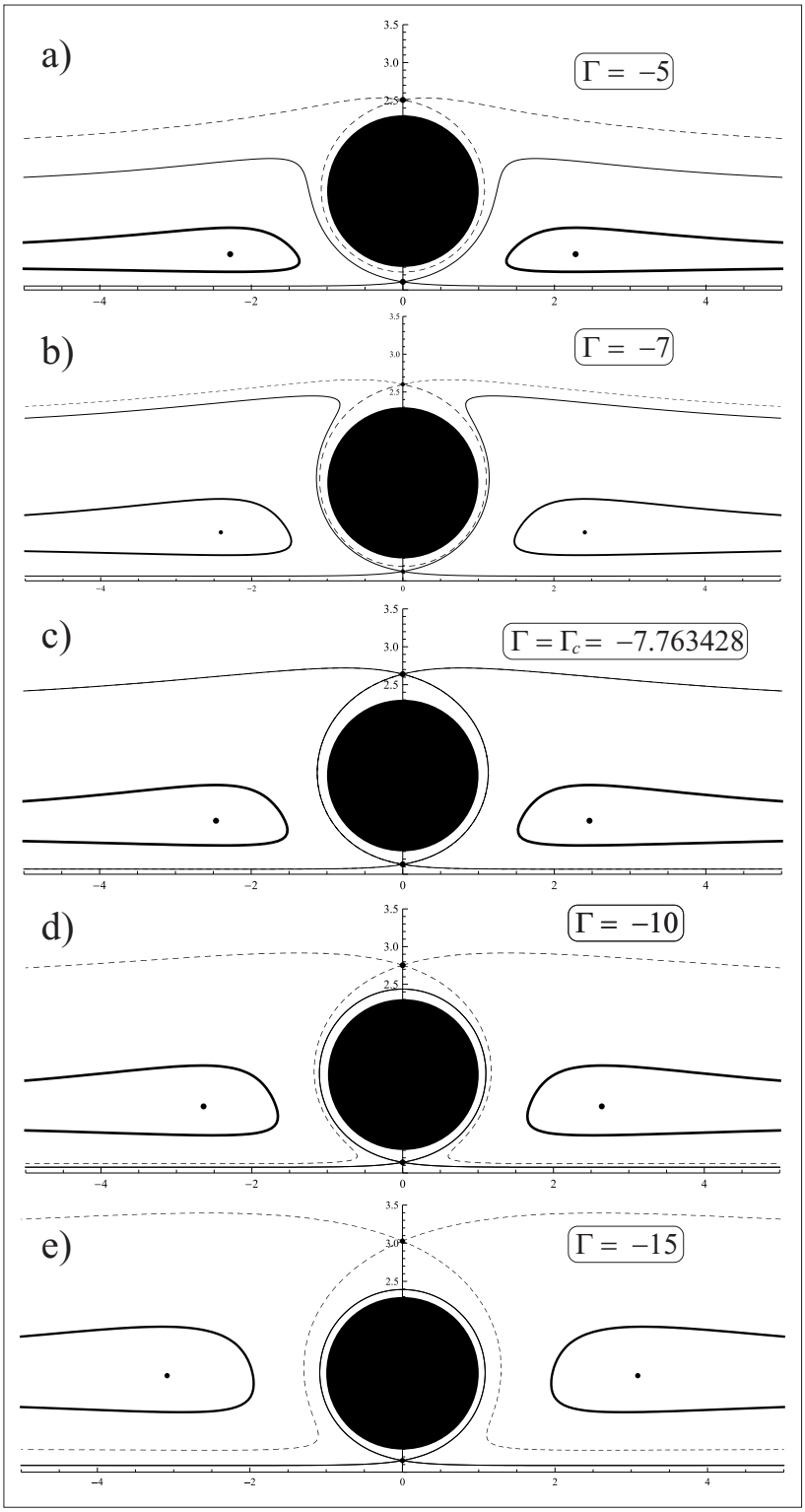

Figure 5.15 Transition in the phase portrait as the vortex intensity Γ increases while the cylinder gap is kept constant at 0.3 (the arrows are omitted and can be inferred from the previous figure).

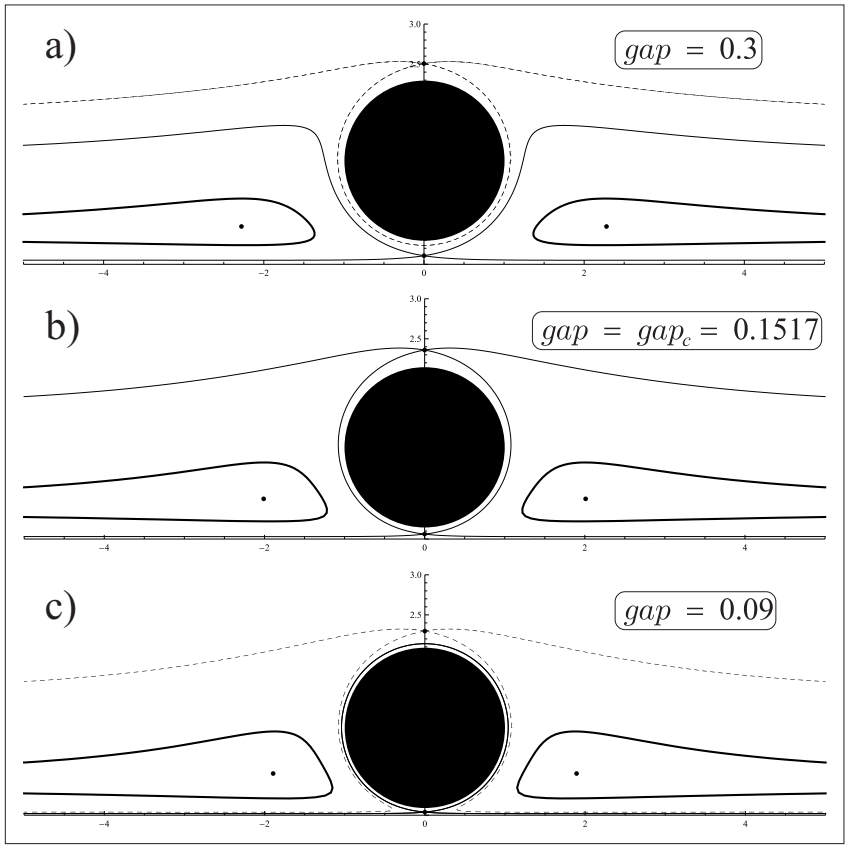

Figure 5.16 Transition in the phase portrait as the cylinder gap decreases while the vortex intensity is kept constant at $\Gamma = -5$.

the change in the gap acts in opposition to the change in the vortex intensity, i.e., to obtain a transition like the one depicted in Fig. 5.15, it is necessary to decrease the gap, without changing Γ. Fig. 5.16 shows such a transition for a fixed value of the vortex intensity $\Gamma = -5$. It is observed that the critical gap value for which the heteroclinic loop is formed is approximately $\text{gap}_c = 0.1517$. Fig. 5.17 shows a diagram illustrating the topological patterns in phase space. Phase transitions similar to these were also observed by Sakajo in a system consisting of the dynamics of a single vortex in the region between three circular cylinders and an outer circular boundary (Ref. [29] Fig. 3b-c in particular).

It is possible to observe in this Fig. 5.16 that the stationary positions corresponding to the centers move away from the cylinder as the gap is increased. This result is in qualitative agreement with the experimental measurements made by Wei-Jung Lin et al. [5] as we will see later.

5.4.4 Comparison with Experiments: Stationary Positions

Fig. 5.18 shows a superposition between the experimental observation by Wei-Jung Lin et al. [5], and the calculated curve of equilibria (red curve) for a gap equal to 0.2. As can be readily verified, the experimental stationary position does not lie on the predicted

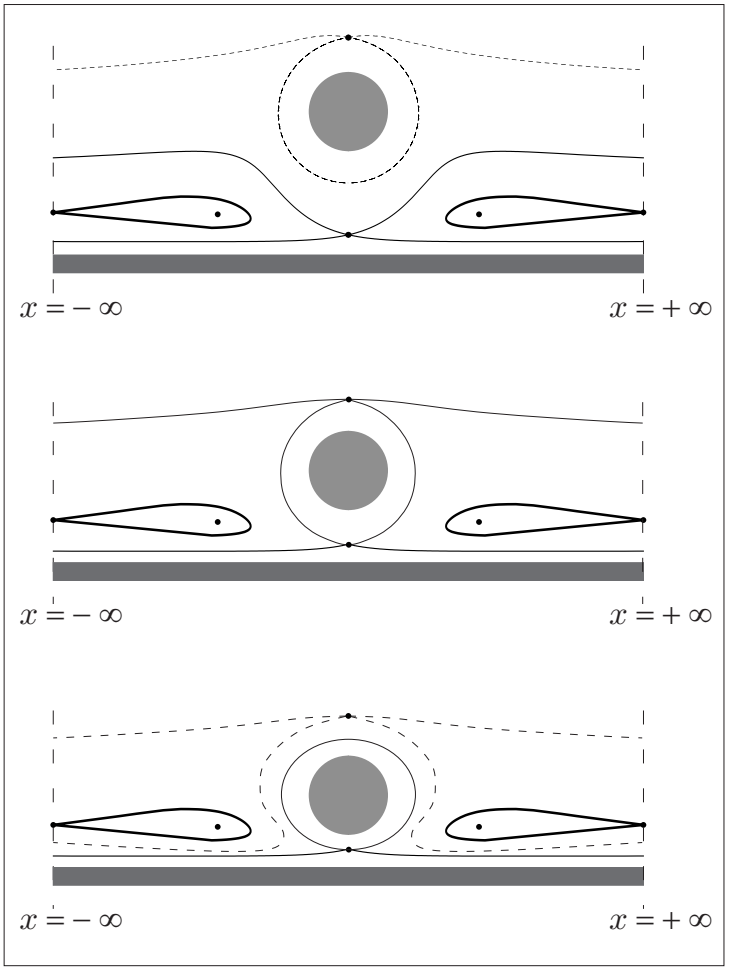

Figure 5.17 Diagram illustrating the topological changes in the phase portrait due to the variation of the plane-cylinder gap.

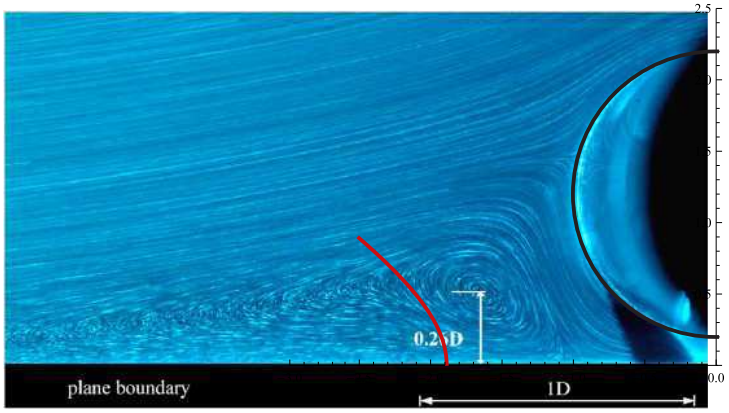

Figure 5.18 Comparison between the experimental observation and the calculated stationary positions curve for cylinder-plane gap of 0.2.

stationary configurations curve. To attain a better agreement, it is necessary to make use of an additional degree of freedom that was not considered so far: the flow circulation around the cylinder.

As discussed earlier in Sec. 4.3, the circulation γ around the cylinder can be controlled by properly placing vortices at the infinity. The complex potential for the case of one vortex of intensity Γ in an incident stream, with circulation γ around the cylinder is obtained by adding to the previously calculated complex potential, Eq. (5.20), the term related to the vortex at infinity, using Eq. (4.17). The complex potential then reads

$$W(z, z_v) = W_U(\zeta(z)) + \Gamma G_0(\zeta(z), \zeta(z_v)) - \gamma G_1(\zeta(z), \beta)\,, \tag{5.60}$$

where β is the point at the complex ζ-plane that is mapped to infinity (in the present case, $\beta = -i$) and G_1 is calculated using Eq. (4.18),

$$G_1(\zeta, \beta) = \frac{1}{2\pi i} \log \left(\frac{\omega(\zeta, \beta)}{|\bar{\beta}|\, \omega\left(\zeta, \theta_1\left(\frac{1}{\bar{\beta}}\right)\right)} \right)\,, \tag{5.61}$$

where θ_1 is given by Eq. (5.8).

To calculate the stationary positions for this new situation where the circulation γ around the cylinder does not vanish, it is necessary to change the Hamiltonian $H^{(z)}$ given in Eq. (5.32) to account for the vortex at infinity. This is done by including the streamfunction due to such a vortex in the definition of ψ_0 which was given in Eq. (5.22) in the case of vanishing circulation. The Hamiltonian $H^{(z)}$ is given by the same Eq. (5.32), rewritten below:

$$H^{(z)}(z_1, \bar{z}_1) = \Gamma\, \psi_0\left(\zeta(z_1), \overline{\zeta(z_1)}\right) - \frac{\Gamma^2}{4\pi} \log \left| \frac{P'(1, r_0)}{P\left(\zeta(z_1)\,\overline{\zeta(z_1)}\,, r_0\right)} \right| + \frac{\Gamma^2}{4\pi} \log \left| \frac{2\sqrt{d^2 - s^2}}{(\zeta(z_1) + i)^2} \right|\,, \tag{5.62}$$

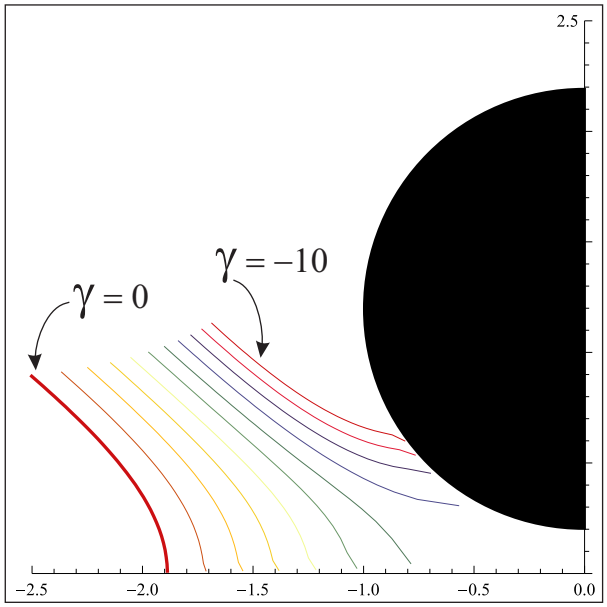

Figure 5.19 Stationary position curves for $gap = 0.2$. Following each curve the vortex intensity varies from $\Gamma = -0.1$ (closer to the plane) to $\Gamma = -10$ (away from the plane). Each curve is for a fixed integer value of the circulation γ around the cylinder.

with

$$\psi_0\left(\zeta, \bar{\zeta}\right) = \mathrm{Im}\left[W_U(\zeta) - \gamma G_1(\zeta, \beta)\right] \ . \tag{5.63}$$

With these modifications it is possible to calculate the new stationary positions as we change the circulation γ around the cylinder and the vortex intensity Γ. Fig. 5.19 shows a set of 11 stationary position curves, each for a fixed integer value of the circulation γ around the cylinder. The thick red curve on the left corresponds to $\gamma = 0$, which is the case treated before, shown in Fig. 5.18.

By comparing Fig. 5.19 with the experimental observation in Fig. 5.18, we see that the curve corresponding to the value of $\gamma = -3$ (orange) is the one that best approximates the experimental stationary configuration, see Fig. 5.20. The point on the curve where the stationary position lies is $z_v = -1.6939 + 0.5257i$ and the vortex intensity is $\Gamma = -4.5$. Fig. 5.21 is a streamline pattern obtained by introducing the experimental parameters estimated in Fig. 5.20 ($U = 1$, $z_v = -1.6939 + 0.5257i$, $\Gamma = -4.5$, $\gamma = -3$) into the complex potential (5.60).

The necessity to impose a negative (clockwise) circulation around the cylinder to approximate the stationary configuration observed is in qualitative agreement with the experiments. To see this, first we recall that in the case of flows past a cylinder (with no other boundaries) studied in Chapter 3, the circulation is zero because of the up-down symmetry of the system. When the additional plane boundary is present, the flow is no longer symmetrical and one expects a non-vanishing circulation around the cylinder. For this circulation to be negative, the average velocity above the cylinder must be higher than below it, and this is indeed observed in the experiments. According to Lin's paper

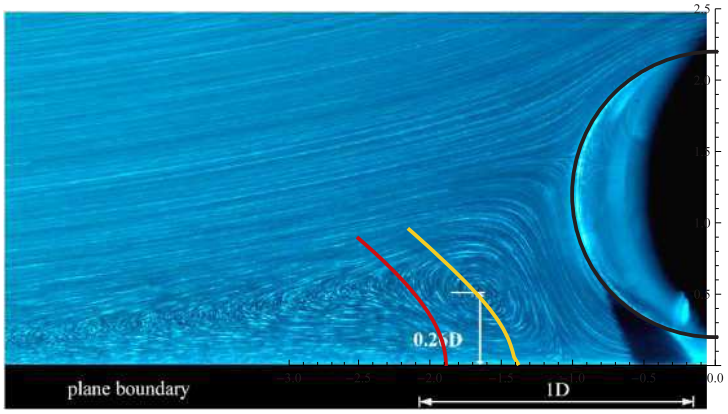

Figure 5.20 Comparison between the experimental observation and the calculated stationary position curves for $\gamma = 0$ (red) and $\gamma = -3$ (orange).

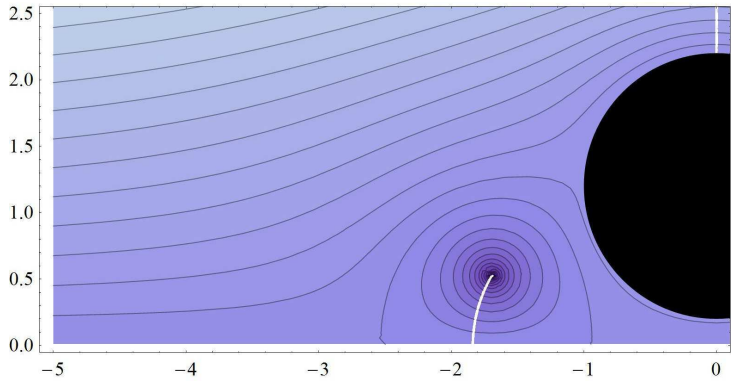

Figure 5.21 Streamline pattern produced with the estimated experimental parameters $U = 1$, $z_v = -1.6939 + 0.5257\,i$, $\Gamma = -4.5$ and $\gamma = -3$.

[5]: "The recirculating eddy upstream of the circular cylinder forms just like an obstacle to the approaching flow near the plane boundary. As the gap ratio decreases, enlargement of this eddy prominently deflects part of the fluid from upstream of the plane boundary over the top of the circular cylinder and thus reduces the flow passing through the gap."

As anticipated at the end of the previous section, the stationary position tends to move away from the cylinder as the gap increases. Fig. 5.22 shows three different measurements made by Lin [5] that illustrate the change in the vortex position. For each configuration, we estimated the experimental parameters for the vortex intensity Γ and the circulation around the cylinder γ. The fact that the circulation around the cylinder tends to decrease (in modulus) as the gap increases is expected, since the flow above and below the cylinder tends to be "more symmetric" as the distance between the cylinder and the wall increases. Also, since the vortex intensity is smaller in the case of the largest gap, the deflection of the incoming stream by the vortex is reduced, therefore contributing to the reduction of the circulation around the cylinder.

Thus said, it is fair to mention that the point vortex model not only explains the exis-

tence of a stationary configuration upstream the cylinder, but is also in good qualitative agreement with several experimental observations.

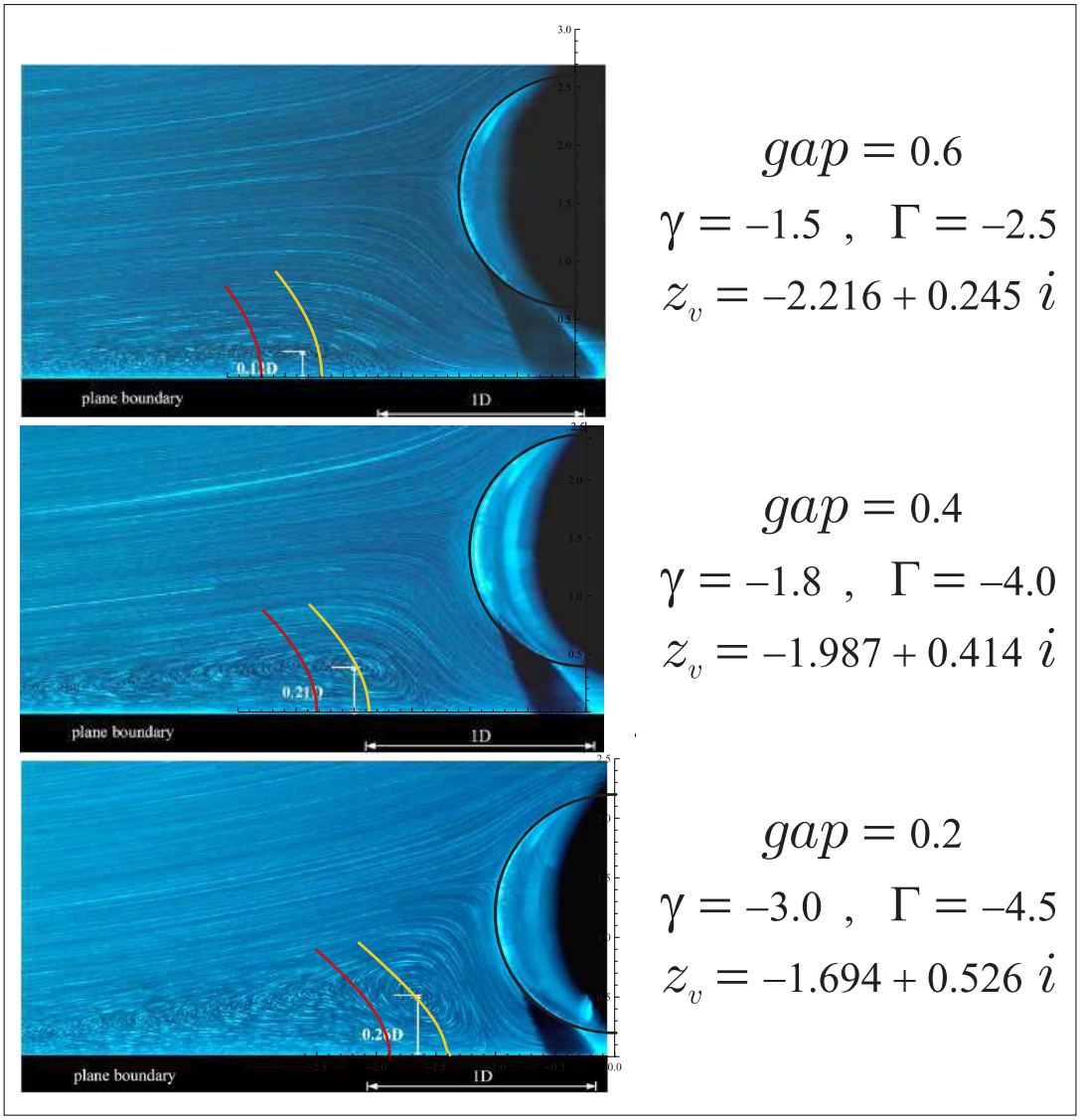

Figure 5.22 On the left, the experimental measurements made by Lin [5]. The estimated experimental parameters are shown on the right of the figure. The red curve corresponds to the system having circulation around the cylinder $\gamma = 0$, while the orange curve is for the value of γ estimated on the right.

CHAPTER 6

CONCLUSIONS

In this thesis, we have applied the point vortex model to study the dynamics of vortices in the presence of solid obstacles. Two different systems were treated: the Föppl system, in which a pair of vortices move in a uniform stream around a circular cylinder in an otherwise unbounded domain, and the system consisting of a single vortex near a circular cylinder placed above an infinite plane wall, also in a uniform stream.

In the first problem, we obtained, using standard complex analysis techniques, the vortices stationary positions and showed that, in addition to the Föppl equilibrium and the equilibrium on the normal line, found in Föppl's original paper (Ref. [15]), the system possesses a hitherto unnoticed nilpotent saddle point at infinity, whose homoclinic loops define the region of nonlinear stability of the Föppl equilibrium. This important observation allowed us to completely characterize the phase portrait of this system within the symmetric subspace. We have also performed the linear stability analysis of the fixed points under symmetric and antisymmetric perturbations. We obtained the eigenvalues and eigenvectors for each fixed point, and, by numerically integrating the nonlinear equations of motion, we studied the dynamics resulting from antisymmetrical perturbations of the equilibrium configurations. We argued that the dynamics resulting from these perturbations of the Föppl equilibrium is responsible for the instability that leads to vortex shedding and the development of the so-called von Karman vortex street, a hypothesis first confirmed by Tang and Aubry [19] via direct numerical simulations (DNS) of the Navier-Stokes equations.

Next, we studied the problem of a single vortex near a cylinder placed above a plane wall. The presence of a secondary boundary (the plane) makes this problem much harder to treat analytically. A recent mathematical apparatus, based on the so-called Schottky-Klein prime function, was used to study the vortex dynamics in this multiply connected domain. The stationary positions were calculated by numerically maximizing the Hamiltonian and the phase portrait of the system was computed. We showed that the point vortex model could explain the existence of the stationary configuration upstream the cylinder observed in the experiments. Moreover, the model results are in qualitative agreement with some experimentally observed features of this system such as: (i) the negative circulation around the cylinder; (ii) the reduction of the absolute value of this circulation as the cylinder-plane gap increases; (iii) the variation of the stationary positions as the gap changes. We also observed that the phase portrait of the system undergoes a topological transition, as we vary either the vortex intensity or the cylinder-plane gap beyond some critical values. Topological transitions like the one observed in our system were reported by Sakajo in Ref. [29]. In particular, in Fig. 3b-c of this paper, a transition very similar to the one we found is reported in the analysis of the dynamics of a single vortex inside a circular domain with obstacles.

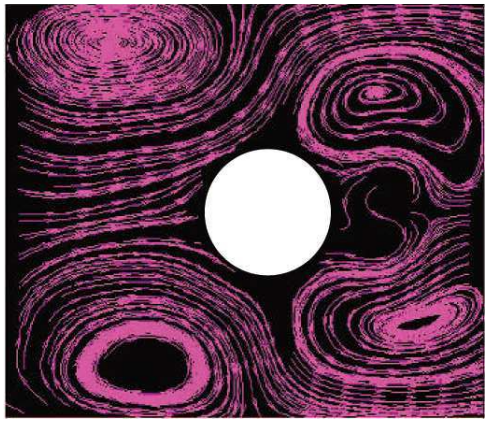

Figure 6.1 Configuration with four vortices observed in the flow of superfluid helium around a cylinder placed in a channel (figure from Ref. [6]).

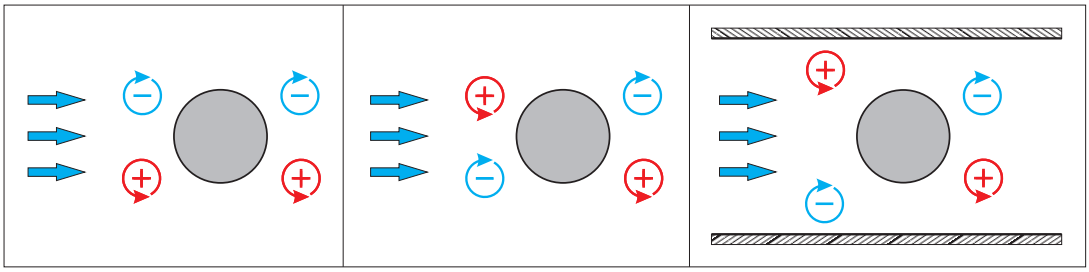

Figure 6.2 Configurations with both vortex pairs having the same signs (left) and opposite signs (center). Configuration including the channel, without the rectangular symmetry (right).

One possible extension of this work is to consider systems involving a higher number of vortices. In a recent publication Zhang and Sciver [6] observed a very interesting four-vortex configuration in the flow of superfluid helium around a cylinder placed in a channel, as shown in Fig. 6.1. An analytical study of this system by means of the point vortex model would be very interesting. As an initial step towards it we have analyzed the problem of a pair of vortex pairs in the vicinity of a circular cylinder in an otherwise unbounded domain. We have reproduced the known stationary configuration (Ref. [21]) where the vortex pairs have the same signs before and after the cylinder, and are symmetrically located, see the scheme on left side of Fig. 6.2. However, for the case observed in the experiments of Fig. 6.1, where the vortex pairs have opposite signs, there is no possible stationary configuration with the same rectangular symmetry, shown schematically on the center of Fig. 6.2. A next step would be to consider the problem of a pair of vortex pairs around the cylinder in a channel, as shown in the right side of Fig. 6.2. To attack this problem, one should first find a conformal map from the fluid domain to some other simpler region, say, an annulus, where the analysis could be done via the Schottky-Klein prime function formalism presented in Chapter 4.

In the case of flows around a cylinder placed above a plane wall, there are several studies regarding the influence of the wall in the vortex shedding phenomenon (see for

example Refs. [5], [25] and [26]). In this situation, because the system does not have the up-down symmetry present in the Föppl case, maybe it could have a Föppl-like stationary configuration behind the cylinder in which one of the vortices is stronger than the other. Also, it has been experimentally observed by Price et al. in Ref. [26] that the boundary layers from above and below the cylinder clearly separate differently from each other for small gap values. The analysis of the stability properties of a (possible) Föppl-like stationary configuration of a pair of point vortices behind the cylinder may shed some light into these important questions.

BIBLIOGRAPHY

[1] J. R. Chambers, "Concept to Reality: Contributions of the Langley Research Center to U.S. Civil Aircraft of the 1990s," tech. rep., National Aeronautics and Space Administration (NASA), 2011.

[2] M. V. Dyke, *Album of Fluid Motion*. The Parabolic Press, 1982.

[3] P. K. Kundu and I. M. Cohen, *Fluid Mechanics*. Academic Press, 2002.

[4] D. G. Crowdy, "A new calculus for two-dimensional vortex dynamics," *Theor. Comput. Fluid Dyn.*, vol. 24, pp. 9–24, 2010.

[5] W. J. Lin, C. Lin, S. C. Hsieh, and S. Dey, "Flow characteristics around a circular cylinder placed horizontally above a plane boundary," *J. Eng. Mech.*, vol. 135, pp. 697–716, 2009.

[6] T. Zhang and S. W. V. Sciver, "Large-scale turbulent flow around a cylinder in counterflow superfluid 4He (He (II))," *Nature Physics*, vol. 1, pp. 36–38, 2005.

[7] D. J. Acheson, *Elementary Fluid Dynamics*. Oxford University Press, 1990.

[8] P. G. Saffman, *Vortex Dynamics*. Cambridge University Press, 1992.

[9] H. von Helmholtz, "Über integrale der hydro-dynamischen gleichungen, welche den wirbelbewegungen entsprechen," *Journal für die reine und angewandte Mathematik*, vol. 55, pp. 25–55, 1858.

[10] G. R. Kirchhoff, *Vorlesungen über matematische Physik - Mechanik*. Teubner, Leipzig, 1876.

[11] C. C. Lin, "On the motion of vortices in two dimensions I: existence of the Kirchhoff-Routh function," *Proc. Natl. Acad. Sci.*, vol. 27, pp. 570–575, 1941.

[12] G. L. Vasconcelos, M. N. Moura, and A. M. J. Schakel, "Vortex motion around a circular cylinder," *Phys. Fluids*, vol. 23, p. 123601, 2011.

[13] H. Aref, "Vortex dynamics of wakes," *Nelin. Dinam.*, vol. 2, pp. 411–424, 2006. Paper in russian, english version available at: `http://www.fluid.dtu.dk/upload/fluid.dtu/hassan%20div%20+%20pdf%20filer/moscow_paper.pdf`.

[14] T. W. G. de Laat, "Eigenfrequencies of vortex-pair equilibria near an elliptic cylinder or a flat plate in uniform flow," *Phys. Rev. E.*, vol. 75, p. 036302, 2007.

[15] L. Föppl, "Wirbelbewegung hinter einem kreiszylinder," *Sitzb. Bayer. Akad. Wiss.*, vol. 1, pp. 1–17, 1913.

[16] "The Mathematica Book Online." `http://reference.wolfram.com/legacy/v5_2/TheMathematicaBook/MathematicaReferenceGuide/SomeNotesOnInternalImplementation/A.9.4.html`.

[17] M. Baumgartner, O. Dean, V. Patel, J. Schweitzer, and E. V. Beek, "Solving ODEs with mathematica." `https://controls.engin.umich.edu/wiki/index.php/Solving_ODEs_with_Mathematica#Algorithms_Used_by_Mathematica`, 2006.

[18] L. Perko, *Differential Equations and Dynamical Systems*. Springer, 1991.

[19] S. Tang and N. Aubry, "On the symmetry breaking instability leading to vortex shedding," *Phys. Fluids*, vol. 9, pp. 2550–2561, 1997.

[20] A. Roshko, "On the development of turbulent wakes from vortex streets," Tech. Rep. 1191, National Advisory Committee for Aeronautics (NACA), 1954.

[21] A. Elcrat, B. Fornberg, M. Horn, and K. Miller, "Some steady vortex flows past a circular cylinder," *J. Fluid Mech.*, vol. 409, pp. 13–27, 2000.

[22] D. G. Crowdy and J. S. Marshall, "Analytical formulae for the Kirchhoff-Routh path function in multiply connected domains," *Proc. Roy. Soc. A.*, vol. 461, pp. 2477–2501, 2005.

[23] P. Koebe, "Abhandlungen zur theorie der konformen abbildung," *Acta Mathematica*, vol. 41, pp. 305–344, 1918.

[24] C. C. Lin, "On the motion of vortices in two dimensions II: some further investigations on the Kirchhoff-Routh function," *Proc. Natl. Acad. Sci.*, vol. 27, pp. 575–577, 1941.

[25] P. W. Bearman and M. M. Zdravkovich, "Flow around a circular cylinder near a plane boundary," *J. Fluid Mech.*, vol. 89, pp. 33–47, 1978.

[26] S. J. Price, D. Summer, J. G. Smith, K. Leong, and M. P. Païdoussis, "Flow visualization around a circular cylinder near to a plane," *J. Fluids Struct.*, vol. 16(2), pp. 175–191, 2002.

[27] E. R. Johnson and N. R. McDonald, "The motion of a vortex near two circular cylinders," *Proc. R. Soc. A*, vol. 460, pp. 939–954, 2004.

[28] D. G. Crowdy and J. S. Marshall, "The motion of a point vortex around multiple circular islands," *Phys. Fluids*, vol. 17, p. 056602, 2005.

[29] T. Sakajo, "Equation of motion for point vortices in multiply connected circular domains," *Proc. R. Soc. A*, vol. 465, pp. 2589–2611, 2009.

APPENDIX A

PUBLICATION

G. L. Vasconcelos, M. N. Moura, and A. M. J. Schakel, "Vortex motion around a circular cylinder," *Phys. Fluids*, vol. 23, p. 123601, 2011.

Vortex motion around a circular cylinder

G. L. Vasconcelos,[a] M. N. Moura, and A. M. J. Schakel
Laboratório de Física Teórica e Computacional, Departamento de Física, Universidade Federal de Pernambuco, 50670-901, Recife, Brazil

(Received 30 May 2011; accepted 18 November 2011; published online 9 December 2011)

The motion of a pair of counter-rotating point vortices placed in a uniform flow around a circular cylinder forms a rich nonlinear system that is often used to model vortex shedding. The phase portrait of the Hamiltonian governing the dynamics of a vortex pair that moves symmetrically with respect to the centerline—a case that can be realized experimentally by placing a splitter plate in the center plane—is presented. The analysis provides new insights and reveals novel dynamical features of the system, such as a nilpotent saddle point at infinity whose homoclinic orbits define the region of nonlinear stability of the so-called Föppl equilibrium. It is pointed out that a vortex pair properly placed downstream can overcome the cylinder and move off to infinity upstream. In addition, the nonlinear dynamics resulting from antisymmetric perturbations of the Föppl equilibrium is studied and its relevance to vortex shedding discussed. © *2011 American Institute of Physics*. [doi:10.1063/1.3667269]

I. INTRODUCTION

Flow around a circular cylinder is a classical topic in hydrodynamics that is of fundamental importance to many scientific fields with numerous applications.[1,2] Of particular interest is the formation, at moderate Reynolds numbers, of vortex eddies behind a circular cylinder, which then go unstable at higher Reynolds numbers and evolve into a Karman vortex street.[3,4] Since an analytic treatment of the problem in terms of the Navier-Stokes equation is difficult and the computational cost of direct numerical simulation (DNS) is very high, a particularly useful approach to study the basic features of vortex shedding from bluff bodies is to consider the dynamics of point vortices in an inviscid fluid.

A point-vortex model for the formation of two recirculating, symmetric eddies in the wake of a circular cylinder was first introduced by Föppl.[5] He obtained stationary solutions for a pair of vortices behind the cylinder in a uniform stream and found that the centers of the eddies observed in the experiments lie on the locus of such equilibria—now called the Föppl curve. In addition, Föppl found that these equilibria, although stable against perturbations that are symmetric with respect to the centerline, were unstable against nonsymmetric perturbations. This instability is believed to constitute the origin of the vortex shedding process that leads to the formation of the Karman vortex street.[6] It was later found out independently by several authors[7–9] that Föppl's stability analysis for symmetric perturbations was in error in that the stationary solution behind the cylinder is not exponentially but only marginally stable. Physically, marginal stability implies, for instance, that if a splitter plate is placed behind the cylinder in the center plane of the wake to suppress vortex shedding,[10–12] oscillating forces on the cylinder may still arise owing to the cyclic motion of the vortices around their equilibrium position.[13]

Despite many contributions to the problem, it is fair to say that the nonlinear dynamics of the Föppl system is not yet fully understood. In particular, a more complete picture of vortex-pair dynamics in the presence of symmetric perturbations is lacking, and several aspects of the nonlinear dynamics for nonsymmetric perturbations remain unclear. To address these two issues is the main motivation of the present paper. It should be emphasized at the outset that a better understanding of the dynamical structure underlying the Föppl model is of interest not only because of its practical relevance for vortex shedding but also in its own theoretical right from the viewpoint of nonlinear dynamics.

The Föppl model has inspired a number of studies on several related problems, such as the modeling of vortex wake behind slender bodies in terms of multiple pairs of point vortices,[14–17] the Hamiltonian structure of a circular cylinder interacting dynamically with point vortices,[18–20] the control of vortex shedding,[21–23] and the stability of symmetric and asymmetric vortex pairs over three-dimensional slender conical bodies.[12,24,25] The related problem of desingularization of the Föppl pair in terms of vortex patches of finite area was also studied.[26,27] A recent review on vortex motion past solid bodies with additional references to the Föppl model and related problems can be found in Ref. 28.

After formulating the problem of a pair of counter-rotating point vortices placed in a uniform stream around a circular cylinder in Sec. II, we begin our analysis of the Föppl system in Sec. III by studying its Hamiltonian dynamics restricted to the invariant subspace where the vortices move symmetrically with respect to the centerline. A phase portrait of the system is presented that fully characterizes the dynamics within this symmetric subspace. In particular, we point out that in addition to the two previously known sets of equilibria, namely, the Föppl equilibrium and the equilibrium on the axis bisecting the cylinder perpendicularly to the uniform flow, the system possesses a hitherto unnoticed nilpotent saddle at infinity. We show, furthermore, that the homoclinic orbits associated with this nilpotent saddle

[a]Author to whom correspondence should be addressed. Electronic mail: giovani@df.ufpe.br.

delimit the region of closed orbits around the Föppl equilibrium. We proceed in Sec. IV to study the linear and nonlinear dynamics resulting from antisymmetric perturbations of the Föppl equilibrium. In the linear regime, a mistake that went undetected in Föppl's expressions[5] for the corresponding eigenvalues is now corrected. As for the nonlinear dynamics, the unstable manifold associated with the Föppl equilibrium is computed numerically, and its close relation to the vortex shedding instability is pointed out. The linear stability analysis of the equilibria on the normal line with respect to symmetric and antisymmetric perturbations is also presented—for the first time, it seems—and the respective nonlinear dynamics is investigated numerically. A discussion of the physical relevance of our findings and our main conclusions are presented in Sec. V.

II. PROBLEM FORMULATION

We consider the motion of a pair of point vortices of same strength and opposite polarities around a circular cylinder of radius a and in the presence of a uniform stream of velocity U, as illustrated in Fig. 1. It is convenient to work in the complex z-plane, where $z=x+iy$, and place the center of the cylinder at the origin. The upper and lower vortices are located at positions $z_1=x_1+iy_1$ and $z_2=x_2+iy_2$, respectively. The complex potential $w(z)=\phi(x,y)+i\psi(x,y)$, with ϕ being the velocity potential and ψ the stream function, is given by[29]

$$w(z)=U\left(z+\frac{a^2}{z}\right)+\frac{\Gamma}{2\pi i}\ln\frac{z-z_1}{z-a^2/\bar{z}_1}-\frac{\Gamma}{2\pi i}\ln\frac{z-z_2}{z-a^2/\bar{z}_2}, \tag{1}$$

where Γ is the circulation of the vortex at z_1 and bar denotes complex conjugation. In Eq. (1), the first two terms represent the incoming flow and its image (a doublet at the origin) with respect to the cylinder, the third term gives the contributions to the complex potential from the upper vortex and its image, and similarly, the last term contains the contributions from the lower vortex and its image. As can be inferred from Fig. 1, a necessary condition for a steady configuration to exist is that the upper (lower) vortex be of negative (positive) circulation, hence, only the case $\Gamma<0$ is of interest to us here.

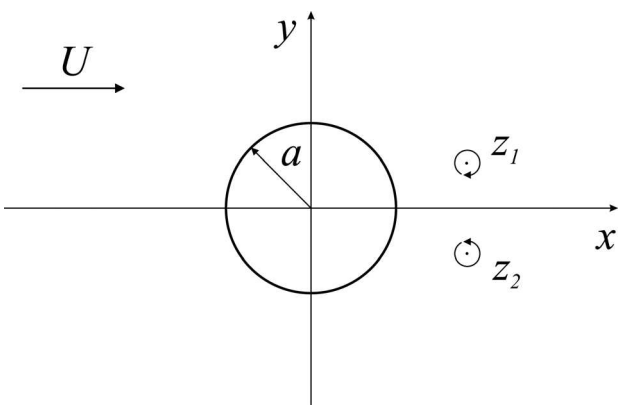

FIG. 1. A pair of vortices behind a circular cylinder in a uniform stream.

In dimensionless variables

$$z'=\frac{z}{a},\quad t'=\frac{U}{a}t,\quad w'=\frac{w}{Ua},\quad \kappa=-\frac{\Gamma}{2\pi Ua}>0, \tag{2}$$

the complex potential (1) becomes

$$w(z)=z+\frac{1}{z}+i\kappa\ln\frac{(z-z_1)(1-\bar{z}_2z)}{(z-z_2)(1-\bar{z}_1z)}, \tag{3}$$

where the prime notation has been dropped. According to standard theory of point vortices in an inviscid fluid, any given vortex moves with the velocity of the flow computed at the position of that vortex, excluding its own contribution to the flow. It then follows from Eq. (3) that the velocity $\mathbf{u}_1=(u_1,v_1)$ of the vortex located at z_1 is given by

$$u_1-iv_1=1-\frac{1}{z_1^2}-i\kappa\left(\frac{1}{z_1-z_2}-\frac{\bar{z}_1}{1-z_1\bar{z}_1}+\frac{\bar{z}_2}{1-z_1\bar{z}_2}\right), \tag{4}$$

or more explicitly,

$$u_1=1-\frac{x_1^2-y_1^2}{r_1^4}-\kappa\left(\frac{y_1-y_2}{r_1^2+r_2^2-2(x_1x_2+y_1y_2)}+\frac{y_1}{r_1^2-1}-\frac{y_1r_2^2-y_2}{1+r_1^2r_2^2-2(x_1x_2+y_1y_2)}\right), \tag{5a}$$

$$v_1=-2\frac{x_1y_1}{r_1^4}+\kappa\left(\frac{x_1-x_2}{r_1^2+r_2^2-2(x_1x_2+y_1y_2)}+\frac{x_1}{r_1^2-1}-\frac{x_1r_2^2-x_2}{1+r_1^2r_2^2-2(x_1x_2+y_1y_2)}\right), \tag{5b}$$

where $r_i^2=x_i^2+y_i^2$, $i=1,2$. The velocity $\mathbf{u}_2=(u_2,v_2)$ of the second vortex is obtained by simply interchanging the indexes $1\leftrightarrow 2$ in Eq. (5) and letting $\kappa\to-\kappa$.

III. DYNAMICS ON THE SYMMETRIC SUBSPACE

It is not difficult to see from Eq. (5) that if the vortices are initially placed at positions symmetrically located with respect to the centerline, i.e., $z_2(0)=\bar{z}_1(0)$, then this symmetry is preserved for all later times, i.e., $z_2(t)=\bar{z}_1(t)$ for $t>0$. In this section, we study the dynamics within this invariant symmetric subspace, where the motion of the lower vortex is simply the mirror image of that of the upper vortex with respect to the centerline. Symmetry can be enforced experimentally by placing a splitter plate behind the cylinder in the center plane of the wake.[5,10]

With $x_2=x_1$ and $y_2=-y_1$, Eq. (5) reduces to

$$u=1-\frac{x^2-y^2}{r^4}+\kappa y\left[\frac{r^2+1}{(r^2-1)^2+4y^2}-\frac{1}{r^2-1}-\frac{1}{2y^2}\right], \tag{6a}$$

$$v=-2\frac{xy}{r^4}-\kappa x\left[\frac{r^2-1}{(r^2-1)^2+4y^2}-\frac{1}{r^2-1}\right]. \tag{6b}$$

Here, the subscripts have been dropped with the understanding that in the remainder of the section we restrict our attention to the upper vortex.

A. Hamiltonian dynamics and phase portrait

As is well known, the equations of motion for point vortices in a two-dimensional inviscid flow, first derived by Kirchhoff, can be formulated as a Hamiltonian system.[3,4] The dynamics of point vortices in the presence of closed, rigid boundaries was shown by Lin[30] to be also Hamiltonian with the same canonical symplectic structure as in the absence of boundaries. For a vortex pair placed in a uniform stream around a circular cylinder, the phase space is four-dimensional and has a two-dimensional (2D) invariant subspace corresponding to symmetric orbits. The Hamiltonian restricted to the 2D symmetric subspace is given by[31]

$$H(x,y) = y\left(1-\frac{1}{r^2}\right) - \frac{\kappa}{2}\ln\frac{y(r^2-1)}{\sqrt{(r^2-1)^2+4y^2}}. \tag{7}$$

The corresponding dynamical equations

$$\dot{x} = \frac{\partial H}{\partial y}, \quad \dot{y} = -\frac{\partial H}{\partial x}, \tag{8}$$

where dot denotes time derivative, yield Eq. (6) upon identifying (u, v) with $(\dot{x}, \dot{y})$.

A phase portrait of this Hamiltonian system for $\kappa = 45/32$ is presented in Fig. 2, where the curves shown are (unevenly spaced) level sets of the Hamiltonian Equation (7). [For convenience, these curves were obtained from a direct numerical integration of Eq. (6).] A detailed description of the main features of this phase portrait will be given below, starting with an analysis of the various equilibrium points and their stability. The related problem of the symmetric "moving Föppl system," where the cylinder advances through the fluid followed by the vortex pair, was recently considered by Shashikanth *et al.*,[18] but there the phase portrait[19] is quite different from the one shown in Fig. 2, because of the additional degrees of freedom related to the velocity of the moving cylinder.

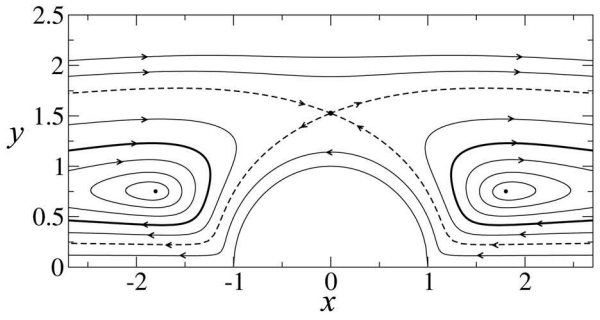

FIG. 2. Phase portrait for the symmetric Föppl system with $\kappa = 45/32$. The isolated black dots are the Föppl equilibria. The dashed curves are the stable and unstable branches of the separatrix associated with the equilibrium point on the normal line, and the thick solid lines are the homoclinic loops of the equilibrium point at infinity; see text.

B. Equilibrium points

The equilibrium positions for the vortex are obtained by setting $u = v = 0$ in Eq. (6). Three types of equilibrium points can be identified.

1. Föppl equilibria

The locus of possible equilibrium positions (x_0, y_0) for the upper vortex found by Föppl[5] is the curve

$$r_0^2 - 1 = 2r_0 y_0, \tag{9}$$

with corresponding strength

$$\kappa = \frac{(r_0^2+1)(r_0^2-1)^2}{r_0^5}. \tag{10}$$

Along the Föppl curve (9), the vortex strength increases with distance from the center of the cylinder and diverges linearly for $r_0 \to \infty$. For the equilibrium point on the edge of the cylinder ($r_0 \to 1$), the strength vanishes. Notice that Eq. (9) yields two branches of solution: one in which the vortex pair is behind the cylinder ($x_0 > 0$) and the other where the vortex pair is in front of the cylinder ($x_0 < 0$). The former case models the formation of vortex eddies behind a cylinder in a uniform stream and was the primary motivation of Föppl's original study.[5] The latter case has attracted far less attention, because it is not usually observed in experiments. We note, however, that recirculating eddies are observed in front of a circular cylinder near a plane boundary when the gap between the cylinder and the plane is sufficiently small.[32] In this context, the Föppl equilibrium upstream of the cylinder may eventually be relevant for flows around a half-cylinder placed on a plane wall (or for the closely related situation where a splitter plate is attached to the front of the cylinder), although we are unaware of specific experiments in this setting.

2. Equilibria on the normal line

This corresponds to the upper vortex being located on the line bisecting the cylinder perpendicularly to the incoming flow,[15] that is,

$$x = 0, \qquad y = b, \qquad b > 1, \tag{11}$$

with strength

$$\kappa = \frac{2(b^2-1)(b^2+1)^2}{b(b^4+4b^2-1)}. \tag{12}$$

As in the Föppl solution, the strength tends to zero when the edge of the cylinder is reached ($b \to 1$) and diverges linearly with distance from the center of the cylinder. At large distances, the vortex strength for this equilibrium is about twice that of a Föppl pair located at the same distance from the origin.

3. Equilibrium at infinity

Equation (6) also yields equilibrium points at the positions

$$x = \pm\infty, \qquad y_\infty = \frac{\kappa}{2}. \tag{13}$$

To the best of our knowledge, the existence of this additional equilibrium point at infinity was not noted before. Its physical origin, however, can be easily understood, as it corresponds to the equilibrium configuration for a vortex pair placed in a uniform stream (without the cylinder). At points infinitely far from the cylinder, the flow induced by the image system (inside the cylinder) becomes negligible, and hence, a stationary configuration is possible if the vortices with given circulation $\pm\kappa$ are placed at the appropriate distance ($=\kappa$) from each other.

C. Stability analysis

The linear stability analysis of the equilibria described above is presented next, together with a discussion of the *nonlinear* stability of the Föppl equilibrium.

1. Föppl equilibria

Consider a perturbation of the Föppl equilibrium (9) parameterized as $z = z_0 + \Delta z$, where $\Delta z = \xi + i\eta$, with ξ and η being infinitesimal (real) quantities. Linearization of Eq. (6) then yields the following dynamical system:

$$\begin{pmatrix} \dot{\xi} \\ \dot{\eta} \end{pmatrix} = A \begin{pmatrix} \xi \\ \eta \end{pmatrix}, \tag{14}$$

where the matrix A reads

$$A_{11} = -A_{22} = -\frac{x_0(r_0^4 - 3r_0^2 + 2)}{r_0^8}, \tag{15}$$

$$A_{12} = \frac{4r_0^8 + 5r_0^6 + 2r_0^4 - 5r_0^2 + 2}{2r_0^9}, \tag{16}$$

$$A_{21} = -\frac{2x_0^2(r_0^4 + r_0^2 + 2)}{r_0^7(r_0^2 + 1)}. \tag{17}$$

Its eigenvalues λ are given by

$$\lambda^2 = -\frac{3r_0^6 + 5r_0^4 + 13r_0^2 - 5}{r_0^{10}} < 0, \tag{18}$$

for $r_0 > 1$. The eigenvalues are, thus, purely imaginary and not a complex pair with negative real part as found by Föppl.[5] In other words, the Föppl equilibrium is a center and not a stable focus. Our Eq. (18) agrees with the expression for the eigenvalues of the symmetric modes obtained in Ref. 7 from the linearization of the full 4D dynamical system. As can be seen from Fig. 2, the Föppl solution is in fact a nonlinearly stable center, meaning that when the vortex is displaced from its equilibrium position by a small (but finite) amount, it executes a periodic motion around that point, corresponding to the closed orbits in the figure. This periodic motion around the Föppl equilibrium has been observed in numerical simulations of the model carried out by de Laat and Coene.[13] Note that since the eigenvalues given in Eq. (18) do not depend explicitly on the coordinate x_0, it follows that the two Föppl equilibria, downstream and upstream of the cylinder, have identical stability properties, as is evident from Fig. 2. This means, in particular, that if vorticity can be generated upstream of the cylinder then stationary recirculating eddies could form in front of the cylinder—a situation observed, for instance, in flows around a cylinder placed above a plane wall.[32]

2. Equilibria on the normal line

Linearization of Eq. (6) around the equilibrium point $z = ib$ yields, for the matrix A,

$$A_{11} = A_{22} = 0, \tag{19}$$

$$A_{12} = \frac{b^8 + 10b^6 - 8b^4 + 14b^2 - 1}{b^3(b^2 - 1)(b^4 + 4b^2 - 1)}, \tag{20}$$

$$A_{21} = \frac{2(b^2 - 1)(3b^2 - 1)}{b^3(b^4 + 4b^2 - 1)}. \tag{21}$$

The eigenvalues λ of this matrix are determined by

$$\lambda^2 = \frac{2(3b^2 - 1)\left(b^8 + 10b^6 - 8b^4 + 14b^2 - 1\right)}{b^6(b^4 + 4b^2 - 1)^2} > 0, \tag{22}$$

which yields a pair of real eigenvalues, $\lambda_\pm = \pm\sqrt{\lambda^2}$. The equilibrium point on the normal line is, therefore, a saddle, having a stable and unstable direction, as is also evident from the phase portrait shown in Fig. 2. The eigenvectors $\mathbf{w}_\pm$ associated with the eigenvalues $\lambda_\pm$, respectively, read

$$\mathbf{w}_\pm = \begin{pmatrix} \pm\sqrt{A_{12}/A_{21}} \\ 1 \end{pmatrix}. \tag{23}$$

Although it was known from numerical simulations[13] that the equilibrium point on the normal line is unstable (against generic symmetric perturbations), it seems that an explicit linear stability analysis for this case was not carried out before, perhaps because these equilibria were not considered physically relevant since they are not observed in experiment.[5] However, when the full nonlinear dynamics is considered, the stable and unstable eigendirections $\mathbf{w}_\pm$ give origin to the respective stable and unstable separatrices, indicated by the dashed curves in Fig. 2. In this sense, the existence of an equilibrium point on the normal line is dynamically felt by a vortex even if it is placed far from this "unphysical" equilibrium.

3. Equilibrium at infinity

The matrix A of the linearized system around the equilibrium point at infinity is given by

$$A = -\frac{2}{\kappa}\begin{pmatrix} 0 & 1 \\ 0 & 0 \end{pmatrix}, \tag{24}$$

which is nilpotent and has two zero eigenvalues. To study the stability of this equilibrium point, one needs to examine the nonlinear contributions. To this end, we note that for $|x| \to \infty$ and $y \approx y_\infty$, Eq. (6b) assumes the form

$$\dot{y} = -\frac{\kappa}{x^3}. \tag{25}$$

It then follows from a theorem in ordinary differential equations[33] that, in view of the cubic term in Eq. (25), the equilibrium point is a *degenerate* or *nilpotent* saddle,[34] for which the two eigenvectors are the same. The behavior of trajectories in the neighborhood of a generic nilpotent saddle is illustrated in Fig. 3. The behavior near the nilpotent saddle at $x = \pm\infty$ and $y = y_\infty$ can be described as follows. A vortex placed very far downstream and below (above) the line $y = y_\infty$ will move away from (towards) the equilibrium point at $x = \infty$. Similarly, a vortex placed very far upstream will move away from (towards) the equilibrium point at $x = -\infty$ if $y > y_\infty$ ($y < y_\infty$).

The stable and unstable separatrices associated with the nilpotent saddle at infinity form two homoclinic loops,[34] called nilpotent saddle loops, which are indicated in Fig. 2 by thick solid lines and correspond to the level curves passing through this equilibrium point,

$$H(x,y) = H(\pm\infty, y_\infty) = \frac{\kappa}{2}\left(1 - \ln\frac{\kappa}{2}\right). \tag{26}$$

The nilpotent saddle loops encircle the Föppl equilibria and define their region of nonlinear stability, in the sense that vortex trajectories are closed for initial positions inside the loops and unbounded otherwise. In this way, the nilpotent saddle at infinity, which went unnoticed until now, allows us to fully characterize the nonlinear stability of the Föppl equilibrium.

For unbounded orbits, the long-time asymptotic behavior depends on the location of the vortex initial position with respect to the separatrices associated with the equilibrium point on the normal line. A vortex placed downstream of the cylinder between the nilpotent saddle loop and the separatrices of the equilibrium point on normal line will eventually be convected away by the free stream; see Fig. 2. In particular, if the vortex starts very far behind the cylinder at a position that is below the nilpotent saddle loop and above the stable separatrix, it first moves towards the cylinder, turns around the Föppl equilibrium, and is then "reflected" back to infinity. Even more surprising trajectories arise if the vortex is placed downstream below the stable separatrix, for it will be close enough to its image below the centerline to be able to overcome the cylinder and move off to infinity upstream. (A related phenomenon occurs in the inviscid coupled motion of a cylinder initially at rest and a vortex pair starting at infinity with no imposed background flow.[35] When the cylinder is less dense than the fluid, it is found that if the vortices are released sufficiently above the centerline they reverse relative to the moving cylinder; otherwise, they move over and past the cylinder.) Unbounded trajectories for the Föppl system also result for initial positions upstream of the cylinder: (1) if placed above the stable separatrix, the vortex moves downstream to infinity and (2) if placed between the stable separatrix and the nilpotent saddle loop, the vortex goes around the Föppl equilibrium in front of the cylinder and returns to infinity upstream; see Fig. 2. It is again the hitherto unnoticed nilpotent saddle at infinity, together with the precise nature of the equilibrium point on the normal line, which allows us to go beyond linear stability analysis and capture the full phase portrait in the symmetric subspace.

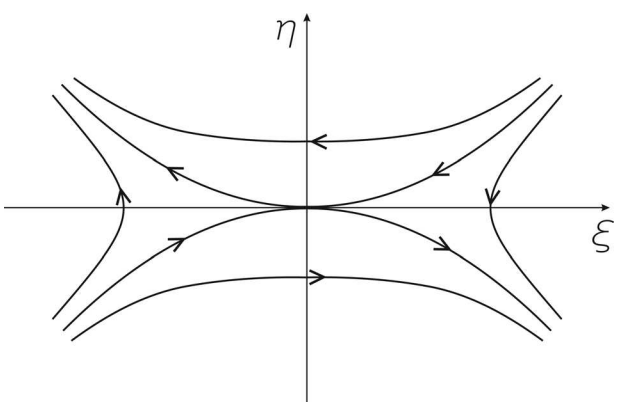

FIG. 3. Trajectories near a nilpotent saddle.

We stress that closed orbits exist only when the flow is symmetric. Nonsymmetric perturbations inevitably cause the vortex pair to move off to infinity, as we demonstrate next.

IV. NONSYMMETRIC DYNAMICS

In this section, the effect of antisymmetric perturbations on the equilibria of the Föppl system is studied. We begin by observing that the dynamics of two counter-rotating point vortices possesses a *conjugation symmetry*. To describe this symmetry, let $z_1(t; z_{1,0}, z_{2,0})$ and $z_2(t; z_{1,0}, z_{2,0})$ denote the trajectories of the upper and lower vortices, respectively, with initial positions $z_{1,0}$ and $z_{2,0}$. For the dynamical system defined by Eq. (5) and the corresponding equation for the second vortex, one can verify that the following relations hold:

$$z_1(t; \bar{z}_{2,0}, \bar{z}_{1,0}) = \overline{z_2(t; z_{1,0}, z_{2,0})}, \tag{27a}$$

$$z_2(t; \bar{z}_{2,0}, \bar{z}_{1,0}) = \overline{z_1(t; z_{1,0}, z_{2,0})}. \tag{27b}$$

In other words, for any given pair of initial positions, $z_{1,0}$ and $z_{2,0}$, there exists a "conjugate pair" of initial positions, $\bar{z}_{2,0}$ and $\bar{z}_{1,0}$, such that the vortex trajectories of the first pair are the complex conjugate of those of the second pair.

Any perturbation of a vortex-pair equilibrium can be written as the superposition of a symmetric perturbation and an antisymmetric one. To be precise, antisymmetric perturbations are of the form

$$z_1 = z_0 + \Delta z, \qquad z_2 = \bar{z}_0 - \overline{\Delta z}, \tag{28}$$

where z_0 denotes a generic equilibrium point and $\Delta z = \xi + i\eta$. Since the antisymmetric subspace of the full 4D phase space is invariant under linear dynamics, we can focus on the upper vortex in carrying out our linear stability analysis.

A. Föppl equilibria

Linearization of Eq. (5) around the Föppl equilibrium (9) with respect to antisymmetric perturbations (28) yields

$$\begin{pmatrix} \dot{\xi} \\ \dot{\eta} \end{pmatrix} = B \begin{pmatrix} \xi \\ \eta \end{pmatrix}, \tag{29}$$

where the matrix B is given by

$$B_{11} = -B_{22} = \frac{x_0\left(r_0^4 + 3r_0^2 - 2\right)}{r_0^8}, \tag{30}$$

$$B_{12} = \frac{3r_0^6 - 5r_0^2 + 2}{2r_0^9}, \tag{31}$$

$$B_{21} = \frac{4r_0^8 + 3r_0^6 - 4r_0^4 - 5r_0^2 + 2}{2r_0^9}. \tag{32}$$

This matrix has a pair of real eigenvalues, $\lambda_\pm = \pm\sqrt{\lambda^2}$, where

$$\lambda^2 = \frac{3r_0^6 + 3r_0^4 - 3r_0^2 + 1}{r_0^{10}}. \tag{33}$$

The Föppl equilibrium is, therefore, a saddle with respect to antisymmetric perturbations, while it is a center with respect to symmetric perturbations, as seen earlier. That is, the Föppl equilibrium is a *saddle-center* of the full 4D dynamical system.[36] We note in passing that, although Föppl obtained a pair of real eigenvalues for the case of antisymmetric perturbations, his original formulae for the eigenvalues are in error.[37] Our expression (33) is in agreement with the eigenvalues of the skew-symmetric modes obtained by Smith[7] from the linearization of the full dynamical system. The eigenvectors $\mathbf{w}_\pm$ associated with the eigenvalues $\lambda_\pm$ are readily computed, with the result

$$\mathbf{w}_\pm = \begin{pmatrix} (\lambda_\pm + B_{11})/B_{21} \\ 1 \end{pmatrix}. \tag{34}$$

In Fig. 4, we show in solid curves the pair of vortex trajectories obtained by slightly displacing the vortices from their equilibrium positions in the directions defined by the unstable eigenvector $\mathbf{w}_+$, while the trajectories obtained by slightly displacing the vortices in the opposite directions are shown in dashed curves. The latter pair of trajectories is the complex conjugate of the former by conjugation symmetry. Note that for the first pair of trajectories, the lower vortex initially moves towards the centerline and upstream, while the upper vortex moves away from the centerline and downstream. At later times, the vortex pair moves off to infinity with the lower vortex trailing behind the upper vortex. For the second pair of trajectories, the upper and lower vortices switch roles; see Fig. 4. In the flow of a real fluid past a cylinder, the two basic instabilities associated with displacements along the unstable directions $\pm\mathbf{w}_+$ happen alternately and constitute the origin of vortex shedding that leads to the formation of the Karman vortex street.[6] In like manner, the suppression of vortex shedding by placing a splitter plate behind the cylinder[10,11] is consistent with the fact that the Föppl equilibrium is nonlinearly stable with respect to symmetric perturbations; see Sec. V for further discussions on vortex shedding and its suppression by a splitter plate.

For small, generic antisymmetric perturbations, the vortices move along trajectories that follow closely the ones depicted in Fig. 4. Whether a vortex pair eventually moves up or down is determined by the initial position of the upper vortex relative to the stable direction $\mathbf{w}_-$, which is indicated in Fig. 4 by the short straight line passing through the Föppl equilibrium. If the initial position of the upper vortex is to the right (left) of the stable direction, then the vortex pair asymptotically moves upwards (downwards). This explains the behavior seen in the numerical simulations reported in Ref. 25, where nearby initial positions around the Föppl equilibrium were found to lead to close-by trajectories.

Since any degree of antisymmetry in the initial perturbation causes the vortex pair to move off to infinity, the Föppl equilibrium is unstable under generic perturbations. As an example, Fig. 5 shows vortex trajectories obtained by displacing the Föppl pair (at $r_0 = 2$) by the amounts $\Delta z_1 = \Delta z_2 = -0.25 + i0.005$. During the linear stage, the trajectories are a superposition of a symmetric orbit and a growing mode associated with the antisymmetric component of the perturbation, which ultimately leads to asymptotic trajectories with the vortices moving parallel to each other.

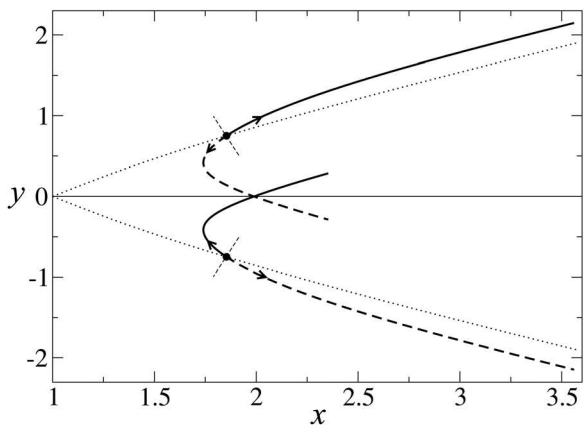

FIG. 4. Vortex trajectories for antisymmetric perturbations of the Föppl equilibrium for $\kappa = 45/32$, in which case $x_0 = \sqrt{55}/4$ and $y_0 = \pm 3/4$ (black dots). The solid and dashed curves are the trajectories starting along the unstable directions w_+ and $-\mathrm{w}_+$, respectively, while the short straight lines indicate the axes defined by the stable direction w_-. The dotted lines represent the loci of the Föppl equilibria.

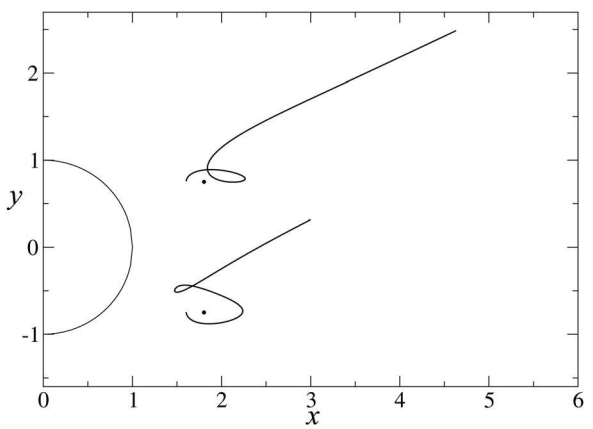

FIG. 5. Trajectories resulting from a generic perturbation $\Delta z_1 = \Delta z_2 = -0.25 + i0.005$ of the Föppl pair at $r_0 = 2$ (black dots).

B. Equilibria on the normal line

For antisymmetric perturbations of the equilibrium (11) on the normal line, the matrix B assumes the form

$$B_{11} = B_{22} = 0, \tag{35}$$

$$B_{12} = \frac{2\left(3b^6 + b^4 + 5b^2 - 1\right)}{b^3(b^2-1)(b^4+4b^2-1)}, \tag{36}$$

$$B_{21} = \frac{b^2-1}{b^3}, \tag{37}$$

with eigenvalues λ given by

$$\lambda^2 = \frac{2\left(3b^6 + b^4 + 5b^2 - 1\right)}{b^6(b^4+4b^2-1)} > 0. \tag{38}$$

This yields a pair of real eigenvalues, $\lambda_\pm = \pm\sqrt{\lambda^2}$, with respective eigenvectors,

$$\mathbf{w}_\pm = \begin{pmatrix} \pm\sqrt{B_{12}/B_{21}} \\ 1 \end{pmatrix}. \tag{39}$$

In Fig. 6, we show the vortex trajectories (solid curves) obtained by slightly displacing the vortices from their equilibrium position along the unstable direction $\mathbf{w}_+$ for $b=2$. The initial motion here is somewhat similar to what is seen for a Föppl pair, in the sense that one vortex moves upstream towards the centerline and the other moves downstream away from the centerline. The main difference is that for later times, the vortices now end up moving upstream. The long-time dynamics in this case is also more sensitive on the initial conditions; for somewhat larger perturbations, the vortices are eventually carried away by the free stream. An example where this happens is indicated by the dashed curves in Fig. 6, which represent the vortex trajectories for the antisymmetric perturbation $\Delta z = 0.16$.

As already argued in Sec. III C 2, although the equilibrium point on the normal line is not directly observed in experiments, it is important to know its instability properties under both symmetric and antisymmetric perturbations. This knowledge contributes to a better understanding not only of the full nonlinear dynamics of the Föppl system but also of more general flows, such as the case of stationary vortex patches above and below the cylinder in a uniform stream, where similar unstable modes are observed.[27]

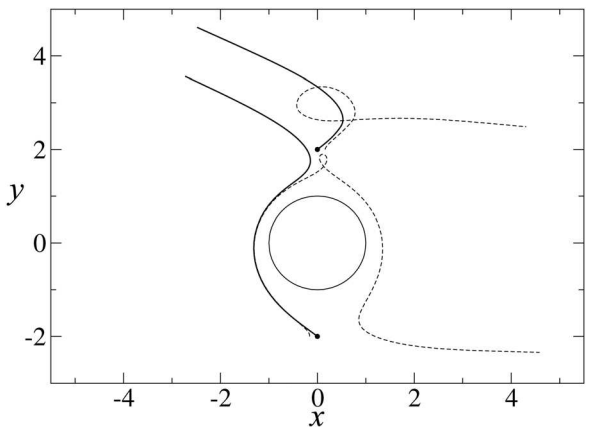

FIG. 6. Vortex trajectories (solid curves) associated with the unstable direction w_+ of the equilibrium at $z = \pm 2i$ (black dots). The dashed curves are trajectories resulting from the antisymmetric perturbation $\Delta z = 0.16$.

V. DISCUSSION AND CONCLUSIONS

In this paper, we have investigated a two-dimensional vortex model for the formation of recirculating eddies behind a fixed cylinder placed on a uniform stream. The model, which was first introduced by Föppl[5] almost a century ago, has two main simplifying assumptions: (1) the fluid is treated as inviscid, and hence the flow is potential and (2) the size of the vortex core is neglected, and so the vortices are considered to be point-like. In spite of these simplifications, the model is known to be in qualitative agreement with real flows past a cylinder, as was already pointed out by Föppl in his original paper. Several novel features of the Föppl model have been obtained in the present work, which help one to better understand the basic dynamics of vortex shedding behind a cylinder.

In real flows, governed by the Navier-Stokes equations, stationary vortices behind a cylinder are formed at moderate Reynolds number ($Re < 50$). As the Reynolds number increases past $Re \approx 50$, the configuration loses its symmetry and becomes unstable. New vortices then start to form alternately on both sides of the cylinder, while the vortices further downstream break away and develop into a Karman vortex street, as described by Föppl.[5] It has been argued by Roshko[10] that "possibly the breaking away should be regarded as primary, resulting in asymmetry." The analysis presented in Sec. IV A makes it clear that the reverse scenario is more plausible; the asymmetrical disturbances induce the instability of the vortex pair which then breaks away from the cylinder. As vorticity is continuously generated from the separated boundary layer on both sides of the cylinder, new vortices are formed and alternately shed into the far wake of the cylinder according to the unstable modes shown in Fig. 4. DNSs of two-dimensional flows past a cylinder performed by Tang and Aubry[6] have confirmed that the mechanism for the instability of the symmetric eddies in real flows is qualitatively described by the instability of the point-vortex model.

It is experimentally observed[10,11] that vortex shedding is suppressed if a splitter plate is installed behind the cylinder in the center plane of the wake. The presence of the splitter plate tends to enforce symmetry of the flow with respect to the centerline, thus effectively reducing the appearance of antisymmetric disturbances behind the cylinder. The suppression of vortex shedding in this case is thus entirely consistent with the fact that the Föppl equilibria of the vortex-point model are nonlinearly stable against symmetric perturbations and that vortex shedding is induced by unstable antisymmetric modes, as discussed above. This scenario has been confirmed by DNS of flows past a cylinder with symmetry imposed along the centerline recently performed by Kumar *et al.*[38] The problem of stationary configurations for vortex flows past a cylinder with patches of constant vorticity has also been studied numerically by Elcrat *et al.*[26,27]

These authors found two families of solutions, representing desingularized versions of the Föppl and the normal equilibria, respectively, which have the same stability properties as the corresponding point-vortex equilibria.

In conclusion, we have seen that the Föppl model, where a pair of counter-rotating point vortices move around a circular cylinder in the presence of a uniform stream, is a rich nonlinear dynamical system whose features—notably its stability properties—bear a direct relevance to our understanding of the vortex shedding mechanism in real flows. The results obtained here should, in principle, carry over to more general geometries, such as vortex motion around a plate or around a cylinder with noncircular cross section.

ACKNOWLEDGMENTS

This work was supported in part by the Brazilian agencies CNPq and FACEPE. One of the authors (A.M.J.S.) acknowledges financial support from CAPES, Brazil through a visiting professor scholarship.

[1]M. M. Zdravkovich, *Flow Around Circular Cylinders, Fundamentals*, Vol. 1; *Applications*, Vol. 2 (Oxford University Press, Oxford, 1997).
[2]B. M. Sumer and J. Fredse, *Hydrodynamics Around Cylindrical Structures* (World Scientific, Singapore, 2006).
[3]P. G. Saffman, *Vortex Dynamics* (Cambridge University Press, Cambridge, 1992).
[4]J.-Z. Wu, H.-Y. Ma, and M.-D. Zhou, *Vorticity and Vortex Dynamics* (Springer, Berlin, 2006).
[5]L. Föppl, "Wirbelbewegung hinter einem Kreiszylinder," Sitzb. Bayer. Akad. Wiss. **1**, 1 (1913).
[6]S. Tang and N. Aubry, "On the symmetry breaking instability leading to vortex shedding," Phys. Fluids **9**, 2550 (1997).
[7]A. C. Smith, "On the stability of Föppl's vortices," J. Appl. Mech. **70**, 610 (1973).
[8]I. Soibelman, private communication, (2011); see also page 43 of Ref. 3.
[9]J. Cai, F. Liu, and S. Luo, "Stability of a vortex pair behind two-dimensional bodies," AIAA Paper 2001-2844, 2001.
[10]A. Roshko, "On the development of turbulent wakes from vortex streets," NACA Technical Report 1191, US Government Printing Office, Washington DC, 1954.
[11]A. Roshko, "Experiments on the flow past a circular cylinder at very high Reynolds number," J. Fluid Mech. **10**, 345 (1961).
[12]J. Cai, F. Liu, and S. Luo, "Stability of symmetric vortices in two dimensions and over three-dimensional slender conical bodies," J. Fluid Mech. **480**, 65 (2003).
[13]T. W. G. D. de Laat and R. Coene, "Two-dimensional vortex motion in the cross-flow of a wing-body configuration," J. Fluid Mech. **305**, 93 (1995).
[14]D. D. Seath, "Equilibrium vortex positions," J. Spacecr. Rockets **8**, 72 (1971).
[15]D. Weihs and M. Boasson, "Multiple equilibrium vortex positions in symmetric shedding from slender bodies," AIAA J. **17**, 213 (1979).
[16]K. G. Miller, "Stationary cornex vortex configurations," Z. Angew. Math. Phys. **47**, 39 (1996).
[17]B. Protas, "Higher-order Föppl models of steady wake flows," Phys. Fluids **18**, 117109 (2006).
[18]B. N. Shashikanth, J. E. Marsden, J. W. Burdick, and S. D. Kelly, "The Hamiltonian structure of a two-dimensional rigid circular cylinder interacting dynamically with N point vortices," Phys. Fluids **14**, 1214 (2002); (Erratum: Phys. Fluids **14**, 4099 (2002)).
[19]B. N. Shashikanth, "Symmetric pairs of point vortices interacting with a neutrally buoyant two-dimensional circular cylinder," Phys. Fluids **18**, 127103 (2006).
[20]A. V. Borisov, I. S. Mamaev, and S. M. Ramodanov, "Dynamic interaction of point vortices and a two-dimensional cylinder," J. Math. Phys. **48**, 065403 (2007).
[21]S. Tang and N. Aubry, "Suppression of vortex shedding inspired by a low-dimensional model," J. Fluids Struct. **14**, 443 (2000).
[22]B. Protas, "Linear feedback stabilization of laminar vortex shedding based on a point vortex model," Phys. Fluids **16**, 4473 (2004).
[23]B. Protas, "Center manifold analysis of a point vortex model of vortex shedding with control," Physica D **228**, 179 (2007).
[24]J. Cai, F. Liu, and S. Luo, "Stability of symmetric and asymmetric vortex pairs over slender conical wings and bodies," Phys. Fluids **16**, 424 (2004).
[25]D. H. Bridges, "Toward a theoretical description of vortex wake asymmetry," Prog. Aerosp. Sci. **46**, 62 (2010).
[26]A. Elcrat, B. Fornberg, M. Horn, and K. Miller, "Some steady vortex flows past a circular cylinder," J. Fluid Mech. **409**, 13 (2000).
[27]A. Elcrat, B. Fornberg, and K. Miller, "Stability of vortices in equilibrium with a cylinder," J. Fluid Mech. **544**, 53 (2005).
[28]B. Protas, "Vortex dynamics models in flow control problems," Nonlinearity **21**, R203 (2008).
[29]L. M. Milne-Thomson, *Theoretical Hydrodynamics*, 5th ed. (Dover, New York, 1996).
[30]C. C. Lin, "On the motion of vortices in two dimensions–I and II," Proc. Natl. Acad. Sci. U.S.A. **27**, 570 (1941).
[31]L. Zannetti, "Vortex equilibrium in flows past bluff bodies," J. Fluid Mech. **562**, 151 (2006).
[32]W.-J. Lin, C. Lin, S.-C. Hsieh, and S. Dey, "Flow characterization around a circular cylinder placed horizontally above a plane boundary," J. Eng. Mech. **135**, 697 (2009).
[33]L. Perko, *Differential Equations and Dynamical Systems* (Springer, New York, 1991).
[34]M. Han, C. Shu, J. Yang, and A. C.-L. Chian, "Polynomial Hamiltonian systems with a nilpotent critical point," Adv. Space Res. **46**, 521 (2010).
[35]I. Eames, M. Landeryou, and J. B. Flór, "Inviscid coupling between point symmetric bodies and singular distributions of vorticity," J. Fluid Mech. **589**, 33 (2007).
[36]L. M. Lerman and Y. L. Umanskiy, *Four-dimensional Integrable Hamiltonian Systems with Simple Singular Points* (American Mathematical Society, Providence, 1998).
[37]The formula for the matrix element X' given in Eq. (17) of Ref. 5, which corresponds to the matrix element B_{21} in our Eq. (32), is in error.
[38]B. Kumar, J. J. Kottaram, A. K. Sing, and S. Mittal, "Global stability of flow past a cylinder with centreline symmetry," J. Fluid Mech. **632**, 273 (2009).

This volume has been typeset in LaTeXwith the UFPEThesis class (www.cin.ufpe.br/~paguso/ufpethesis).